UNIVERSITY OF SOUTHAMPTON

FACULTY OF ENGINEERING AND APPLIED SCIENCE

Department of Electronics and Computer Science

Q-SWITCHED FIBRE LASERS FOR DISTRIBUTED SENSING APPLICATIONS

by Gareth P. Lees

A Thesis submitted for the degree of

DOCTOR OF PHILOSOPHY

September 1998

UNIVERSITY OF SOUTHAMPTON

ABSTRACT

FACULTY OF ENGINEERING AND APPLIED SCIENCE

DEPARTMENT OF ELECTRONICS AND COMPUTER SCIENCE

Doctor of Philosophy

Q-SWITCHED FIBRE LASER SOURCES FOR DISTRIBUTED SENSING APPLICATIONS

by Gareth P. Lees

This thesis examines pulsed fibre sources for distributed sensing applications. A number of Q-switched fibre laser sources optimised for high peak powers, narrow linewidth and short pulse duration are described. The source specifications were dictated by the requirements of Raman and Brillouin distributed sensing systems. The spatial resolution of distributed sensors is related to the pulse width whereas the range is dependent on the power launched into the sensing fibre. Brillouin distributed sensors also require that the source linewidth is less than 10 GHz, the separation between the Rayleigh and Brillouin backscattered light. This constraint on laser linewidth leads to coherent Rayleigh noise on the Rayleigh backscattered trace. This noise can be reduced by a technique of frequency shift averaging. A Q-switched laser incorporating this technique was developed, which resulted in a Brillouin distributed temperature sensor with a temperature resolution of 1.4°C and a spatial resolution of 10metres over a range of 6.5km.

The development of high power Q-switched fibre lasers leads to the possibility of generating Raman shifted pulses at wavelengths of 1.64-1.65μm. Interest in this wavelength region stems from the increase in sensitivity to fibre micro-bend losses at these higher wavelengths and the ability to monitor the fibre whilst carrying out live data transmission. A diode pumped, pulsed source at 1.64μm producing 8Watt, 10ns pulses through a process of Raman generation was demonstrated. Q-switched laser technology was also used to increase the dynamic range of 1.65μm OTDR. The technique utilised delayed Raman amplification of the 1.65μm signal pulse by a co-propagating 1.53μm pump pulse. Amplification occurs when the two pulses overlap. The position of the overlap is determined by the initial delay between the pulses and the fibre dispersion. An increase in dynamic range of 17.5dB has been observed and the 1.65μm OTDR range was extended to in excess of 100km.

Table of Contents

Acknowledgements

During my work at the Optoelectronics Research Centre, many people have provided valuable input to my research. I would especially like to thank my supervisor Dr Trevor Newson for his continuous technical and moral support. Special thanks are due to Adrian Leach and Arthur Hartog of York Sensors for their helpful discussion and debate. Thanks are also due to Martin Cole for supplying the fibre gratings and Dr Peter Wait for giving generously his time for discussion.

Last, but in no way least, I would like to thank my family and friends for their support throughout my research. Above all to my wife, Amanda, for her love and encouragement.

Glossary

AOD	Acousto-Optic Deflector
AOM	Acousto-Optic Modulator
ASE	Amplified Spontaneous Emission
CRN	Coherent Rayleigh Noise
CW	Continuous Wave
DBR	Distributed Bragg Reflector
DFB	Distributed Feedback
DTS	Distributed Temperature Sensor
ESA	Excited State Absorption
FIMT	Fibre in Metallic Tube
FSAV	Frequency Shift Averaging
LPR	Landau-Placzek Ratio
MZ	Mach-Zehnder
OTDR	Optical Time Domain Reflectometry
RF	Radio Frequency
RTTR	Real Time Thermal Rating
ULR	Ultra-long Range
WDM	Wavelength Division Multiplexer

Chapter One

Introduction

The principal aim of this thesis is to investigate novel Q-switched fibre laser configurations as pulsed sources for a wide range of applications from commercial distributed temperature sensing systems to spectroscopy. The development of Q-switched laser sources and their implementation into optical fibre distributed temperature sensors are explored in detail in this work.

The device specifications which are important in the field of distributed temperature sensing are high spatial and temperature resolutions. The pulsed laser characteristics which fulfil these specifications are short pulse widths to achieve the required spatial resolution and high peak powers to generate a large signal from which the temperature information is extracted. During the course of this work a number of different Q-switched lasers were modelled, constructed and evaluated experimentally. This had two desired objectives, 1) to satisfy the source requirements for both Raman and Brillouin based distributed sensors and 2) to understand the dynamics of Q-switched fibre lasers. Q-switched lasers using different dopants and novel fibre structures were investigated along with a number of different methods of Q-switching.

The applications of Q-switched fibre lasers are many and two of these applications were demonstrated in this work. The principal application is distributed sensing, or any application which relies on an OTDR mode of operation. The second application demonstrated was based on Raman gain. When a pulse of light is transmitted down a fibre, light at the stokes Raman shifted wavelength will experience gain. It is this principle which led to the demonstration of an 8watt, 10ns pulse at 1.64μm. Using the same Raman gain principle the light from a Q-switched laser was used to increase the dynamic range of OTDR at 1.64μm.

The work carried out is based primarily on the author's own research. Any material adopted from other sources is clearly referenced and introduced to make this account more comprehensive.

The thesis is divided as follows:

Chapter 2 explores the concept of optical fibre distributed temperature sensing. This includes a theoretical overview of both the Raman and Brillouin mechanisms and how their physical characteristics can be used to obtain spatially resolved temperature and strain measurements. It also provides a literature review of past work in the field of distributed temperature sensing. The chapter also outlines the specifications required for a suitable pulsed laser source for both Raman and Brillouin sensing.

Chapter 3 provides an overview of Q-switched fibre lasers, starting with the historical background. Different methods of Q-switching fibre lasers, and the use of different dopants and fibre types to increase the performance of Q-switched fibre lasers are discussed.

Chapter 4 provides a quantitative model for the Q-switched fibre laser. This allows parameters such as peak power and pulse width to be modelled with respect to fibre length, mirror reflectivity and cavity losses.

Chapter 5 describes the experimental work carried out with regards to Q-switched fibre laser sources for distributed sensing. A number of designs were experimentally investigated with the aim of increasing understanding of Q-switched laser dynamics and to provide ultimately Q-switched fibre lasers which fulfil the specifications required by both Raman and Brillouin temperature sensors.

Chapter 6 utilises the laser sources developed in this research and applies the source to construct a Brillouin distributed temperature sensor.

Chapter 7 describes the investigation of a novel method for increasing the dynamic range of 1.65μm OTDR systems. This novel method utilises the high peak powers obtained from the

Q-switched Erbium doped fibre lasers to generate and amplify signals in the 1.6μm wavelength region using Raman gain.

Chapter 8 is the final chapter of this work and provides a summary of the results of each chapter and states the overall conclusions of the thesis.

Chapter Two

Optical Fibre Distributed Temperature Sensing

2.1 Introduction

Optical fibre temperature sensors have been the subject of research for a number of years [1][2][3]. Optical fibre distributed temperature sensors (DTS) enable the temperature profile along a length of fibre to be continuously monitored. The sensors operate on the powerful optical time domain reflectometry (OTDR) principle where a pulse of light is transmitted down the fibre and the light which is backscattered within the numerical aperture of the fibre is measured. The time between sending the pulse of light into the fibre and detecting the backscattered light provides a measure of the distance along the fibre. The physical characteristics of the backscattered light can provide valuable information on fibre parameters such as optical attenuation, temperature and strain. The backscattered light is characterised by three scattering mechanisms, Rayleigh, Raman and Brillouin, each of which provide different information regarding the fibre characteristics. In this chapter a detailed investigation of the use of both Raman and Brillouin scattering mechanisms for temperature sensing systems is carried out.

2.2 Distributed Temperature Sensing using Raman Scattering

2.2.1 Theory of Raman Scattering

In a molecular structure there exist molecular vibrational modes. The energy of these vibrational modes can be expressed in terms of phonons, the quanta of the molecular vibrations. It is the interaction between the incident light and these molecular vibrations which gives rise to inelastic scattering processes such as Raman. The molecular vibrations can be categorised into two types, either high frequency 'optical' vibrations which gives rise to Raman scattering or the lower frequency 'acoustic' vibrations which gives rise to Brillouin scattering.

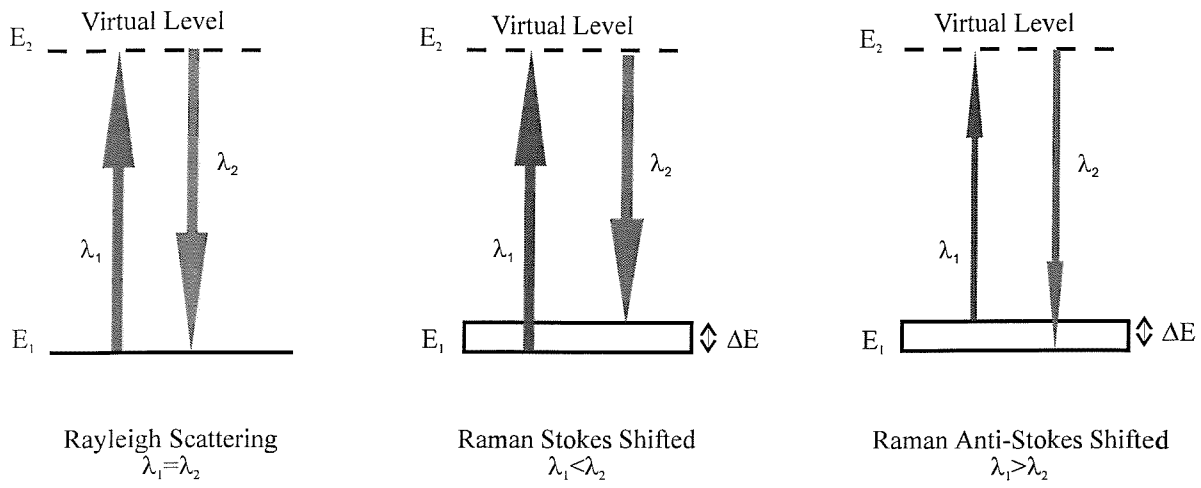

***Figure 2-1** - Rayleigh and Raman Scattering*

Figure 2-1 shows a simple schematic of the molecular vibrational energy levels in a glass and illustrates the inelastic Rayleigh process in which the light is scattered from the molecular lattice without any change in energy. The Raman Stokes and anti-Stokes processes are also shown in which the incident photon undergoes a change in energy, ΔE, either through accepting energy from the molecular vibrations (phonon annihilation) or giving up energy to the molecular vibrations (phonon creation). The energy distribution of the thermally generated molecular vibrations follows Boltzmann statistics, which means that the density of phonons in the higher vibrational energy states is generally less than the lower states, and hence the probability of anti-Stokes scattering is less. This can be seen experimentally in Figure 2-2 where the anti-Stokes band is weaker than the Stokes band. Although the anti-Stokes band is the weaker of the two, it is more sensitive to temperature as the percentage change in signal for a given temperature variation is higher than the Stokes. The temperature dependence of the Raman signal arises from the thermal population of the lattice vibrational energy states or phonons and it is this thermal population which is interrogated by the incident light.

Another important property of Raman scattering is the broadband nature of the Stokes and anti-Stokes bands. The molecules in the glass lattice all experience different local electric fields because of the non-crystalline, amorphous nature of the glass. The molecules therefore all have different vibrational energies. It is this non-crystalline form of the silica glass which gives the Raman scattering its distinctive broadband nature. Raman scattering can extend over a large wavelength range up to $1000cm^{-1}$ from the incident wavelength with

the peak occurring at 440cm^{-1}. Figure 2-2 shows the spontaneous anti-Stokes and Stokes signals as a function of wavenumber [5].

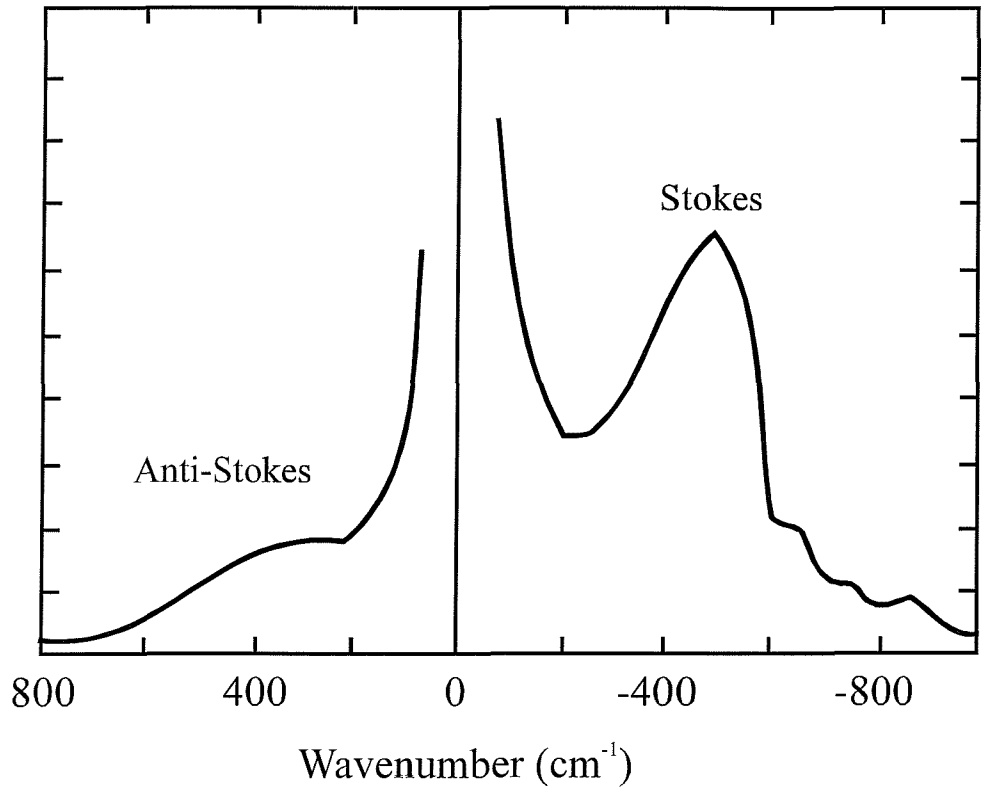

Figure 2-2 *- Plot showing the Stokes and anti-Stokes Raman signals as a function of wave number [5]*

2.2.2 Raman Distributed Temperature Sensing Systems

The first demonstration of optical fibre distributed temperature sensing using Raman backscattered light was shown in 1985 [1]. This initial experiment measured the ratio of the intensity of Stokes and anti-Stokes backscattered signals in order to provide an absolute temperature measurement along the length of the fibre. Importantly this measurement is independent of the pump light intensity, launch conditions, fibre composition and fibre geometry. However due to the large wavelength separation (≈200nm at λ=1530nm) between the Stokes and anti-Stokes signals, a correction has to be made for the difference in fibre attenuation at these wavelengths.

The ratio R(t) of Stokes to anti-Stokes signals is given by the formula:

$$R(t) = (\frac{\lambda_s}{\lambda_a})^4 \cdot \exp(-\frac{hc\nu}{kt}) \qquad (2\text{-}1)$$

where λ_s and λ_a are the measured Stokes and anti-Stokes wavelengths, ν is their wavenumber separation from the pump in metres^{-1}, h is Planck's constant, c is the speed of light, k is Boltzmann's constant and t is the absolute temperature of the fibre core [1].

Although the intensities of both the Stokes and anti-Stokes signals depends on temperature, in many systems (York DTS 80, 800) only the weaker but more temperature sensitive anti-Stokes signal is used. This results in a simplified operation of the device [6]. However, the anti-Stokes signal can only be used to measure absolute temperatures when a reference length of fibre at a constant known temperature is used to calibrate the sensor.

In the next section Raman distributed temperature sensing systems, currently available from York Sensors, are investigated along with the laser source characteristics which are required for their operation.

2.2.2.1 Source Considerations for Raman DTS systems

A schematic showing the principle of operation of a commercial Raman based optical fibre distributed temperature is shown in Figure 2-3.

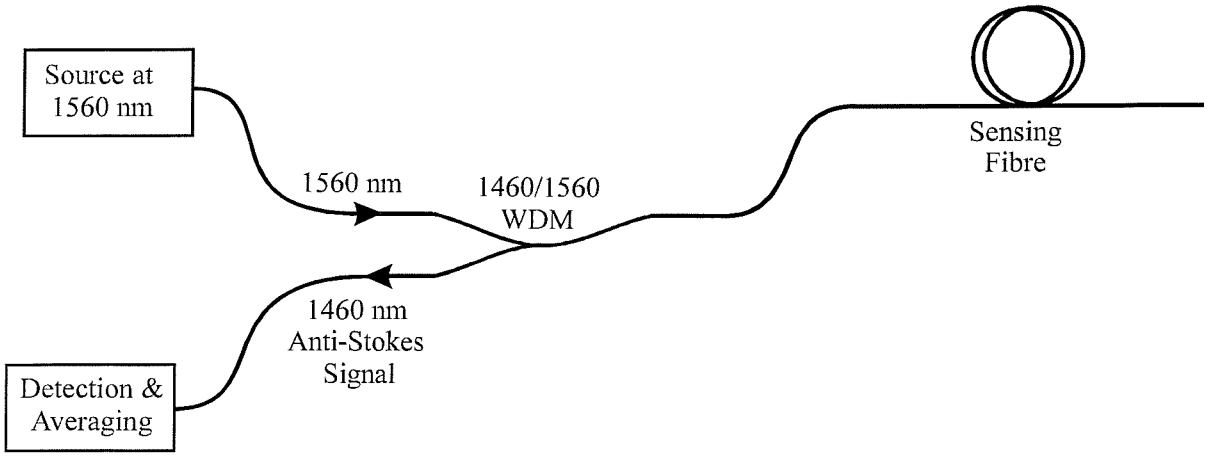

Figure 2-3 *- Schematic of Optical Components in a DTS system*

A laser source launches pulses of light into the sensing fibre using an optical fibre wavelength division multiplexer (WDM). The returning backscattered signal, which is at the anti-Stokes shifted wavelength, then returns through the WDM onto the detector and the associated electronics. The electronics collects the backscattered data from the detector in real-time and then proceeds to average further data to produce the required temperature and spatial resolution. The following section studies the factors to be considered when designing an effective source for Raman DTS.

The choice of operating wavelength for the DTS depends on many factors, not least is the required range of the sensor. At short wavelengths (0.9μm, 1.06μm etc.) the attenuation of single mode fibre is in the region of 1dB/km which is a factor of five times higher than the 0.2dB/km attenuation at 1.55μm. However, the silicon detection technology at the shorter wavelengths benefits from lower noise characteristics than the higher wavelength Germanium detectors. This is caused due to the smaller energy band gap in the Germanium detectors which increases the thermally generated dark current. A typical Silicon photodiode ($1mm^2$) generates a dark current of 20pA compared with a dark current of 600nA from a Germanium photodiode of the same physical dimensions under the same operating conditions (Hamamatsu, S1336-18 Silicon and B1720-02 Germanium photodiodes).

However, the advent of ternary alloys such as Indium Gallium Arsenide (InGaAs) has revolutionised detectors in the near infrared (NIR) regions. A typical $1mm^2$ InGaAs detector (Hamamatsu, G5832-01) has a dark current of 1nA, decreasing to 70pA when cooled to -25°C, which is a significantly better performance than the equivalent Germanium detectors at near infra-red wavelengths. The ternary alloys have lower dark currents because their bandgaps can be tailored to the desired wavelength by adjusting the concentrations of the constituent components.

Sources, such as high power semiconductor lasers (0.9μm) and Neodymium doped Q-switched fibre lasers (1.06μm), which are compatible with the silicon detector technology have been used successfully for short to medium range sensing systems. Semiconductor lasers operating a 0.9μm have been used to produce 3W, 15ns pulses at a 10kHz repetition rate whilst Q-switched Neodymium fibre lasers at 1.06μm have produced 2kW pulses, 1.4ns pulses at a 1kHz repetition rate [7].

The limiting factor for long range sensing systems is the intrinsic attenuation of the signal by the fibre. In order to minimise this effect, a move to the 1.56μm wavelength region reduces the attenuation of the fibre to 0.2dB/km. However there are few sources at this wavelength with the required high power, short pulse characteristics. Semiconductor lasers are readily available at 1.48μm and 1.55μm but provide only low powers, currently limited to 30mW for 1.55μm laser diodes. Because of these low powers the lasers need to be amplified. Recently a long range (>30km) DTS system has been reported using a pulsed 1.55μm semiconductor laser in conjunction with an Erbium doped fibre amplifier. An output power of up to 20Watts was reported [3].

Whatever operating wavelength is selected, the source design for Raman DTS has to fulfil a number of other criteria; i.e. constraints on repetition rate, peak power and pulse width.

The length of the sensing fibre places an unavoidable constraint on the maximum repetition rate of the laser because only one pulse may be launched into the sensing fibre at any one time and a second pulse can only be launched after the backscattered signal from the first pulse has been collected. A 30km length of fibre for example would limit the maximum repetition rate to 3.3kHz. Shorter sensing fibres enable higher repetition rates and therefore faster measurement times to be obtained.

The pulse width of the laser source determines the minimum spatial resolution of the sensor. The shorter the pulse the higher the spatial resolution which can be measured. A 10ns pulse width limits the spatial resolution to 1 metre. An important factor to consider is that the magnitude of the backscattered light is proportional to the energy of the launched pulse. Therefore by decreasing the pulse width to obtain the required spatial resolution, the magnitude of the backscattered signal is reduced, making detection increasingly difficult.

Finally, let us consider the constraints on the peak power of the source. The power of the laser must be below the threshold at which Stimulated Raman scattering occurs. Stimulated Raman scattering can occur at relatively low pump powers because of the long interaction lengths and high power densities which occur within the fibre core. The pump light generates Raman Stokes shifted light as it travels along the fibre. Above a threshold pump power this Raman Stokes shifted light is found to build up exponentially. This can lead to

almost all of the pump power being converted to the Stokes shifted wavelength. The threshold pump power for stimulated Raman scattering is defined as the input pump power required so that the Stokes power becomes equal to the pump power at the fibre output and is given by the formula [8][9]:

$$P_0^{th} = \frac{16 \times A_{eff}}{L_{eff} \times g_R} \qquad (2\text{-}2)$$

where A_{eff} and L_{eff} are the effective area and length respectively and g_R is the Raman gain coefficient (1×10^{-13} m/W).

In order to calculate this threshold, the effective fibre core area, A_{eff}, has to be calculated. This is done by calculating the fibre spot size which is a function of core radius and normalised frequency (V) of the fibre and is given by [11]:

$$w = r \cdot (0.65 + 1.619V^{-\frac{3}{2}} + 2.879V^{-6}) \qquad (2\text{-}3)$$

The normalised frequency V for a typical single mode fibre at 1.55μm with a core radius of 2.5μm and an NA of 0.15 is 1.52. Using these values the spot size is calculated to be 4.4μm. The effective area is then given by the formula:

$$A_{eff} = \pi \cdot w^2 \qquad (2\text{-}4)$$

which gives a value of 60μm^2.

The final parameter to calculate is the effective fibre length. For long pulses this can be calculated using the equation:

$$L_{eff} = \frac{1}{\alpha_p}(1 - \exp(-\alpha_p L)) \qquad (2\text{-}5)$$

where α_p is the pump absorption coefficient of the fibre, which at 1.55μm is $5x10^{-5}$ m^{-1}. The effective length for a 10km length of fibre is 7.87km, using these values and a pulse width greater than 30ns, the threshold power for stimulated Raman scattering is 1.26Watts

When the pulse width becomes short (less than 20-30ns) then a second factor becomes dominant when calculating the effective length. This factor is due to the significant wavelength difference between the pump and the signal (100nm). The difference in group velocities at the two wavelengths leads to pulse walk-off where the pump and signal pulses move apart as they travel down the fibre [10]. The walk-off distance is given by:

$$L_w = \frac{W}{D \cdot \Delta\lambda} \qquad (2\text{-}6)$$

where W, is the pulse width, D is the fibre dispersion parameter (17ps nm^{-1} km^{-1}) and $\Delta\lambda$ is the wavelength separation between the pump and signal, 100nm. For a 10ns pulse, L_w is 5km. Figure 2-4 shows how L_w and L_{eff} vary with pulse width.

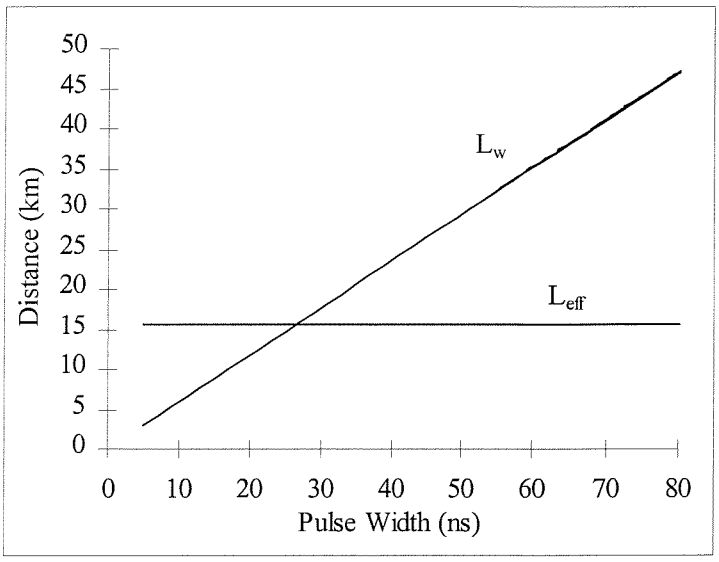

Figure 2-4 *- A plot of walk-off length (L_w) and effective length (L_{eff}) against pulse width for a 30km length of sensing fibre. At pulse widths less than 28ns the walk-off length becomes the dominant factor.*

For a 30km length of fibre, with a pulse width of 100ns, the effective length would be 15.5km, and coupled with the effective area and the gain coefficient the threshold pump

power for stimulated Raman would be 620mW. This increases to 1.63Watts with a pulse width of 10ns due to pulse walk-off effects.

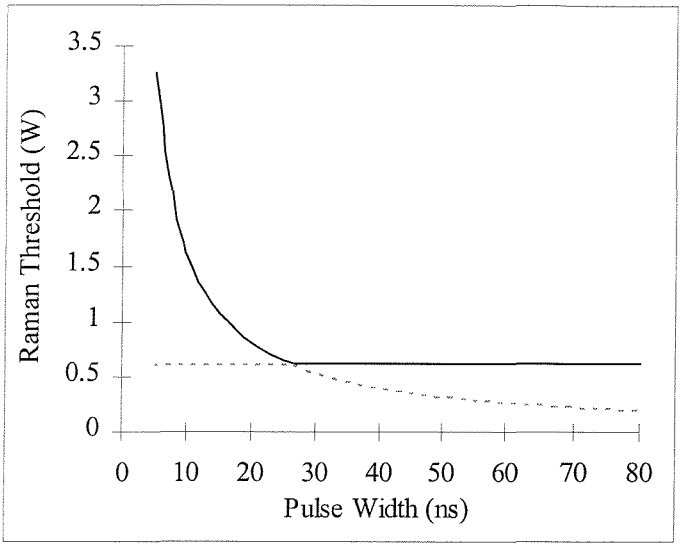

Figure 2-5 *- Plot of Raman threshold against Pulse Width (ns) for a 30km sensing fibre*

Figure 2-5 shows the variation of Raman threshold with pulse width, illustrating the increase of the Raman threshold with short pulses.

The maximum peak power which can be launched into the sensing fibre is limited by this Raman threshold. However as the backscattered Raman signal is proportional to the launched pump power, the launched power should be made as high as possible within this threshold, in order to maximise the backscattered signal.

The next section leaves Raman scattering for temperature sensing and investigates the alternative Brillouin scattering mechanism, which can be used to measure both temperature and strain along the sensing fibre.

2.3 Distributed Temperature Sensing using Brillouin Scattering

The Brillouin temperature sensor operates on the same OTDR principle as the Raman based system, i.e. a pulse of light is transmitted down the fibre and the backscattered Brillouin signal is interrogated. As we shall see, one advantage of Brillouin scattering over Raman, is that the backscattered signal contains information on both temperature and strain along the length of the fibre. It is therefore possible to construct a simultaneous distributed temperature and strain sensor. This thesis focuses on suitable sources for this type of sensor. In the following sections the theory of Brillouin scattering will be considered along with the differences between this and the previously examined Raman scattering.

2.3.1 Theory of Brillouin Scattering

The fundamental difference between Raman and Brillouin scattering stems from the fact that 'acoustic' phonons participate in Brillouin scattering whereas 'optical' phonons participate in Raman scattering. Spontaneous Brillouin scattering results from the interaction between the pump light beam and thermally generated acoustic waves within the fibre (acoustic phonons). The thermally generated acoustic waves occur over a wide range of frequencies determined by discrete phonon energies, but it is only frequencies satisfying the Bragg condition which gives rise to Brillouin scattering (Figure 2-6).

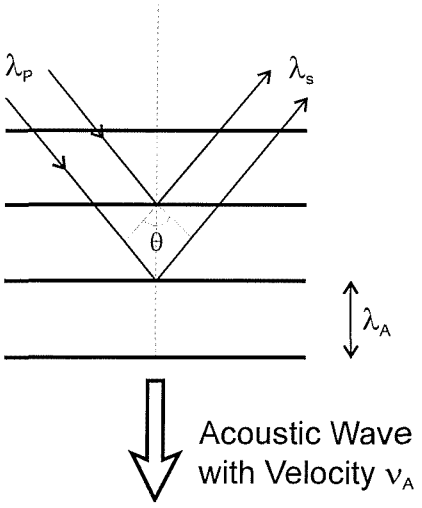

Figure 2-6 *- Illustration of Bragg scattering from a moving acoustic wave of wavelength* λ_A

The Bragg condition for scattering is given by:

$$2n\lambda_A \sin\frac{\theta}{2} = \lambda_P \qquad (2\text{-}7)$$

where n is the refractive index, λ_A and λ_P and the acoustic and pump light wavelengths respectively and θ, is the angle between the incident and scattered light.
By substituting

$$\lambda_A = \frac{v_A}{\upsilon_A} \qquad (2\text{-}8)$$

where v_A is the acoustic velocity, we obtain an expression for the acoustic frequencies, υ_A, which satisfies the Bragg condition:

$$\upsilon_A = \frac{2n}{\lambda_p} \cdot v_A \cdot \sin\frac{\theta}{2} \qquad (2\text{-}9)$$

This expression gives a quantitative value for the frequency shift experienced by the light which is scattered from the acoustic waves (phonons). It is dependent on the velocity of the acoustic waves (acoustic velocity in silica [12] = 5960m/s), the angle between the incident and scattered light wavefronts and the wavelength of the pump light. The expression gives a maximum frequency shift when the light is scattered in a backward direction and zero in the forward direction. The two maximum positions correspond to the Stokes and anti-Stokes shifted signals where the pump light travels co- and counter-propagating to the acoustic wave and is Doppler shifted down and up by a frequency, υ_A given by equation 2-9. If we consider only these maximum positions where $\theta=\pi$, then equation 2-9 reduces to:

$$\upsilon_A = \frac{2n \cdot v_A}{\lambda_P} \qquad (2\text{-}10)$$

where, n, is the refractive index (1.46), v_A, is the acoustic velocity in silica (5960m/s), and λ_P is the wavelength of the pump light. This expression gives a value for the maximum

frequency shift experienced by the pump light due to scattering by the acoustic waves. At a wavelength of 1.53μm the frequency shift for Brillouin scattering is calculated to be 11.3GHz whilst for Raman scattering it is approximately 12.5THz i.e. three orders of magnitude larger.

It has been shown that this spontaneous Brillouin frequency shift increases linearly with both strain [13] and temperature [14]. The strain and temperature dependence of the Brillouin frequency shift may be represented by the following equations:

$$\upsilon_A(\varepsilon) = \upsilon_A(0) + C_S \cdot \varepsilon \qquad (2\text{-}11)$$

$$\upsilon_A(T) = \upsilon_A(T_R) + C_T \cdot (T - T_R) \qquad (2\text{-}12)$$

where ε is the strain on the fibre, T is the temperature and T_R is a reference temperature. The constants of strain and temperature are found to be C_S = 0.048MHz/με and C_T = 1.1MHz/K [15].

These equations show that measurements on the Brillouin frequency shift are dependent on both strain and temperature. As it is not possible to determine which of the two measurands (temperature or strain) is causing the frequency shift it would be necessary to introduce a second fibre which is isolated from either temperature or strain in order to determine simultaneously the measurands.

Another method to resolve either temperature or strain is to measure the Brillouin intensity along with the frequency shift. This provides two sets of coupled equations with can be solved to provide information on both the strain and temperature profile along a single optical fibre.

The intensity of the Brillouin signal is proportional to both temperature and strain, with a temperature sensitivity of 0.3% K^{-1} [16] and a strain sensitivity of 9.03×10^{-4}% $\mu\varepsilon^{-1}$ [17].

The intensity of the Brillouin signal is given by the equation [18]:

$$I_B = \frac{I_R \cdot T}{T_f\left(\rho \cdot \upsilon_a^2 \cdot B_T - 1\right)} \qquad (2\text{-}13)$$

where I_B and I_R are the Brillouin and Rayleigh intensities, respectively, B_T is the isothermal compressibility, T_f is the fictive temperature, υ_a is the acoustic velocity, ρ is the density and T is the ambient temperature. Both the density and the acoustic velocity are temperature dependent, however the density dependence is very small and is usually neglected. It is the temperature and strain dependence of the Young's modulus and Poisson ratio that manifests itself as a change in the acoustic velocity [19] that generates the change in Brillouin intensity.

This thesis concentrates on the measurement of the Brillouin intensity as a function of temperature. Without an effective method of generating the Brillouin signal and measuring its intensity, a distributed strain and temperature sensing device cannot be realised.

The small frequency separation between the Rayleigh and Brillouin signals leads to a rigid criterion on the linewidth of the pump source if the Brillouin intensity is to be measured. A pump source with a linewidth greater than the maximum Brillouin frequency shift would generate Rayleigh backscattered light which would obscure the Brillouin signal, making detection impossible. This is illustrated in Figure 2-7.

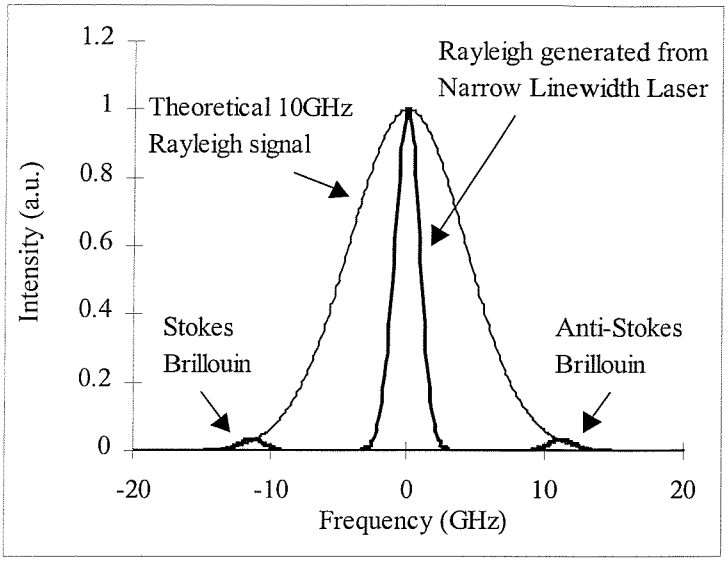

***Figure 2-7** - Plot showing the Rayleigh and Brillouin spectra obtained with a narrow linewidth 2GHz source overlaid with a theoretical Rayleigh signal with a 10GHz linewidth width*

A theoretical value of the Rayleigh spectrum with a width of 10GHz is overlaid onto an experimental plot. The experimental plot shows a central Rayleigh peak and the Stokes and anti-Stokes Brillouin signals either side. The intensity of the spontaneous Stokes and anti-Stokes Brillouin signals is 30 times smaller than that of the Rayleigh signal. The width of the Brillouin scattered signals equals that of the pump (in this case 2GHz) broadened by plus and minus the natural Brillouin linewidth which is of the order of approximately 50MHz.

2.3.2 Brillouin Distributed Temperature Sensing Systems

Many techniques are available to extract the temperature information from the Brillouin signal. These range from direct detection of the Brillouin signal, heterodyne methods and interrogation of the Brillouin loss or gain characteristics.

The heterodyne technique [20][21] involves mixing the backscattered signal with a local oscillator to resolve the Brillouin frequency shift. The first Brillouin heterodyne system was reported in 1992 [20]. Two single frequency Nd:YAG lasers were used as the pulsed light

source and the local oscillator. The frequency difference between the two lasers was tuned around the Brillouin shift, to mix the light down to a frequency so that a low bandwidth coherent receiver could be used for detection. A range of 11km was measured with a spatial resolution of 100m and a strain and temperature accuracy of 50με and 3K. Temperature and strain however were not resolvable from each other.

The Brillouin loss or gain technique [22] utilises the Brillouin interaction between pulsed and CW optical beams counter-propagating in an optical fibre. When the optical frequency of the counter-propagating CW beam is greater than that of the pulsed beam by a frequency equal to the Brillouin shift then the CW beam experiences a loss and the pulsed beam is amplified. Using this technique the Brillouin frequency shift can be resolved. Because of the counter-propagating nature of this technique, access is required to both ends of the sensing fibre. This renders the technique unsuitable for pre-installed fibre cable or cables where access can only be gained from one end. Another concern arising from the counter-propagating technique is that in the event of the sensing fibre being damaged the sensing system would stop operating.
The direct detection technique [16] determines the temperature profile along a length of optical fibre by measuring the intensity of the Brillouin backscattered light which is captured within the numerical aperture of the fibre. It is this technique which this thesis expands upon.

Before using the changes in Brillouin intensity to measure temperature, it is important to determine whether the intensity, like the frequency shift, is dependent on the strain applied to the fibre. Recent experiments have concluded that the intensity of the Brillouin signal is dependent on the strain applied to the fibre [17][15]. It was shown that a strain of 333με causes the same change in intensity as a temperature change of 1°C. Through private communication with optical fibre cable companies and in previously published work on strain measurements in optical fibre cable [23], it is reasonable to assume that under normal operating conditions fibre cable can be laid within a strain tolerance of less than 600με. This residual strain applied to the fibre during the installation process causes a Brillouin intensity change approximately equivalent to a 2°C temperature change. This would give a 2°C error on the temperature measurement due to fibre strain.

However the work on the Brillouin temperature sensor is the initial stage of a combined distributed temperature and strain sensor. With both the frequency shift and the intensity change being monitored, values for both the temperature and strain profile can be assessed independently. The ratio of the Rayleigh backscattered signal to the Brillouin signal is calculated in order to determine whether the changes in intensity are due to local attenuation of the fibre (splice losses, micro-bending) or the required temperature variation. This is known as the Landau-Placzek ratio and is useful because of the insensitivity of the Rayleigh backscattered light to changes in temperature [16].

What then are the possible advantages of using Brillouin scattering to measure temperature?

- One major factor is that the Brillouin gain, $g_B=5x10^{-11}m/W$, is larger than the peak Raman gain, $g_r=1x10^{-13}m/W$ resulting in a larger backscattered signal for a given launched power. This helps to overcome the fact that the sensitivity of the Brillouin to temperature is lower at 0.3%/K than the anti-stokes Raman at 0.8%/K.
- Due to the narrow wavelength separation between the Rayleigh and Brillouin, the pump wavelength can be chosen so that both the pump and Brillouin signals lie in the low loss wavelength region of silica fibre (1.53μm). Whereas in the case of Raman scattering, the pump and Raman signals are separated by 100nm, giving the anti-Stokes and Stokes wavelengths a higher attenuation.
- Another consequence of the narrow wavelength separation between the Brillouin signal and its pump is that the wavelength can be chosen to lie within the Erbium gain spectrum. This would allow for the possible optical amplification of the weak backscattered Brillouin signal.
- Brillouin signals can be used to monitor both temperature and strain.

There are however a number of disadvantages in shifting from a Raman based temperature sensor to a Brillouin based system:

- In order to resolve the Brillouin signal from the Rayleigh, the Brillouin based system requires a high power, short pulse and narrow linewidth source. In a Raman based system, the linewidth is less of an issue, making it is easier to develop sources for use in

this type of sensor. It is one of the aims of this research to develop a narrow linewidth source for Brillouin based temperature sensing.

- A narrow bandwidth optical filter (Mach-Zehnder or Fabry-Perot interferometer etc.) is also required to separate the Brillouin signal from the Rayleigh, whereas a cheaper, bulk dichroic filter can be used in a Raman based sensor.

2.3.2.1 Source considerations for Brillouin DTS systems

As we have seen the Brillouin signal is close to the Rayleigh signal in wavelength, a system therefore needs to be devised which allows the Rayleigh and Brillouin signals to be spectrally resolved. In order to do this the source and detection sections of the system must be considered along with cost and commercial viability.

The source is a major component of the DTS system and needs to be reliable, cheap to manufacture and able to generate a Brillouin signal with sufficient magnitude to produce a long range sensor. The source must have a linewidth of less than the Brillouin frequency shift so that the generated Rayleigh does not obscure the Brillouin signal. Similarly, like the Raman DTS, the source must fulfil criteria regarding the pulse width which determines the system spatial resolution. It must also provide an ideal peak power of just below the threshold at which stimulated Brillouin or Raman scattering occurs.

The threshold for stimulated Brillouin scattering places a constraint on the maximum power which can be launched into the optical fibre. The expression for the Brillouin threshold is given by [8][9]:

$$P_0^{th} = \frac{21 \cdot A_{eff}}{L_{eff} \cdot g_B} \qquad (2\text{-}14)$$

where A_{eff} and L_{eff} are the effective area and length and g_B is the Brillouin gain ($5\text{x}10^{-11}$ m/W). The effective area A_{eff} is calculated in equation (2-4) as $60\mu m^2$. The effective interaction length is given as half the pulse width i.e. for a 100ns pulse L_{eff}=10metres. This is because of the counter-propagating nature of the pump and the backward stimulated Brillouin. Therefore if we decrease the pulse width the Brillouin threshold will increase

proportionally and the upper limit on the launched power will be dictated by the stimulated Raman threshold. If we plot the Brillouin threshold given by equation (8-6) and the Raman threshold given by (3-2) we can see that for pulse widths less than 400ns stimulated Raman dominates whereas pulse widths above this stimulated Brillouin dominates.

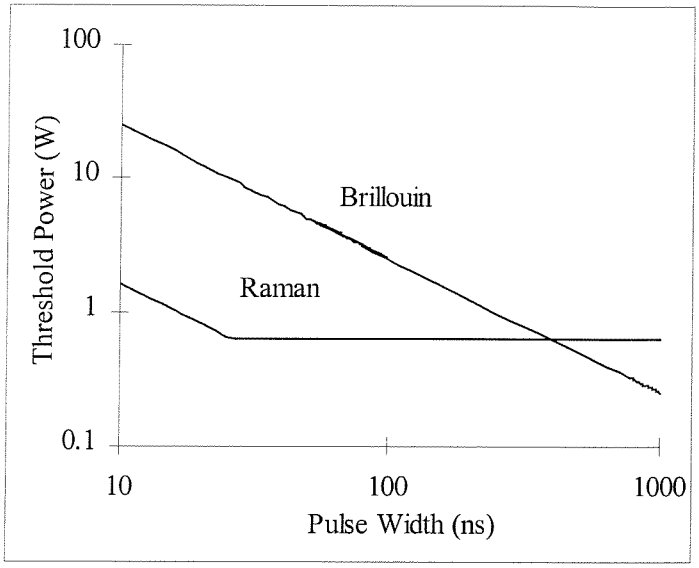

Figure 2-8 *- Figure showing the threshold values for both Brillouin and Raman for various pulse widths*

For sensing applications where spatial resolutions of less than 40metres are required then stimulated Raman is the main limitation on the maximum peak power, which for a 30km sensing fibre and a 100ns pulse width is approximately 600mW.

When using the narrow linewidth source to measure the Rayleigh it was found that the signal contained coherent Rayleigh noise (CRN) It is necessary to reduce this in order to achieve the required temperature resolution. This problem is dealt with by the technique of frequency shift averaging (FSAV), which involves taking the results at discrete wavelengths over a range and then averaging the results [24].

2.4 Applications of Distributed Temperature Sensing Systems

Current leading edge DTS systems (York DTS 800) can monitor the temperature profile along a length of fibre in excess of 30km with a temperature resolution of 2°C and spatial resolution of 8m.

The main commercial markets for DTS systems are in the areas of power utilities, process industries and fire detection. Each of these applications has different requirements on spatial resolution, response speed, range etc. For example, power utilities require long range DTS systems to monitor hot spots in power transmission lines.

Power transformers are often operated at well below maximum efficiency to avoid heating effects. By continuously monitoring the temperature profile of these power cables, they can be operated at much higher power levels, maximising power transport in times of peak demand. The freedom of optical fibre sensors from electromagnetic interference (EMI) makes them ideal for this application. Furthermore modern power transmission lines have optical fibre built into the cable which makes integrating the DTS simple. Long range sensors are however essential if large power networks are to be monitored. Figure 2-9 shows a typical plot of the temperature distribution along a subterranean power cable [25]. As we can see the variation in temperature along the cable is 16°C, quite a substantial range. This data was taken without any power in the cable and shows only the ambient temperature variation along a length of cable. The heated sections may well run alongside underground heating ducts and the cooler sections through damp areas of earth.

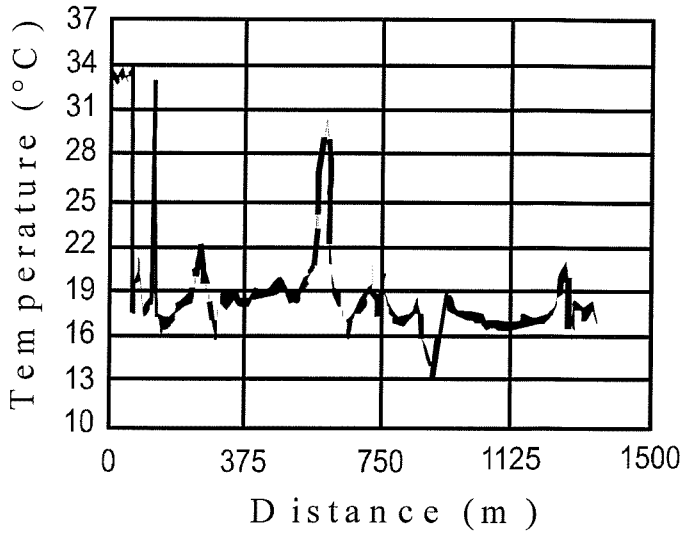

Figure 2-9 *- Data from Raman Distributed Temperature Sensor for an subterranean power cable [25]*

Another application requiring high spatial resolution rather than long range, involves monitoring chemical processes occurring in brick-lined reactors, ovens, dryers, pressure vessels etc. A high resolution and response time will allow leaks and failures in such containers to be pinpointed with an accuracy of less than a metre and because of the distributed nature of the sensor, positioning of discrete sensors at possible fault locations is not necessary.

2.5 Conclusions

In this chapter the theory of both Raman and Brillouin scattering mechanisms have been described and related to distributed sensing applications. The source requirements, peak power, pulse width, linewidth and repetition rate, for both the Raman and Brillouin optical fibre distributed sensors were examined. The constraint on source peak power for short pulse widths, of less than 400ns, was found to be the onset of stimulated Raman, whereas for pulses widths greater than this, the onset of stimulated Brillouin. With this information, we have ascertained the requirements for novel laser sources which will improve the current technology in the fields of both Raman and Brillouin based distributed sensors. It is the aim of this thesis to investigate and develop these laser sources.

2.6 References

[1] J.P.Dakin and D.J.Pratt: 'Distributed Optical Fibre Raman Temperature Sensor Using a Semiconductor light source and detector', *Electronics Letters*, Vol. 21, No. 13, pp.569-570, (1985)

[2] A.H.Hartog, A.P.Leach and M.P.Gold: 'Distributed Temperature Sensing in Solid Core Fibres', *Electronics Letters*, Vol. 21, No. 23, pp.1061-1062, (1985)

[3] T.Wakami and S. Tanaka: '1.55μm Long Span Fibre Optic Distributed Temperature Sensor', *International Conference on Optical Fibre Sensors OFS 94*, pp.134-137, Glasgow, UK, (1994)

[4] C.Kittel: 'Introduction to Solid State Physics: Sixth Edition', *John Wiley Publishing*, ISBN 0-471-87474-4, (1986)

[5] J.P.Dakin: 'Review Article: Multiplexed and Distributed Optical Fibre Sensor Systems', *J. Phys E: Sci. Instrum.*, Vol. 20, pp.954-967, (1987)

[6] York Sensors Limited, York House, Abbey Park Industrial Estate, Romsey, Hampshire, SO51 3AQ, UK

[7] I.Abdulhalim, C.N.Pannell, K.P.Jedrzejewski and E.R.Taylor: 'Acousto-optically Q-switched fibre laser under first order operation emitting pulses with 2kW peak power and 1.4ns duration', *9th International Conference on Optical Fibre Sensors OFS 93*, pp.229-232, Firenze, Italy (1993)

[8] G.P.Agrawal: 'Non Linear Fibre Optics: Second Edition', *Academic Press*, ISBN 0-120-45142-5, (1995)

[9] R.G.Smith: 'Optical Power Handling Capacity of Low Loss Optical Fibres as Determined by Stimulated Raman and Brillouin Scattering', *Applied Optics*, Vol.11, No.11, pp.2489-2494, (1972)

[10] R.H.Stolen and A.M.Johnson: 'The Effect of Pulse Walkoff on Stimulated Raman Scattering in Fibres', *IEEE Journal of Quantum Electronics*, Vol.QE-22, No.11, pp.2154-2160, (1986)

[11] D.Marcuse: 'Theory of Dielectric Optical Waveguides: Second Edition', *Academic Press*, ISBN 0-124-70951-6 , (1991)

[12] N.P.Bansal and R.H.Doremus: 'Handbook of Glass Properties', *Academic Press*, (1986)

[13] T.Horiguchi, T.Kurashima and M.Teteda: 'Tensile Strain Dependence of Brillouin Frequency shift in silica optical fibres', *IEEE Photonics Technology Letters*, Vol. 1, No. 5, pp.107-108, (1989)

[14] T.Kurashima, T.Horiguchi and M.Teteda: 'Thermal effects on Brillouin frequency shift in jacketed optical silica fibres', *Applied Optics*, Vol. 29, No. 15, pp.2219-2222, (1990)

[15] T.R.Parker, M.Farhadiroushan, V.A.Handerek and A.J.Rogers: 'A Fully Distributed Simultaneous Strain and Temperature Sensor using Spontaneous Brillouin Backscatter', *IEEE Photonics Technology Letters*, Vol.9, No.7, pp.979-981, (1997)

[16] P.C.Wait and T.P.Newson: 'Landau-Placzek Ratio applied to Distributed Fibre Sensing', *Optics Communications*, Vol. 122, pp.141-146, (1996)

[17] K.De Souza, P.C.Wait and T.P.Newson: 'Characterisation of Strain Dependence of the Landau-Placzek ratio for distributed sensing', *Electronics Letters*, Vol. 33, No. 7, pp.615-616, (1997)

[18] J.Schroeder, R.Mohr, P.B.Macedo and C.J.Montrose: 'Rayleigh and Brillouin scattering in K_2O-SiO_2 glasses', *Journal of American Ceramic Society*, Vol.56, No.10, pp.131, (1973)

[19] S.Timoshenko: 'Theory of Elasticity', *Macgraw Hill*, Chapter 12, (1934)

[20] T.Kurashima, T.Horiguchi, H.Izumita, S.Furukawa and Y.Koyamada: 'Brillouin Optical-fiber time domain reflectometry', *Tech. Dig. International Quantum Electronics Conference*, pp.42-44, Vienna, Austria, (1992)

[21] K.Shimizu, T.Horiguchi, Y.Koyamada and T.Kurashima: 'Coherent Self-Heterodyne Brillouin OTDR for Measurement of Brillouin Frequency Shift Distribution in Optical Fibers', *Journal of Lightwave Technology*, Vol. 12, No. 5, pp.730-736, (1994)

[22] X.Bao, D.J.Webb and D.A.Jackson: '22km Distributed Strain Sensor using Brillouin loss in an Optical Fibre', *Optics Communications*, Vol. 104, pp.298-302, (1994)

[23] M.Tateda, T.Horiguchi, T.Kurashima, and K. Ishihara: 'First Measurement of Strain Distribution Along Field-Installed Optical Fibers Using Brillouin Spectroscopy', *Journal of Lightwave Technology*, Vol. 8, No. 9, pp.1269-1272, (1990)

[24] K.Shimizu, T.Horiguchi and Y.Koyamada: 'Characterisatics and Reduction of Coherent Fading Noise in Rayleigh Backscattering Measurements for Optical Fibers and Components', *Journal of Lightwave Technology*, Vol. 10, No. 7, pp.982-987, (1992)

[25] A.Hartog: 'Distributed Fibre-Optic Temperature Sensor', *Sensor and Transducer Conference*, pp.1-9, Esher, Surrey, UK, (1994)

Chapter Three

Q-Switched Fibre Lasers

3.1 Historical Background to fibre lasers

The first demonstration of laser action was observed in ruby (Cr^{3+}/Al_2O_3) in the early parts of 1960 [1]. This was rapidly followed by a paper entitled "Proposed Fibre Cavities for Optical Masers" by Snitzer which outlined the advantages of incorporating a laser gain medium into a dielectric waveguide [2]. This insight to the use of waveguides for laser resonators led to the rapid development of multimode, side pumped, Neodymium doped fibre lasers in 1961 [3] and Erbium/Ytterbium doped fibre lasers operating at 1.54μm in 1965 [4]. The side pumping of these lasers was however inefficient and only low power pulsed operation could be achieved. Increased pump efficiency was achieved by the first longitudinal pumped fibre laser structure, which was developed by Stone & Burrus in 1973 [5]. This led the way to present day, laser diode pumped fibre devices.

Advances in fibre fabrication techniques (leading to efficient rare earth doping of single mode fibre) and the development of high power pump lasers, have renewed the interest in fibre laser technology.

The advent of the Erbium doped fibre amplifier in 1987 revolutionised the telecommunications industry making obsolete the conventional electro-optic repeaters previously needed for long distance telecommunications [6]. In just two years after the first laboratory demonstration of Erbium doped amplifiers they were already being used in submarine transmission cables [7]. Modern Erbium doped fibre amplifiers deliver small signal gains in excess of 40dB for only modest pump powers. Many active fibre devices, such as broadband, tuneable, high power Q-switched and CW [8][9] sources have resulted from the development of the Erbium doped fibre amplifier and high power pump sources.

Recent developments include the high output power Er^{3+}/Yb^{3+} cladding pumped fibre lasers [10], single longitudinal mode fibre lasers [11] and Q-switched Erbium [13] and Neodymium [12] doped fibre lasers. The long lifetimes of the upper lasing levels of both the Neodymium and Erbium ions make them ideal for Q-switched operation in which energy is stored in the upper lasing level and then released as an intense pulse of light. These high power fibre pulsed sources can be used in a variety of applications including optical time domain reflectometry (OTDR) and specialised optical fibre distributed temperature sensors.

3.2 Q-switched Fibre Lasers

We now consider a number of systems involving various dopants and fibre geometries, which are suitable for the development of Q-switched fibre lasers and operate at a wavelength of 1.5μm, which is an important criterion for long range sensing applications. In particular we look at co-doping the Erbium with Ytterbium and also the affect of increasing the fibre core area.

3.2.1 Introduction to the Erbium-Silica system

Optical fibres doped with Erbium were developed for use as both optical amplifiers and lasers and are of great importance because of their operation at the third telecommunications window. Erbium fibre devices have the following advantages: broad gain bandwidth, high gain, high saturation output power, polarisation independent gain, no cross-talk, low noise figure and low insertion loss. There are many pump bands for the Erbium/Silica system. Figure 3-1 shows a simplified energy level diagram of Erbium ions in a silica glass host. The pump bands at 514, 650, 807, 980 and 1480nm all offer highly efficient pumping potentials. The lack of excited state absorption (ESA) from both the 980 and 1480nm pump bands [*14*] and the availability of high power semiconductor laser diodes at these wavelengths, make them particularly attractive. Gain efficiencies of 7.8dB/mW [15] and 2.1dB/mW [*16*] have been achieved using the 980 and 1480nm bands respectively. The higher pump efficiency gained from the 980nm band coupled with the availability of higher

power laser diodes available at this wavelength lead us to choose this over the 1480nm band.

This 980nm pumping from the ground state to the $^4I_{11/2}$ is followed by a non-radiative multi-phonon relaxation from the pump band into the $^4I_{13/2}$ metastable band. The time constant for this transition has been measured to be approximately 6μs [18]. This is fast compared to the 10ms lifetime of the radiative $^4I_{13/2}$ - $^4I_{15/2}$ lasing transition. The long lifetime of the lasing transition, in conjunction with the high pump intensities that can be achieved in the fibre core, enables a substantial population inversion to be attained.

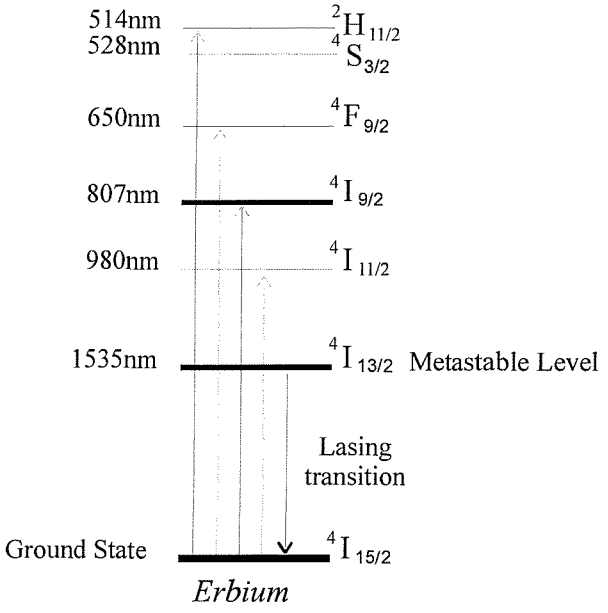

***Figure 3-1** - Simplified Energy Level Diagram for Erbium ions in Silica Glass*

Figure 3-1 does not show the Stark splitting of the Erbium energy levels which occurs due to the effect of the local electric field of the glass on the Erbium ions. This Stark splitting of the $^4I_{13/2}$ and the $^4I_{15/2}$ levels is responsible for the broad emission and absorption cross-sections of the Erbium metastable transition that gives us the advantage of a broad gain bandwidth (approximately 80nm).

3.2.2 Introduction to Erbium/Ytterbium co-doped systems

Optical fibres doped with Erbium are suitable for optical amplifiers and lasers operating in the low loss region of standard silica optical fibre. For practical purposes, (i.e. compact, low power consumption etc), the Erbium doped fibre must be laser diode pumped. However, since the operating wavelength of pump laser diodes varies with temperature and the $^4I_{11/2}$ - $^4I_{15/2}$ absorption of Erbium is spectrally narrow (~16nm [17]), fluctuations in the temperature of the pump laser diode will lead to a change in performance of the fibre amplifier or laser device. With the shift towards cooler-less 980nm pump laser diodes, which reduce power consumption for long haul telecommunications systems, the effects of temperature dependent performance become increasingly important due to the absence of any temperature control mechanism. One solution to this problem is to sensitise the Erbium doped fibre with Ytterbium [19]. Figure 3-2 shows the energy level diagram of the combined Erbium/Ytterbium system.

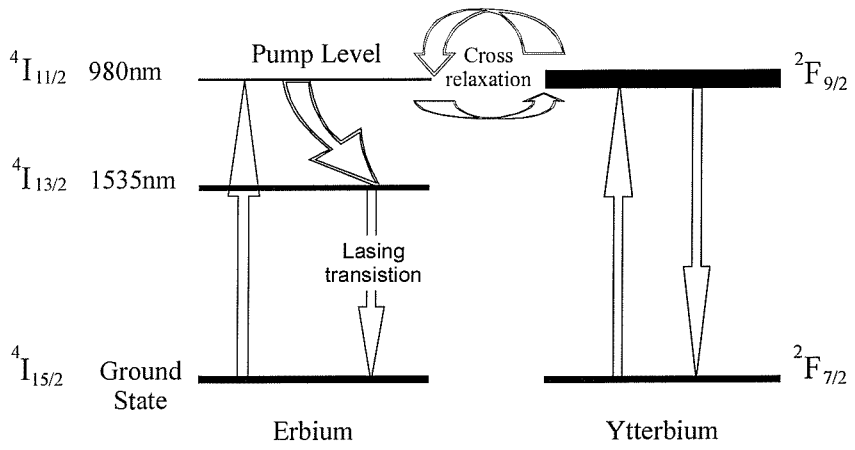

***Figure 3-2** - Schematic of Er^{3+}/Yb^{3+} Energy level scheme*

The sensitising of Erbium with Ytterbium offers an alternative route to pumping the Erbium metastable level ($^4I_{13/2}$). The Ytterbium absorbs the pump light and then, by a process of cross-relaxation between adjacent Erbium and Ytterbium ions, allows the energy to be transferred. Figure 3-3 shows the spectral attenuation for both the Erbium and Erbium/Ytterbium systems. The attenuation for the Erbium shows two narrow bands at both

the 807nm and 980nm wavelengths; corresponding to the $^4I_{15/2} \rightarrow {}^4I_{11/2}$ and $^4I_{15/2} \rightarrow {}^4I_{9/2}$ pump transitions respectively.

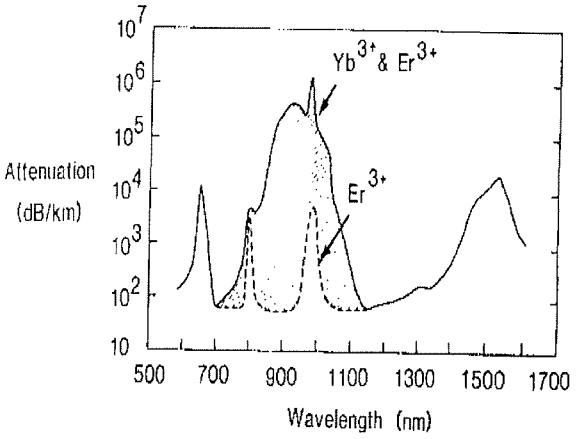

Figure 3-3 *- Spectral attenuation of Er and Er/Yb ions in silica*

The attenuation of the Erbium/Ytterbium co-doped system covers the wide wavelength range 800-1070nm; this is caused by the Stark splitting of the $^4F_{5/2}$ Ytterbium level. The broadband characteristics of the Erbium/Ytterbium co-doped system enables pumping over a wide range of wavelengths, thus relieving the constraint on the temperature (hence wavelength) stability of the pump laser diodes. The broadband nature is also advantageous because it allows pumping in the 810nm wavelength region where pump laser diodes are cheaper than the alternative 980nm diodes. However pumping at the 980nm wavelength still has the advantage that it is free from exited state absorption (ESA).

The addition of the Ytterbium ion also has the added advantage of increasing the pump absorption. This is potentially beneficial for short laser devices that require either single frequency operation [21] or short round-trip times. The increased pump absorption is also utilised in double clad fibre structures [20]. These consist of a single mode Er^{3+}/Yb^{3+} core surrounded by a second cladding which provides a multimode waveguide for pumping the core. The doped core can hence be efficiently pumped by multi-stripe high power diode arrays. Typically the ratio of the Ytterbium to Erbium ions is in the region of 20:1.

However, the lifetime of the Erbium $^4I_{11/2}$ level places a constraint on the Ytterbium transfer of energy. At 4-6μs [18] this is sufficiently fast to allow back-transfer of energy from the Erbium ions to the Ytterbium.

3.2.3 Large Mode Area Fibre

In this section we consider a novel fibre geometry which improves the energy storage in the fibre. There exist two methods of increasing the energy stored within a fibre, either by increasing the Erbium concentration or increasing the core area.

Increasing the Erbium concentration eventually leads to clustering of the Erbium ions, this decreases the pump efficiency by the process of co-operative up conversion between adjacent Erbium ions [22]. This process is illustrated in Figure 3-4 whereby an excited ion transfers its energy to a nearby excited ion resulting in one ion being excited to the $^4I_{9/2}$ state whilst the other returns to the ground state. The ion in the $^4I_{9/2}$ state will then relax back to the metastable level by a non-radiative decay. This process causes a loss in pump efficiency as it has taken two pump photons to excite only one Erbium ion.

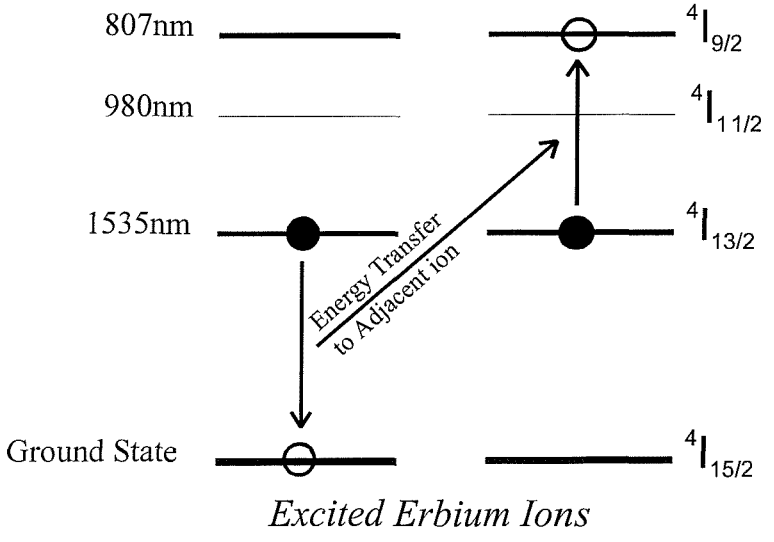

***Figure 3-4** - Schematic showing the process of co-operative Upconversion*

The other method of increasing the stored energy in Erbium doped fibre is by increasing its core area. A recent numerical model has proposed that in order to achieve maximum energy extraction a large mode field area is necessary [23]. Recently this principle was demonstrated experimentally by using a large mode area fibre in a multi-stage power amplifier to obtain pulse energies in excess of 150μJ [24].

The large mode area fibre is constructed by increasing the area of the fibre core. One limitation on increasing the core area is that the fibre must remain single mode at the signal wavelength. In order to increase the core area and satisfy this constraint, the numerical aperture (NA.) of the fibre must be decreased accordingly. This can be illustrated by Equation (3-1) which gives an expression for the normalised frequency (V) in terms of core radius, numerical aperture and wavelength.

$$V = \frac{2\pi}{\lambda} r \cdot NA. \qquad (3\text{-}1)$$

For single mode operation the normalised frequency must lie in the range $1.4<V<2.405$. If we increase the core radius, r, then we must make corresponding decreases in the NA. of the fibre in order for the normalised frequency to remain in the required range. Decreasing the NA. of the fibre is achieved by reducing the refractive index between the fibre core and cladding.

This fibre geometry has a number of disadvantages. Firstly, by decreasing the refractive index difference between the core and the cladding the fibre becomes less guiding and therefore more sensitive to bend losses. Secondly, by increasing the fibre core area the fibre becomes incompatible with other fibre devices such as couplers and WDMs. This limits the use of compact high power fibre pigtailed pump modules for pump sources.

There are two major advantages of using a large mode area fibre. First, for a given absorbed pump power, increasing the mode area reduces the amplified spontaneous emission (ASE). The reduction of ASE allows an increase in stored energy to be obtained. This is analogous

to using multiple amplifiers in parallel. The combined ASE resulting from amplifiers in parallel is smaller than that which would result from equivalent amplifiers in series.

Secondly, the increased mode area also increases the threshold for non-linear Raman and Brillouin effects. These occur at high powers and cause the pulse energy to be shifted to longer wavelengths. The increase in mode area of the fibre allows higher powers to be generated in amplifier and laser devices before non-linear effects cut in and degrade performance.

3.2.4 Q-switched Fibre laser Theory

Q-switching is a widely used laser technique for producing short intense pulses of light. In this process, a high loss is inserted into the laser cavity to prevent feedback. The continuous pumping process results in a population inversion, which is larger than usually achieved in an optimised laser cavity. On removing the loss from the cavity, the energy stored in the enhanced population inversion is released in an intense burst of light. This switching from high loss (low Q) to low loss (high Q) can be repeated to produce a train of high power pulses typically only a few tens of nanoseconds in duration.
An illustration of the processes involved in Q-switching is shown in Figure 3-5.

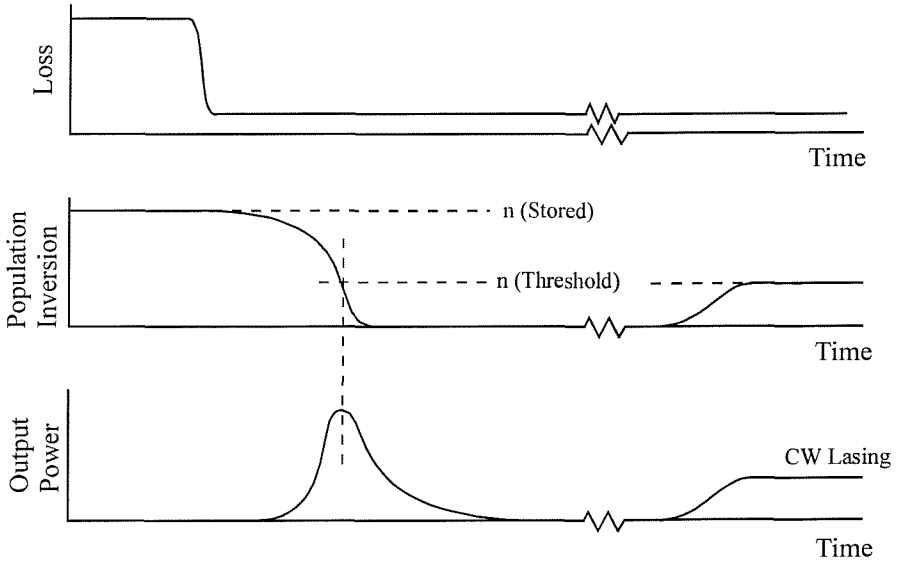

***Figure 3-5** - Diagram showing processes occurring during a Q-switched pulse*

The cavity loss is initially set to a high value. The pumping process enables a population inversion (and thus gain) to build up in the laser cavity that is higher than under CW laser conditions. When switched to a low loss state, the high gain in the cavity rapidly amplifies the spontaneous emission, which then develops into a giant pulse of laser light. This pulse depletes the population inversion and the gain falls rapidly to a value below threshold, where the pulse dies out. If the cavity remains in this low loss state the population inversion will recover to the CW steady state. The high loss should therefore be restored in sufficient time to allow the population inversion to recover its initial high value.

The amount of stored energy in the fibre is limited by the spontaneous emission that exists from the upper laser level to the ground state. The presence of this spontaneous emission causes the population inversion and hence stored energy to be reduced.

3.3 Methods of Q-switching Fibre Lasers

As we have already discussed, Q-switched lasers operate by periodically modulating the loss in the laser cavity. It is important however that the high loss state is sufficient to prevent the occurrence of any CW lasing, which would deplete the population inversion and thus stored energy within the cavity.

Several factors must be examined when considering Q-switching methods. The first is the extinction ratio; this is the ratio of the output of the switch in the high and low loss states. For efficient Q-switching operation, the extinction ratio must be maximised. Insufficient extinction is characterised by CW lasing when the cavity is in a high loss state.

Another important factor to be considered is the switching time of the device. This is the time taken for the device to switch from the high to the low loss state and vice versa. For an efficient Q-switch device, the switching time must be significantly shorter than the pulse build up time. The pulse build-up time is defined as the finite delay between the time when the Q-switch opens and the time when the output power is equal to the steady state power when operating CW [25]. If the Q-switch opening time is greater than the pulse build-up time, two detrimental effects occur:

1) A decrease in pulse energy is observed, as energy is lost through the switch during its opening time.
2) If the opening time of the switch is sufficiently long, multiple output pulses are observed. These secondary pulses can cause measurement and a variety of other errors in practical applications.

To avoid these effects, the opening time required for a Q-switch is typically tens of nanoseconds or faster [25]. However with a high gain system (e.g. an optimised Erbium doped fibre), a fast rise time can lead to a pulsed structure within the Q-switched envelope. The investigation of this behaviour is one of the topics of this research.

Finally, the repetition rate of the device is also an important consideration. Erbium doped Q-switched fibre lasers operate typically in the region of 10Hz to in excess of 10kHz, so suitable devices should cover this range.

3.3.1 Mechanical Chopper

The simplest method of introducing a loss into the cavity is to use a mechanical, rotating, chopper wheel, or other form of mechanical switch such as a rotating mirror. The primary advantage of the mechanical switch is its high extinction ratio, which ensures that lasing does not occur in the high loss state. The laser can only oscillate during the brief interval when a clear path exists between the two mirrors. Another significant advantage is the zero insertion loss when the switch is in the low loss state. Other forms of Q-switching are unable to compete on these two factors. However, the major disadvantage of the mechanical switch is the extremely low switching speed. For a typical chopper wheel (radius - 5cms) this is approximately 100μs, which is very slow compared to other devices. Mechanical switches also suffer from vibration and mechanical noise that lead to problems with pulse to pulse stability.

3.3.2 Acousto-Optic Switches

An acousto-optic modulator (AOM) is an acousto-optic device that relies on an acoustic wave to diffract the optical beam out of the cavity [26][27][28]. An acoustic wave is produced by the application of an RF signal to a transducer that is bonded to the medium in which the acoustic and optical waves interact. This stimulates a travelling acoustic wave in the medium, with a frequency of the applied signal and a velocity dependent upon the material properties of the medium. The acoustic wave generates strain upon the medium that causes the refractive index to be periodically modulated. This periodic modulation, being equivalent to a moving phase grating, may diffract the light incident upon it. An optical beam incident on the modulator at the Bragg angle will be predominantly diffracted into the first order. The incident beam is deflected by the acoustic wave into its diffracted and undiffracted components. The Bragg angle that governs the angle of diffraction is given by:

$$\sin\theta_B = \frac{\lambda \cdot f}{2 \cdot \mathrm{v}} \qquad (3\text{-}2)$$

where f is the acoustic frequency, v, the acoustic velocity, λ, the wavelength and θ_B, the Bragg angle. For a Tellurium Dioxide (TeO_2) acousto-optic modulator, which has an acoustic velocity of 4190m/s [29], operating at a wavelength of 1.55μm, with a 110MHz drive frequency, the Bragg angle is 1.2°.

Acousto-optic modulators offer a number of advantages for Q-switching. They provide high switching speeds (10-100ns) and fast repetition rates (MHz). However, when operating at 1.55μm, they suffer from low diffraction efficiencies, typically in the region of 60-80%.

The switching time of the device is primarily determined by the time required for the acoustic beam to sweep across the optical beam. If we assume a Gaussian beam that is focused into the modulator with a beam waist of 50μm, then the transit time, again assuming a TeO_2 medium would be approximately 12ns.

The diffraction efficiency of the acousto-optic modulator is dependent on a number of variables, notably the RF power, the interaction length and the overlap between the acoustic and optical beams. If the optical beam is focused inside the modulator to increase the rise time performance then this is achieved at the expense of reduced diffraction efficiency or the need for higher RF powers. Conversely failure to focus the optical beam to a sufficiently small diameter will also result in reduced diffraction efficiency, since the acoustic beam fails to intercept the entire optical beam. A trade-off therefore exists between the modulator rise time and diffraction efficiency.

In a Q-switched laser, acousto-optic modulators can be operated in two different regimes, zero and first order, where the feedback into the cavity is provided by the undiffracted and diffracted beams respectively. The choice between the two regimes of operation depends upon the diffraction efficiency of the AOM and the round-trip gain of the cavity. When operating in the zero order regime, switching the modulator on, causes an increase in loss within the cavity. If this loss is not sufficient to prevent CW lasing then the population inversion is clamped to the level at which CW lasing commenced which seriously affects the Q-switching performance. Operating in first order operation, the loss is introduced when the modulator is switched off, and hence there are no problems which arise from the effect of CW lasing. However the lack of CW lasing is bought at the expense of an increase in intra-cavity loss by a factor equal to (diffraction efficiency)^2.

In general, for systems with a low round trip gain, zero order operation is the preferred operating regime and for systems where zero order operation offers insufficient hold-off a move to first order operation is required.

3.3.3 Electro-Optic Switches

The Pockels cell, or electro-optic modulator relies on the application of an electric field to a non-centrosymmetric crystal. This electric field induces a birefringence in the crystal, which rotates the polarisation of the light passing through it. The electro-optic effect can be utilised in two regimes for Q-switching fibre lasers both of which require the Pockels cell to be used

in conjunction with a polarising element. In one form a voltage is applied to the Pockels cell to form a quarter wave plate. On one complete cavity round trip the light is rotated through 90° and is extinguished by the polarising element. Switching the cavity to the low loss state is then achieved by removing the applied electric field. An alternative arrangement is that a quarter wave plate is inserted into the cavity to achieve the high loss condition and then an electric field is applied to the Pockels cell to cancel this effect. This has the advantage that the Pockels cell is in the off state for the long high loss period and is switched on briefly to allow the pulse to build-up. However, it does require an additional quarter wave plate within the cavity.

Electro-optic Q-switching provides the fastest form of Q-switching (<4ns) with good pulse to pulse stability and a high extinction ratio (95-99%). This however is coupled with the need for high-switching voltages, 0-5kV, which can produce severe electrical interference to nearby equipment and high cost.

3.3.4 Mechanical all-fibre modulators

In 1993, Chandonnet *et al* [30] demonstrated a novel all-fibre intensity modulator which could be used as a Q-switch for fibre lasers. This modulator operates by changing the loss in the fibre by coupling out the evanescent field. The fibre is side polished down to the core and a piezoelectric crystal changes the position of an overlay on the surface of the fibre, which has a refractive index matched to the fibre core. This switches the loss in the fibre by coupling out the light.

The switching time was measured to be 175ns from a 10dB to a 3dB attenuation. The maximum repetition rate from this device is 400Hz. The Q-switched laser which was demonstrated when pumped with 100mW of 980nm from a Ti:Sapphire produced pulses with a peak power of 400watts and a 15ns pulse width [30].

3.4 Conclusions

In this chapter a number of systems suitable for the development of Q-switched fibre lasers were investigated. The advantages and disadvantages of Erbium and Erbium/Ytterbium doped silica systems were exposed. We also considered a novel fibre geometry in the form of a large mode area Erbium doped fibre.

The theory and methods of Q-switching were then covered, stating the strengths and weaknesses of the following techniques; mechanical, acousto-optical and electro-optic switches and mechanical all-fibre modulators. In the next chapter we discuss computer modelling of these systems, starting with a mathematical model of an Erbium amplifier. This will predict pump absorption and the effects of spontaneous emission on the stored energy in a continuously pumped Q-switched gain medium.

3.5 References

[1] T.H.Maiman: 'Optical and Microwave – Optical Experiments in Ruby', *Physical Review Letters*, Vol.4, No.11, pp.564-566, (1960)

[2] E.Snitzer: 'Proposed Fibre Cavities for Optical Masers', *Journal of Applied Physics*, Vol.32, No.1, pp.36-39, (1961)

[3] E.Snitzer: 'Optical Maser action of Nd^{3+} in a Barium Crown Glass', *Physics Review Letters*, Vol.7, No.12, pp.444-446, (1961)

[4] E.Snitzer and R.Woodcock: 'Yb^{3+}/Er^{3+} Glass Laser', *Applied Physics Letters*, Vol.6, No.x, pp.45-46, (1965)

[5] J.Stone and C.A.Burrus: 'Nd^{3+} doped SiO_2 lasers in an end pumped fibre geometry', *Applied Physics Letters*, Vol.23, No.7, pp.388-389, (1973)

[6] R.J.Mears, L.Reekie, I.M.Jauncey and D.N.Payne: 'Low Noise Erbium doped fibre amplifier operating at 1.54μm', *Electronics Letters*, Vol.22, No.3, pp.1027-1028, (1987)

[7] N.Edagawa, S.Yamamoto, Y.Namihira, K.Mochizuki and H.Wakabayashi: 'First Field demonstration of optical submarine cable system using LD pumped Erbium doped optical fibre amplifier', *Electronics Letters*, Vol.25, No.19, pp.1278-1280, (1989)

[8] L.Reekie, I.M.Jauncey, S.B.Poole and D.N.Payne: 'Diode Laser Pumped Operation of an Er^{3+} doped single mode fibre laser', *Electronics Letters*, Vol.23, No.20, pp.1076-1078, (1987)

[9] J.D.Minelly, E.R.Taylor, K.P.Jedrzejewski, J.Wang and D.N.Payne: 'Laser Diode Pumped Nd^{3+} doped fibre laser with output powers in excess of 1 Watt', *Proceedings of Conference on Lasers and Electro-Optics (CLEO)*, Paper CWE6, (1992)

[10] J.D.Minelly, W.L.Barnes, R.I.Laming, P.R.Morkel, J.E.Townsend, S.G.Grubb and D.N.Payne: 'Diode Array Pumping of Er^{3+}/Yb^{3+} co-doped fibre lasers and amplifiers', *IEEE Photonics Technology Letters*, Vol.5, No.3, pp.301-303, (1993)

[11] T.Kringlebotn, P.R.Morkel, L.Reekie, J-L,Archambault and D.N.Payne: 'Efficient diode pumped single frequency Er^{3+}/Yb^{3+} fibre laser', *IEEE Photonics Technology Letters*, Vol.5, No.10, pp.1162-1164, (1993)

[12] I.Alcock, A.C.Tropper, A.I.Ferguson and D.C.Hanna: 'Q-switched operation of a Neodymium doped monomode fibre laser', *Electronics Letters*, Vol.22, No.x, pp.84-85, (1986)

[13] R.J.Mears, L.Reekie, S.B.Poole and D.N.Payne: 'Efficient diode pumped CW and Q-switched single mode fibre laser', *Electronics Letters*, Vol.22, No.4, pp.198-199, (1986)

[14] R.I.Laming, M.Farries, P.Morkel, L.Reekie and D.N.Payne: 'Efficient Pump Wavelengths of Erbium Doped Fibre Optical Amplifiers', *Electronics Letters*, Vol.25, No.1, pp.12-14, (1989)

[15] A.Lidgard, D.J.DiGiovanni and P.C.Becker: 'A Comparative Study of an Erbium doped Fibre Amplifier Pumped at 811 and 980nm', *IEEE Journal of Quantum Electronics*, Vol.28, No.1, pp.43-47, (1992)

[16] E.Desurvire: 'Analysis of Erbium Doped Fibre Amplifiers Pumped in the $^4I_{15/2}$ - $^4I_{13/2}$ Band', *IEEE Photonics Technology Letters*, Vol.1, No.10, pp.293-296, (1989)

[17] W.J.Miniscalco, L.J.Andrews, B.A.Thompson, T.Wei and B.T.Hall: 'The effect of glass composition on the performance of Er^{3+} fibre amplifiers', *Fibre Laser Sources and Amplifiers*, SPIE. Vol. 1171, pp.93-102, (1989)

[18] R.S.Quimby, W.J.Miniscalco and B.A.Thompson: 'Quantitative characterisation of clustering in Erbium-doped silica glass fibres', *Fibre Laser Sources and Amplifiers V*, SPIE 93, Vol.2073, paper 1, (1993)

[19] J.E.Townsend, W.L.Barnes, K.P.Jedrzejewski and S.B.Grubb: 'Yb^{3+} Sensitised Er^{3+} doped Silica Optical Fibre with Ultrahigh Transfer Efficiency and Gain', *Electronics Letters*, Vol.27, No.21, pp.1958-1959, (1991)

[20] J.D.Minelly, W.L.Barnes, R.I.Laming, P.R.Morkel, J.E.Townsend, S.G.Grubb and D.N.Payne: 'Diode-array pumping of Er^{3+}/Yb^{3+} co-doped fibre lasers and amplifiers', *IEEE Photonics Technology Letters*, Vol.5, No.3, pp.301-303, (1993)

[21] J.T.Kringlebotn, J-L.Archambault, L.Reekie and D.N.Payne: '1.5μm Er^{3+}/Yb^{3+} Doped Fibre DFB Laser', *Optics Letters*, Vol.19, No.24, pp.2101-2103, (1994)

[22] J.L.Wagaener, P.F.Wysocki, M.J.F.Digonnet, H.J.Shaw and D.J.DiGiovanni: 'Effects of concentration and clusters in Erbium doped fibre lasers', *Optics Letters*, Vol.18, No.23, pp.2014-2016, (1993)

[23] J.Nilsson and B.Jaskorzynska: 'Modelling and Optimisation of low-repetition rate high energy pulse amplification in CW pumped Erbium doped Fibre amplifiers', *Optics Letters*, Vol.18, No.24, pp.2099-2101, (1993)

[24] D.J.Richardson, P.Britton and D.Taverner: 'Diode-pumped, high-energy, single transverse mode Q-switch fibre laser', *Electronics Letters*, Vol.33, No.23, pp.1955-1956, (1997)

[25] A.Seigman: 'Lasers', *University Science Books*, ISBN 0-935702-11-5, (1986)

[26] J.Xu and R.Stroud: 'Acousto-Optic Devices: Principles, Design and Applications', *Wiley Interscience*, ISBN 0-471-61638-9, (1992)

[27] D.Mayden: 'Acousto-optical Pulse Modulators', *IEEE Journal of Quantum Electronics*, Vol. QE-6, No. 1, pp.15-24, (1970)

[28] A.Korpel: 'Acouto-Optics – A Review of Fundamentals', *Proceedings of the IEEE*, Vol. 69, No. 1, pp.48-53, (1981)

[29] A.Yariv: 'Optical Electronics: Fourth Edition', *Harcourt Brace Jovanovich College Publishers*, ISBN 0-03-047444-2, (1991)

[30] A.Chandonnet and G.Larose: 'High-power Q-switched Erbium fibre laser using an all-fibre intensity modulator', *Optical Engineering*, Vol.32, No.9, pp.2031-2035, (1993)

Chapter Four

Modelling of Erbium doped Q-switched Fibre Lasers

4.1 Introduction to Modelling Q-switched Erbium doped Fibre Lasers

Computer modelling is a powerful tool in physics as it can be used to reinforce experimental results and anticipate trends.

Much previous research has focused on the theoretical analysis of Erbium doped fibre amplifiers. A comprehensive treatment of excited state absorption (ESA) on small signal gain has been given by Armitage [1], and the spectral evolution of amplified spontaneous emission (ASE) has been given by Desurvire and Simpson [2]. An in-depth description of Erbium doped fibre amplifiers can be found in Giles and Desurvire [3] which provides valuable information on saturation effects in these systems. This model is particularly useful as it predicts pump absorption and the effects of ASE on the population inversion in the Erbium doped fibre.

In the sphere of Q-switched fibre lasers, a theoretical investigation is provided by Gaeta *et al* [4] who describe the influence of fibre and cavity parameters on the peak power and pulse width of the laser. Their model takes into account the effects of modal overlap between pump and signal fields within the fibre. A more comprehensive and thorough description of Q-switched lasers is presented by Siegman [5]. Of particular importance is his rate equation analysis which can be expanded to obtain a number of useful parameters such as pulse build up time, Q-switched pulse energy and peak power. These equations are described fully in section 4.3.2.

In this chapter we use Giles' model for Erbium fibre amplifiers to calculate parameters such as the stored energy and single pass gain in a doped fibre. This model is then expanded to describe the gain element in a Q-switched fibre laser when in the high loss (low Q) state i.e. to account for the gain depletion caused by the reflection of ASE from a cavity mirror. The calculated gain is then considered to be a lumped element and combined with a rate equation analysis of laser Q-switching (Siegman [5]) to provide a model for Q-switched fibre lasers.

4.2 Modelling of Erbium doped fibre amplifiers

4.2.1 Rate Equation Analysis of Erbium doped fibre amplifiers

In this thesis, a model of an Erbium doped fibre amplifier is used to predict pump absorption and the effects of amplified spontaneous emission (ASE) on the population inversion in the Erbium doped fibre. The numerical analysis of the Erbium system, as shown in Figure 4-1, is described using a coupled rate equation method [3].

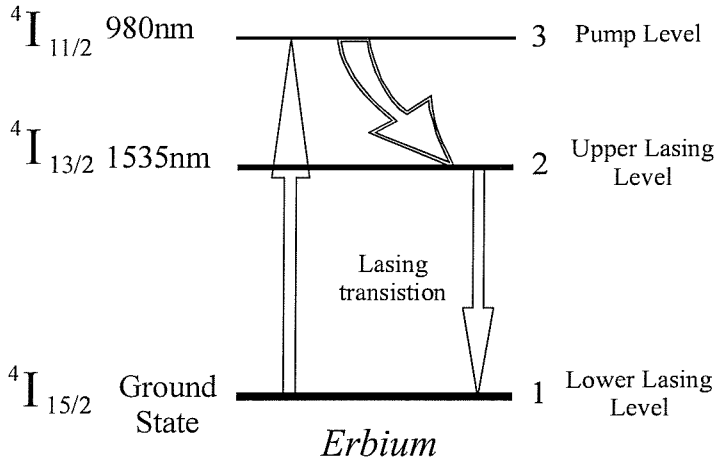

***Figure 4-1** - Schematic showing energy levels for a 980nm pumped Er^{3+} ion*

For laser action to take place a population inversion is needed between two energy levels. In order to build up a population inversion for laser action, ions are pumped from the ground state into an excited state (980nm). They then decay non-radiatively into the upper metastable level. The long lifetime of the metastable level enables a substantial population

inversion to be achieved between this state and, in the case of the Erbium system, the ground state. Ions in the metastable level can undergo radiative decay and fall into the ground state; this decay can be either spontaneous or stimulated emission producing incoherent noise-like emission or coherent laser light respectively. Equations (4-1) and (4-2) describe this behaviour. In order to simplify the two equations the following assumptions are made regarding the Erbium system:

1) When pumping at 980nm, the system is free from excited state absorption (ESA) from the metastable level.
2) The transition rate from the pump band to the metastable level is sufficiently fast (≈6μs) compared with the metastable lifetime (≈10ms), enabling the system to be treated as a quasi-two level system.
3) The wavelength dependence of the emission and absorption cross-sections is neglected.

The rate of change of population densities of ions in the upper and lower lasing levels with time can therefore be written as [3]:

$$\frac{dN_1(z,t)}{dt} = A_{21}N_2 - P_p \cdot \frac{\sigma_{13}\eta_p}{h\upsilon_p A} \cdot N_1 + (P_a^+ + P_a^- + P_s) \cdot \frac{\sigma_{21}\eta_s}{h\upsilon_s A} \cdot N_2 - (P_a^+ + P_a^- + P_s) \cdot \frac{\sigma_{12}\eta_s}{h\upsilon_s A} \cdot N_1$$

(4-1)

$$\frac{dN_2(z,t)}{dt} = -A_{21}N_2 + P_p \cdot \frac{\sigma_{13}\eta_p}{h\upsilon_p A} \cdot N_1 - (P_a^+ + P_a^- + P_s) \cdot \frac{\sigma_{21}\eta_s}{h\upsilon_s A} \cdot N_2 + (P_a^+ + P_a^- + P_s) \cdot \frac{\sigma_{12}\eta_s}{h\upsilon_s A} \cdot N_1$$

(4-2)

The first and second terms on the right hand side of the equation describe the spontaneous emission and the pump rate respectively, whilst the third and fourth terms describe the stimulated emission and absorption rates.

Table 4-1 shows the definitions of the variables and constants used in equations (4-1) and (4-2)

Symbol	Description
N_1, N_2	Population Densities of Upper and Lower lasing levels (m^{-3})
A_{21}	Spontaneous decay rate from the metastable level (s^{-1})
P_p P_s	Pump Power & Signal Power (W)
$P_a^{\pm}$	Forward and Backward ASE powers (W)
σ_{21} σ_{12}	Signal emission and absorption cross-sections (m^2/ion)
σ_{13}	Pump absorption cross-section (m^2/ion)
η_s, η_p	Signal and Pump overlap factors
ν_s, ν_p	Signal and Pump frequencies (s^{-1})
$\Delta\nu$	Equivalent ASE Bandwidth (GHz)
A	Effective Core Area (μm^2)

Table 4-1 *- Definitions for Symbols used in the Rate Equations*

Now consider how the pump power, signal power and ASE vary along the length of the doped fibre. The variation of pump power as a function of distance along the fibre can be written as:

$$\frac{dP_p(z)}{dz} = -P_p \cdot \eta_p \cdot \sigma_{13} \cdot N_1(z) \qquad (4\text{-}3)$$

and because we are assuming that the ions decay immediately to the metastable level, there is no stimulated or spontaneous emission from the pump level to the ground state.

Similarly for the variation of signal power with fibre length, it follows that:

$$\frac{dP_s(z)}{dz} = P_s(z) \cdot \eta_s \cdot (\sigma_{21} N_2 - \sigma_{12} N_1) \qquad (4\text{-}4)$$

which as expected is proportional to the population inversion given by N_2-N_1. The signal is amplified or attenuated depending on the sign of N_2-N_1.

The power of the forward and backward ASE is provided by the expression:

$$\frac{dP_a^{\pm}}{dz} = \pm P_a^{\pm}(z) \cdot \eta_s \cdot (\sigma_{21} N_2 - \sigma_{12} N_1) \pm 2\sigma_{21} N_2(z,t) \eta_s h \nu_s \Delta\nu \qquad (4\text{-}5)$$

where the ± sign denotes the forward or backward travelling ASE respectively. The first term in the expression is simply the growth or decay of the spontaneous emission provided by the population inversion with the gain medium. Whereas the second term in the expression gives a value for the spontaneous emission produced per unit length in the amplifier bandwidth. This is the expression which initiates the evolution of the amplified spontaneous emission.

Using these five equations, a computer model was developed to calculate the variation of pump, signal and ASE powers and population densities along a length of Erbium doped fibre. With no signal present (P_s=0) the model provides the total population inversion or energy stored in a length of pumped Erbium fibre. This result is later used for the Q-switched laser model.

4.2.2 Results obtained from the Erbium fibre amplifier model

Table 4-2 lists the numerical parameters used for this amplifier model, these values are seen as typical for an alumino-silicate Erbium doped fibre.

Parameter	Numerical Value
P_p	45mW
A_{21}	$83s^{-1}$ (τ=12ms)
N_t	$1.716x10^{25}$ m^{-3} 800ppm of Er^{3+}
N.A.	0.15
R	2.5μm
λ	1.55μm
$\Delta\nu$	250GHz or 2nm
A (core area)	$58\mu m^2$
η_s	0.600
η_p	0.811
σ_{12}	$7.0x10^{-25}$ m^2
σ_{21}	$6.5x10^{-25}$ m^2
σ_{13}	$1.75x10^{-25}$ m^2

***Table 4-2** – Numerical Values used in the computer simulation*

The signal and pump overlap factors are calculated to represent the overlap of the signal and pump mode field diameters with the Erbium doped core. They give the fraction of the total signal and pump intensities which are contained within the core of the fibre. We have assumed that both the pump and the signal propagate in the LP_{01} mode and that the dopant distribution is uniform across the core and zero in the cladding (top hat profile). The mode field diameter is then given by equation (4-6) where w is the mode field radius, r the core radius and V is the normalised frequency or V number:

$$w = r(0.65 + 1.619 \cdot V^{-\frac{3}{2}} + 2.879 \cdot V^{-6}) \qquad (4\text{-}6)$$

Using this equation we calculate the mode field radius for the pump and signal wavelengths. We then calculate the fractional intensity which lies within the fibre core to give the overlap factors for the pump and signal (η_p & η_s).

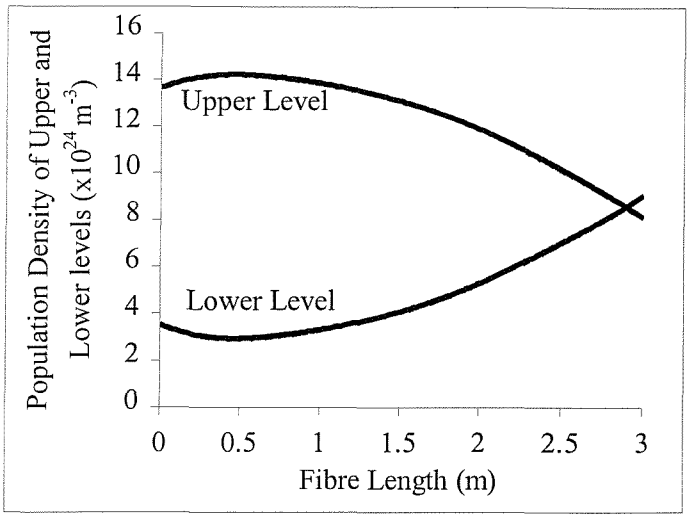

Figure 4-2 *– Variation of the population density of the upper and lower levels along a length of Erbium doped fibre*

The results from the model show the powerful influence of ASE on both the absorbed pump power and the population inversion density (gain) along the fibre. Figure 4-2 shows the population inversion density of the upper and lower levels as a function of distance along the length of the Erbium doped fibre. An interesting point to note is that the population inversion at the near and far ends of the fibre has been depleted. At the near end of the fibre this depletion is due to backward propagating ASE. Whilst at the far end of the fibre, the depletion is caused by both the forward ASE and the lower pump intensity.

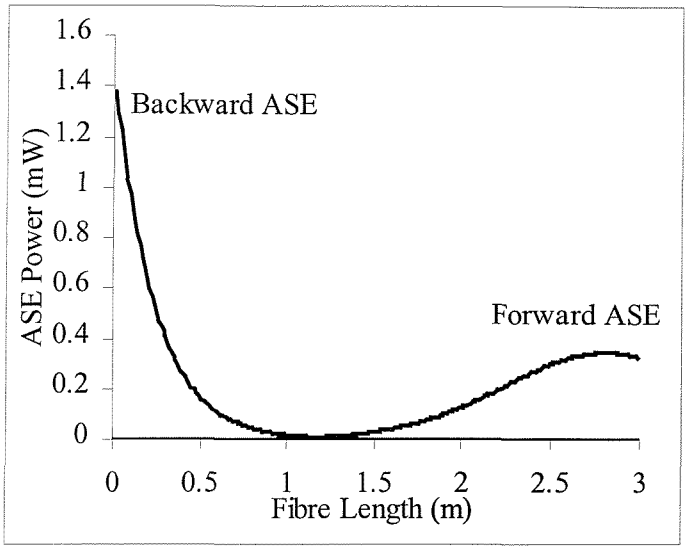

Figure 4-3 *– Variation of Forward and Backward ASE power along a length of Erbium doped fibre*

Figure 4-3 shows the variation in the forward and backward ASE power as a function of distance along the fibre. The ASE is at a minimum close to the centre of the fibre and thus the local gain is at a maximum, as illustrated in figure 4-3. The increased pump intensity and therefore higher population inversion at the front end of the fibre has the effect of allowing the backward travelling ASE to be amplified to a higher value than the forward ASE.

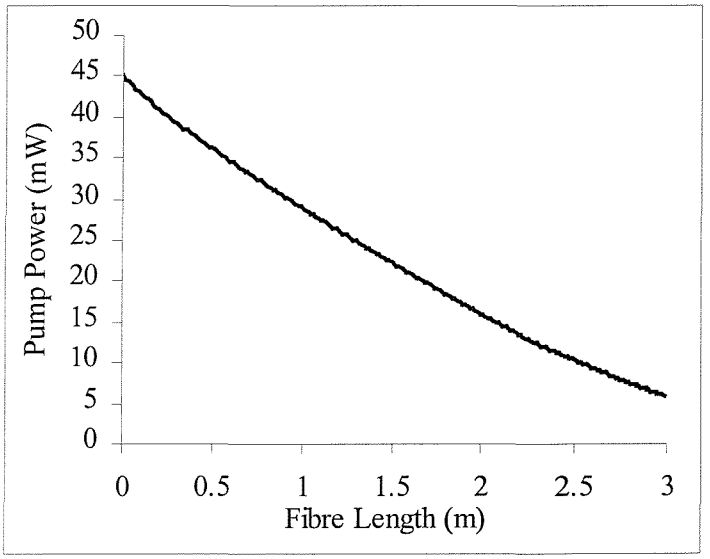

Figure 4-4 *– Variation of Pump Power along the length of Erbium doped fibre*

From these results it is clear that the presence of the ASE has a marked impact on the gain of the amplifier and it is for this reason that power amplifiers contain methods of reducing the ASE. A simple method of achieving this is to put an optical isolator in the centre of the Erbium fibre, which would prevent the build-up of backward ASE [6]. Other more sophisticated methods such as using an AOM to gate pulsed signals through an amplifier chain whilst blocking the ASE can also be used. These methods have the added advantage of decreasing the non-linear Raman effects that occur in long amplifier systems and cause decreased efficiency.

An important concept governing the generation of high energy pulses, is the process of gain saturation which limits the maximum amplification achievable from a fibre amplifier.

4.2.3 Gain Saturation in Erbium doped Fibre Amplifiers

Gain saturation occurs when the signal itself becomes strong enough to deplete the population inversion to such an extent that the rate of signal growth is decreased. A signal propagating through a power fibre amplifier will grow exponentially along the length of the amplifier until saturation effects occur, as illustrated in Figure 4-5.

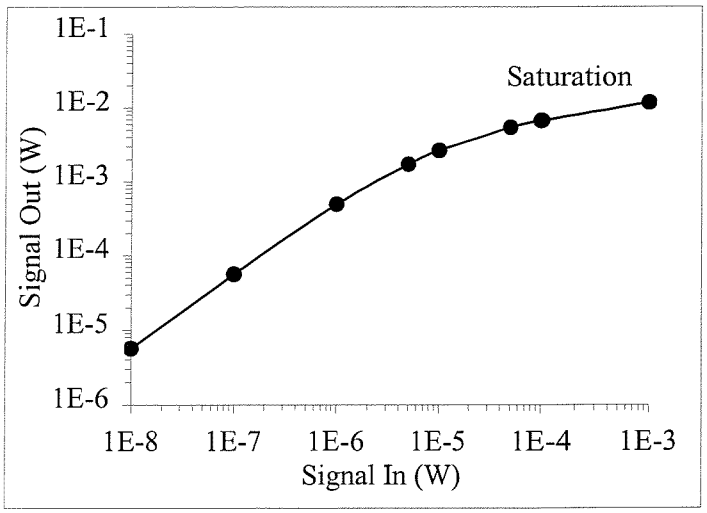

Figure 4-5 *- Results from amplifier model showing the variation of output signal with input signal*

The expression for the saturation intensity is thus vital in determining the maximum power extraction available from a fibre amplifier and in a laser gain medium where the gain can be saturated by the amplified spontaneous emission (ASE). The saturation intensity is defined as (assuming a homogeneously broadened transition) [7]:

$$I_{sat} = \frac{hc}{\lambda \cdot \sigma \cdot \tau_{eff}} \quad \mathrm{W/m^2} \qquad (4\text{-}7)$$

where σ is the transition cross-section and τ_{eff} is the effective lifetime for the transition. For the parameters used in the amplifier model (σ - 6.75×10^{-21} cm^2, τ_{eff} - 12ms) the saturation intensity for a signal at 1.53μm would be approximately $1kW/cm^2$. If the core area is $58\times10^{-8}cm^2$ this would give a saturation power of 0.6mW. The saturation intensity is defined as the input power required to reduce the gain (dB) to a value of half of its small signal value [5]. This is illustrated in Figure 4-6 where the gain falls to half its value at an input signal power of approximately 0.4mW. Importantly the saturation intensity is independent of the pump power since neither the transition cross-section or recovery time depends on the pumping rate. Therefore increasing the pump power for a given fibre diameter does not change the signal power required to reduce the gain by a factor of 2 (saturation power). One method to increase the saturation power is to increase the fibre core area, this technique is applied later to produce high power Q-switched fibre lasers.

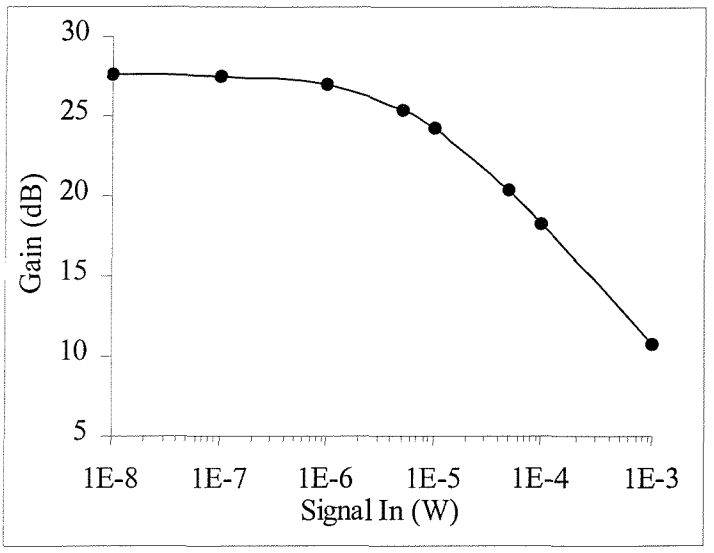

Figure 4-6 *- Figure showing Amplifier Gain as a function of Input Signal*

4.3 Modelling a Q-switched Fibre Laser

Let us now take a more in depth look at a Q-switched laser cavity and the model of the Q-switching process used to explain subsequent experimental observations.

A simple classical rate-equation model for Q-switching is available in many texts on lasers [5][7]. For the purpose of this chapter standard results are applied to a fibre laser geometry to obtain theoretical values for the peak power and pulse width achievable from a Q-switched fibre laser. We can also model the effects of adjusting the fibre length and output coupling on the laser output. The model that has been developed uses the simple Q-switched fibre laser geometry as shown in Figure 4-7.

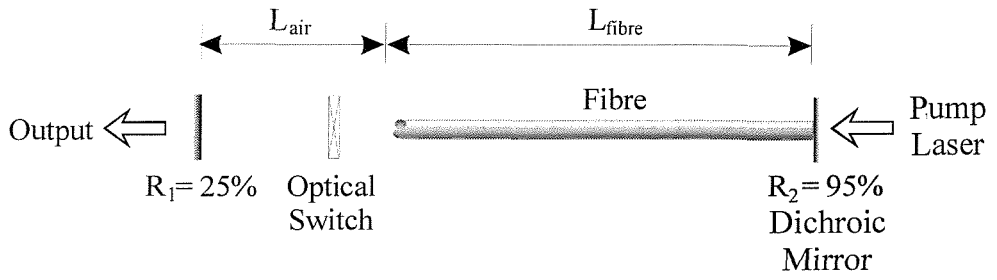

***Figure 4-7** - Schematic for a Q-switched laser*

This consists of a laser medium, in our case a length of Erbium doped fibre, a shutter and two mirrors that make up the laser cavity. The laser medium is pumped through a dichroic mirror with a 980nm laser diode which provides 45mW of launched light into the fibre core. When the shutter is closed the pump generates a population inversion in the medium until equilibrium is reached between the pump and the spontaneous decay. On opening the shutter a rapid build-up of light occurs and a Q-switched pulse is emitted (Figure 4-8).

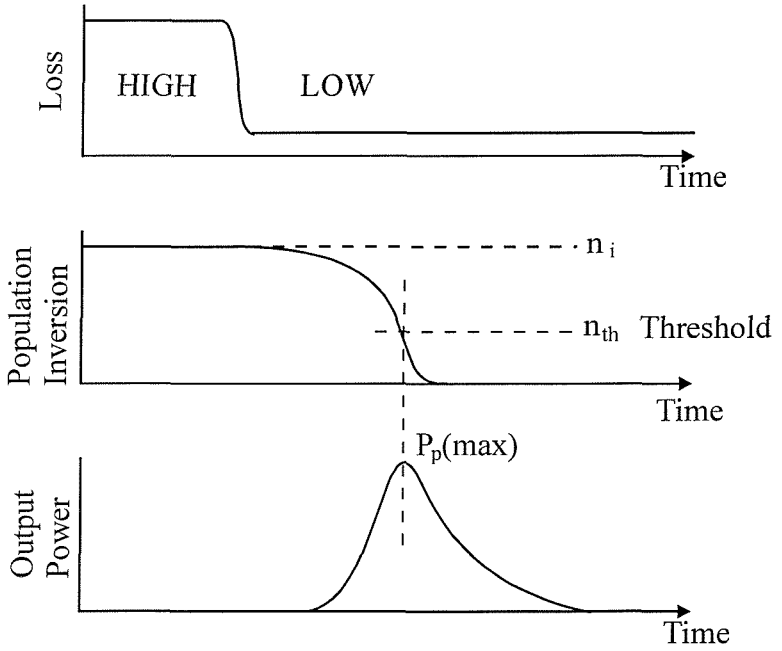

***Figure 4-8** – Sequence of events during the emission of a Q-switched pulse*

In the model certain assumptions are made:

1) The Q-switched process is sufficiently rapid to neglect any influence that the pump and spontaneous emission has on the population inversion within the pulse duration.
2) Excited state absorption within the fibre is neglected.
3) All the surfaces within the cavity are anti-reflection coated and therefore have negligible transmission losses.
4) The rise/fall time of the shutter is fast compared to the cavity round-trip time

The model will provide information on the variation of peak power and pulse width with output coupling and thus the effects of cavity losses on laser performance. This information will be helpful in optimising the cavity configuration. In a later chapter it is experimentally verified that a large core radius promotes the generation of higher pulse energies from fibre amplifiers. The model can be used to predict this.

4.3.1 Modified Amplifier Model

Section 4.2 used a simple rate-equation analysis to calculate the energy stored in a length of pumped Erbium doped fibre. However, before proceeding with the mathematical description of the Q-switched model we need to consider the effect that the laser mirrors have on the stored energy within the laser amplifier. It has been shown previously (Figure 4-3) that in a high gain amplifier the backward ASE can grow to a substantial power (~1mW) a value which is comparable to the saturation power. If this ASE is then reflected back into the cavity by a laser mirror, then in a system with a high single pass gain the amount of stored energy can be substantially reduced. This section provides a more accurate measure of the stored energy in the laser gain medium by modifying the simple rate equation model used in section 4.2 to account for the reflection of the ASE by the laser mirror. As the following results show the reflection of the ASE by laser mirrors has a major effect on the population inversion, ASE and pump power distributions along the length of the fibre.

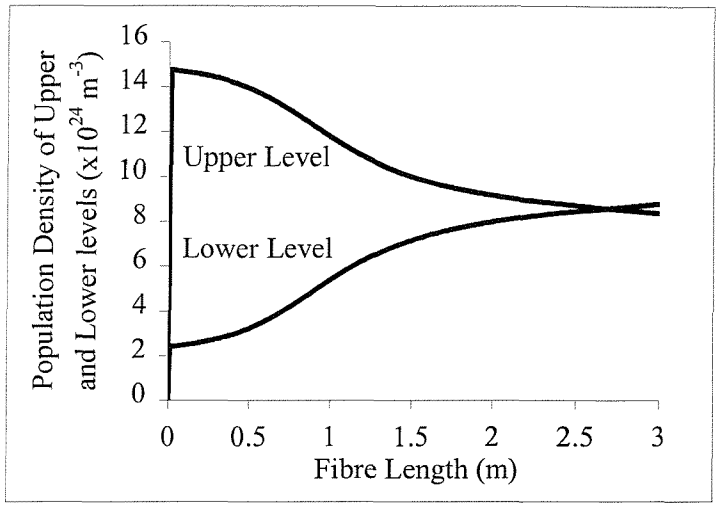

Figure 4-9 *– Variation of Population density of the upper and lower levels along a length of Erbium doped fibre with a 95% reflecting mirror positioned at the near end.*

Figure 4-9 shows the variation of the population densities of both the upper and lower levels of the amplifier. There is a 95% reflecting mirror positioned at the near end of the fibre, this has the effect of reflecting the backward ASE back through the amplifier. It is this second pass of the backward ASE coupled with the lower pump intensity which causes the heavily depleted region at the far end of the fibre. From this plot it is obvious that the reflection of the ASE into the cavity changes, not only the magnitude of the stored energy within the fibre, but also the distribution along the fibre; with, in this case, the maximum population inversion occurring at the near end of the fibre rather than at the centre as it does when no mirrors are present.

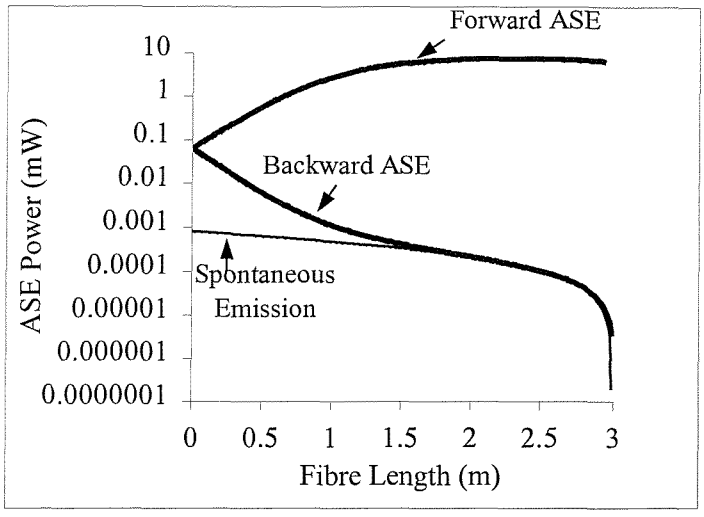

Figure 4-10 *- Variation of forward and backward ASE along a length of Erbium doped fibre with a 95% reflecting mirror positioned at the near end.*

Figure 4-10 shows how the forward and backward ASE varies along the fibre length. In this case the forward ASE comprises of both the backward ASE which has been reflected from the mirror and the ASE which originates from the spontaneous emission of photons at the near end of the fibre. The dominating component of this forward signal is the amplified reflected ASE from the mirror. One point to note is the saturation of the forward signal with a maximum power of 7mW.

The unusual shape of the backward ASE plot at the far end of the fibre is due to the generation of photons in the cavity from purely spontaneous decay. At the far end of the fibre where the forward ASE is saturating the gain (i.e. $N_2 \approx N_1$) no amplified spontaneous emission is expected, however spontaneous emission of photons from N_2 still occurs. In order to verify this the component of the backward ASE which comprises of purely spontaneous emission (Second term in equation (4 –5)) has been plotted.

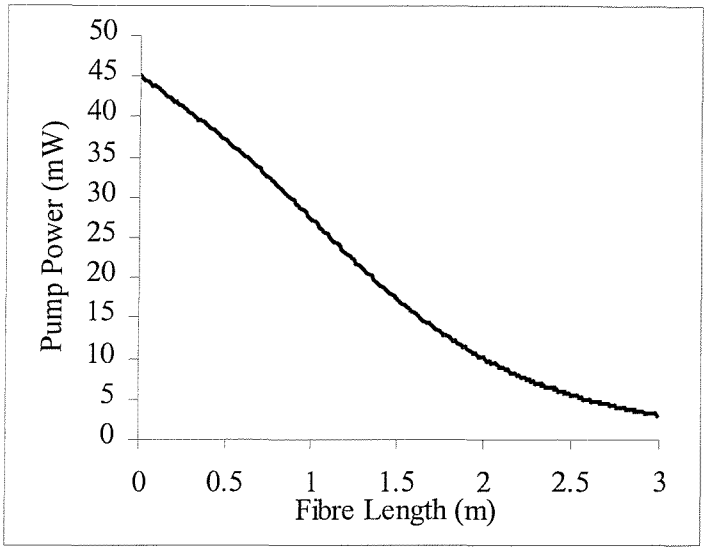

***Figure 4-11** – Variation of Pump power along the length of Erbium doped fibre with a 95% reflecting mirror positioned at the near end.*

The change in distribution of the population inversion along the length of the fibre with the presence of the mirror causes a corresponding change in the pump absorption. At the far end of the fibre with the lower population inversion, an increase in pump absorption is observed.

With the modification to the amplifier model to account for the reflection of ASE from the laser mirror, it was found that the magnitude of the total population inversion is reduced from 10.8×10^{14} to 7.8×10^{14} ions, a reduction of 27%, for a 3m length of fibre. This new model gives a more accurate description of the gain medium in a Q-switched fibre laser when the cavity is in the low Q, high loss state.

4.3.2 Mathematical Description of Q-switched Model

Using the amplifier model developed in the previous section we now have a value for the initial population inversion (n_i) present in the pumped Erbium fibre when the Q-switched laser is in the high loss state. This section provides the equations describing Q-switched behaviour in terms of the cavity losses and the initial population inversion.

Table 4-3 lists some of the more common definitions which will be used in the Q-switched model and their values where appropriate.

Abbreviation	Description	Value & Units
n_{th}	Threshold Population Inversion	
N_p	Number of photons inside the cavity	
R_1, R_2	Reflectivity of Laser Mirrors	0.95 & 0.5
A	Cross-sectional area of fibre	$A_{eff} = 58\mu m^2$
γ	Gain coefficient /unit length	
α_{fibre}	Intrinsic loss of fibre /unit length	$\alpha_{fibre} = 4.6x10^{-5}\ m^{-1}$ (0.2dB/km)
α_{swt}	Single pass switch loss	$\alpha_{swt} = 0.693$ (3dB)
n_{air}, n_{core}	Refractive Index of air and fibre core	$n_{air} = 1$, $n_{fibre} = 1.48$
d	Cavity length	$d = l_{air} + l_g$
L_{fibre}	Length of gain medium (fibre)	metres
l_{air}	Length of air gap	0.15 metres

Table 4-3 *- Parameters used in Q-switched Laser Model*

Consider the Q-switched laser shown in Figure 4-7. After opening the switch, in one round trip of the cavity, the number of photons within the cavity mirrors, N_p, will change, depending on the various loss and gain parameters, to:

$$N_p \rightarrow (R_1 R_2 \cdot e^{2l_{fibre}(\gamma - \alpha_{fibre}) - 2\alpha_{swt}}) N_p \qquad (4\text{-}8)$$

The rate of change in the number of photons with time is therefore given by the change in the number of photons per round trip divided by the time for a round trip .

$$\frac{dN_p}{dt} = \frac{(R_1 R_2 \cdot e^{2l_{fibre}(\gamma - \alpha_{fibre}) - 2\alpha_{swt}} - 1) N_p}{2(l_{air} + n_g l_{fibre}) / c} \qquad (4\text{-}9)$$

The denominator can be abbreviated to the round-trip time of the cavity τ_{RT}, and recognising the criteria for CW lasing threshold to be:

$$R_1 R_2 \cdot e^{2l_{fibre}(\gamma_{th} - \alpha_{fibre}) - 2\alpha_{swt}} = 1 \qquad (4\text{-}10)$$

The threshold gain γ_{th} can be written as:

$$e^{-2l_{fibre}\gamma_{th}} = R_1 R_2 \cdot e^{-2l_{fibre}\alpha_{fibre}-2\alpha_{swt}} \qquad (4\text{-}11)$$

Substituting equation (4-11) into equation (4-9) yields:

$$\frac{dN_p}{dt} = \frac{(e^{2l_{fibre}(\gamma-\gamma_{th})}-1)}{\tau_{RT}} N_p \qquad (4\text{-}12)$$

The round trip time of the cavity can be expressed in terms of the photon lifetime which is the round trip time divided by the fractional number of photons surviving one round trip, in effect the cavity photon decay constant.

$$\tau_p = \frac{\tau_{RT}}{1 - R_1 R_2 \cdot e^{-2(\alpha_{fibre}l_{fibre}+\alpha_{swt})}} \qquad (4\text{-}13)$$

Now if we substitute τ_{RT} from equation (4-13) into equation (4-12) and use the Taylor series expansion, $e^x = 1+x$ then we obtain the equation:

$$\frac{dN_p}{dt} = \frac{1+2l_{fibre}(\gamma-\gamma_{th})-1}{1-(1-2l_{fibre}\gamma_{th})} \cdot \frac{N_p}{\tau_P} = (\frac{\gamma}{\gamma_{th}}-1) \cdot \frac{N_p}{\tau_P} \qquad (4\text{-}14)$$

Now relating the gain to the total number of inverted ions, n, and the threshold gain to the total number of inverted ions at threshold, n_{th}, we arrive at one of the standard equations defining how the number of photons within the laser cavity varies with time.

$$\frac{dN_p}{dt} = (\frac{n}{n_{th}}-1) \cdot \frac{N_p}{\tau_p} \qquad (4\text{-}15)$$

This equation states that if the population inversion (gain) is larger than the threshold value, then the number of photons increases with time, otherwise, they decrease.

We now need to consider a basic rate equation analysis between the two laser levels, whilst still maintaining the assumptions quoted earlier i.e. no pumping or spontaneous emission for the duration of the pulse.

The rate equations can therefore be written as:

$$\frac{dN_1}{dt} = \frac{P_p \eta_s \sigma}{A \cdot h\upsilon} \cdot [N_2 - N_1] \qquad (4\text{-}16)$$

$$\frac{dN_2}{dt} = -\frac{P_p \eta_s \sigma}{A \cdot h\upsilon} \cdot [N_2 - N_1] \qquad (4\text{-}17)$$

Multiplying both sides of the equation by the volume of the gain medium ($A.l_g$) and subtracting gives:

$$\frac{d(N_2 - N_1) \cdot A \cdot l_{fibre}}{dt} = -\frac{2P_p \eta_s \sigma}{A \cdot h\upsilon} \cdot A \cdot l_{fibre} \cdot [N_2 - N_1] \qquad (4\text{-}18)$$

The term $\sigma[N_2\text{-}N_1]$ on the right is equal to γ the gain coefficient per unit length, and the term $(N_2\text{-}N_1).A.l_{fibre}$ is equal to n, the total population inversion. Using Taylor series expansion and some further algebraic manipulation equation (4-18) reduces to:

$$\frac{dn}{dt} = -2 \cdot \frac{N_p}{\tau_p} \cdot \frac{n}{n_{th}} \qquad (4\text{-}19)$$

This is the second fundamental equation that describes the Q-switched behaviour. The factor of two is fundamental in that it states that if the number of photons within the cavity increases by one then the population inversion, n, decreases by two.

Now both equations (4-15) and (4-19) can be used to develop a description of Q-switched behaviour. One final step is needed and that is to normalise the time scale to the photon lifetime within the cavity $T=t/\tau_p$. The two basic equations describing the changing photon number, N_p, and population inversion, n, then become:

$$\frac{dN_p}{dT} = (\frac{n}{n_{th}} - 1)N_p \qquad (4\text{-}20)$$

$$\frac{dn}{dT} = -2\frac{n}{n_{th}}N_p \qquad (4\text{-}21)$$

Now in order to get to the equations for the peak power and pulse width, we have to divide equation (4-20) by (4-21) to remove the time dependence and then we integrate the equation as follows:

$$\int_{N_p(0)\approx 0}^{N_p(\max)} dN_p = \frac{1}{2}\cdot\int_{n_i}^{n_{th}}(\frac{n_{th}}{n} - 1)\cdot dn \qquad (4\text{-}22)$$

Note the limits on the integral, the photon number (N_p) is a maximum when the population inversion crosses the threshold level, this principle is illustrated in Figure 4-8. Therefore the maximum number of photons in the cavity in given by:

$$N_p(\max) = \frac{n_i - n_{th}}{2} - \frac{n_{th}}{2}\ln(\frac{n_i}{n_{th}}) \qquad (4\text{-}23)$$

These photons within the cavity are lost through the various loss processes but it is only the loss through the output mirror which provides the useful output. The maximum optical energy stored in the cavity is given by $(hc/\lambda)\cdot N_p(\max)$ and the fractional loss per round trip at the output mirror divided by the round trip time gives the power at the output:

$$P(\max) = N_p(\max) \cdot \frac{hc}{\lambda} \cdot \frac{1-R_2}{\tau_{RT}} \qquad (4\text{-}24)$$

One more assumption which we will make specific to fibre lasers, is that the initial inversion is significantly higher than the threshold inversion, this has the consequence that we can assume that all the population inversion is converted to photons within the cavity i.e. the final population inversion is zero. This assumption is valid for fibre lasers due to the high pump intensities which can be obtained within the core, as a consequence of the wave-guiding nature of the fibre media.

The pulse energy can then be written as:

$$\begin{aligned} W_{out} &= \frac{n_i}{2} \cdot \frac{hc}{\lambda} \cdot \frac{\text{Output Coupling Loss}}{\text{Total Loss}} \\ &= \frac{n_i}{2} \cdot \frac{hc}{\lambda} \cdot \frac{1-R_2}{1-R_1R_2 \cdot e^{-2(\alpha_{fibre} l_{fibre} - \alpha_{swt})}} \end{aligned} \qquad (4\text{-}25)$$

A good approximation to the pulse width is then the pulse energy divided by the peak power. We now go on to show the relationships between both peak power and pulse width with fibre length and output coupling.

4.3.3 Results from Erbium doped Q-switched Fibre Laser model

The model was developed to anticipate trends and to aid the optimisation of Q-switched laser design. In designing a Q-switched fibre laser there are two physical characteristics that can be adjusted to obtain optimum performance: fibre length and the reflectivity of the

output mirror. In this section we will examine the effects of these parameters on laser performance.

Let us first consider how the peak power changes with fibre length:

From the results shown in Figure 4-12 we observe an initial increase in peak power due to the increase in the magnitude of the stored energy in the fibre. Beyond the optimum length, which is determined by the available pump power and the saturation of the gain by ASE, the peak power then decreases.

The results also show that for very short cavities an increase in pulse width is observed. This is due to the low round trip gain of the cavity, i.e. more round-trips are required for the pulse to build-up and to deplete the inversion to below threshold. However with long fibre lengths the pulse width increases due to the longer round-trip time. There is therefore an intermediate fibre length that produces the shortest pulse widths.

The results obtained from the model are shown in Figure 4-12. From the plot we can see clearly the expected variations of peak power and pulse width with varying cavity length.

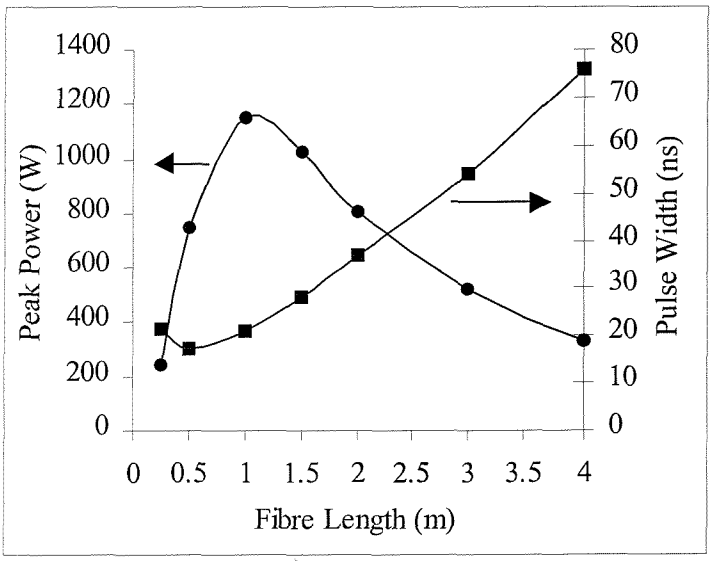

Figure 4-12 *- Variation of Peak Power and Pulse width of a Q-switched Fibre laser as a function of Fibre Length*

These results show that at optimum length for the cavity to obtain high peak powers is approximately 1 metre, with a peak power of 1.2kW and pulse width of 20ns. These results were obtained with a 50% reflectivity output mirror. Shorter pulse widths can be best achieved with shorter lengths of fibre but this is at the expense of peak power.

The accuracy of this theoretical value for the peak power is influenced by the following factors:

1) The model assumes negligible excited state absorption. However the characteristic green glow from the Erbium fibre is evidence that this is not the case. It has been shown that excited state absorption from the upper pump level can play a part in reducing the pump efficiency thus explaining the disparity between the model and experimental results. [8]
2) An uncertainty exists when measuring experimentally fibre parameters such as dopant concentration and emission/absorption cross-sections.
3) The dopant profile tends to be lower in the centre of the fibre core where the single mode signal intensity is a maximum. This non-uniform dopant profile tends to produce a lower population inversion experimentally than the model would predict.
4) Due to the high Erbium concentrations needed for short pulse, high power operation, a reduction of the pump efficiency is often observed due to the process of co-operative up-conversion [8].

The other important parameter which is modelled is the output reflectivity. This is another parameter which, in common with fibre length, can be modified to obtain optimum Q-switched laser performance. Figure 4-13 shows the results of modelling the effect of output mirror reflectivity on peak power and pulse width for a fixed fibre length of 1.0metre. The output mirror reflectivity has no effect on the amount of stored energy within the cavity, as theoretically the mirror would not be visible through the Q-switch in its high loss state. It does however effect the laser threshold (i.e. when the round trip gain equals the losses), by introducing a loss into the cavity, this in turn limits the maximum photon density within the cavity.

The operation of the acousto-optic modulator in first order introduces a round-trip loss equal to the insertion loss x (diffraction efficiency)^2, and is typically 6dB. This is a major intra-cavity loss which corresponds to 75% signal loss per round trip.

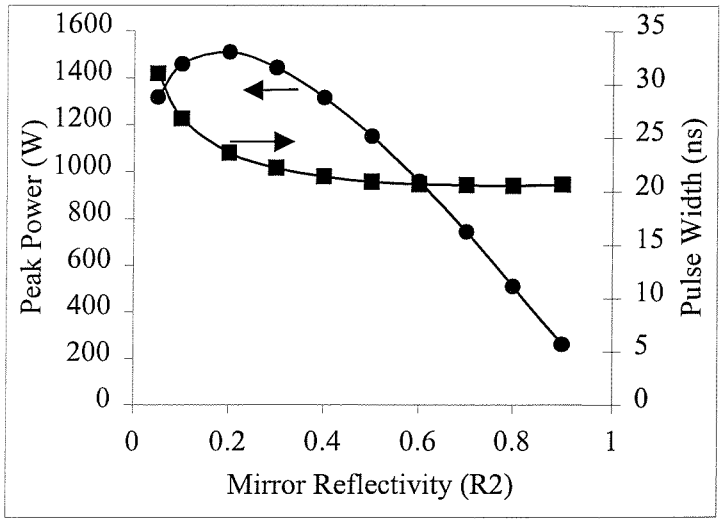

Figure 4-13 *- Dependence of the Peak Power and Pulse Width of a Q-switched fibre laser on Output Coupling (Fibre Length – 1 metre, 6dB intra-cavity round trip loss)*

If the laser cavity consists of a low reflectivity mirror, the output coupling (loss) is high, this produces a higher threshold and therefore lower peak powers. Because the peak powers are lower, more round trips are needed to deplete the stored energy, and therefore longer pulse widths are predicted. As the mirror reflectivity is increased (loss decreases), the threshold goes down and the maximum photon density increases. However due to the high intra-cavity losses, the fraction of this light being emitted as the output laser pulse is reduced and therefore lower peak powers are observed.

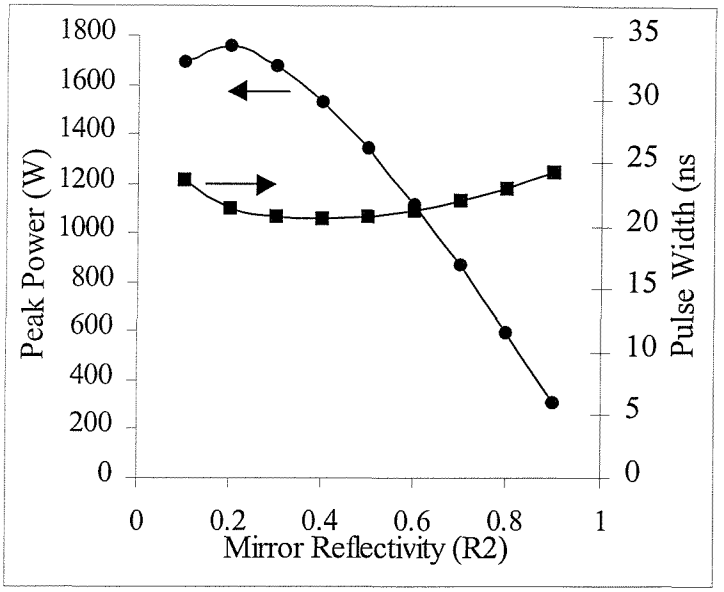

Figure 4-14 *- Dependence of the Peak Power and Pulse Width of a Q-switched fibre laser on Output Coupling (Fibre Length – 1 metre, 3dB intra-cavity round trip loss)*

If, as in Figure 4-14 the intra-cavity losses are decreased, then at high mirror reflectivities (low output coupling) the pulse width again starts to increase. The lower intra-cavity losses and low output losses requires more round-trips to extract the stored energy and an increase in pulse width is observed.

4.3.4 Modelling a Large Mode Area Q-switched Erbium doped Fibre Laser

In the earlier discussion (Section 4.2.3) of gain saturation it was suggested that the saturation power could be increased by using a fibre with a large core area. This fibre type would be beneficial for a Q-switched laser as it would increase the threshold at which gain saturation caused by ASE would occur and therefore increase the magnitude of the stored energy. A larger core area has the added benefit of increasing the threshold at which non-linear Raman and Brillouin effects occur. These non-linear effects reduce efficiency by shifting the intra-cavity power to other wavelengths. Section 4.2.3 calculates the saturation intensity for an Erbium fibre to be $1kW/cm^2$. Therefore a fibre with a $58\mu m^2$ core area gives a saturation power of 0.6mW, increasing to a saturation power of 2.1mW for a $203\mu m^2$ core area.

To make a theoretical comparison between the normal Erbium doped fibre and large mode area (LMA) fibre we will compare systems which operate with the same absorbed pump power. However, due to the increased pump absorption caused by the larger core area, the pump power is increased to 100mW from the 45mW used in the previous models. Lengths of 2.05m of conventional Erbium doped fibre and 1.62m of large mode area fibre were used with 75mW of absorbed pump power.

The parameters used in the model are shown in the table below. The N.A, V-number and core radius were chosen to match the fibres that were used experimentally.

Normal Erbium Doped Fibre	Large Mode Area Fibre
N.A. = 0.15	N.A. = 0.08
Core Radius = 2.5μm	Core Radius = 7.4μm
Effective Core Area = 58μm^2	Effective Core Area = 203μm^2
V = 1.52	V = 2.4
Length = 2.05m	Length = 1.62m
Absorbed Pump Power = 75mW	Absorbed Pump Power = 75mW

Table 4-4 *– Parameters of Normal and Large Mode area Erbium doped Fibre used in the Model*

The principle behind using a large mode area (LMA) fibre is to reduce the small signal gain whilst increasing the amount of stored energy within the fibre. The large core area reduces the pump intensity within the core, this in turn generates a lower population inversion density which suppresses the generation of amplified spontaneous emission. This is illustrated in Figure 4-15 which shows the population densities of both the upper and lower levels for conventional Erbium fibre and large mode area fibre.

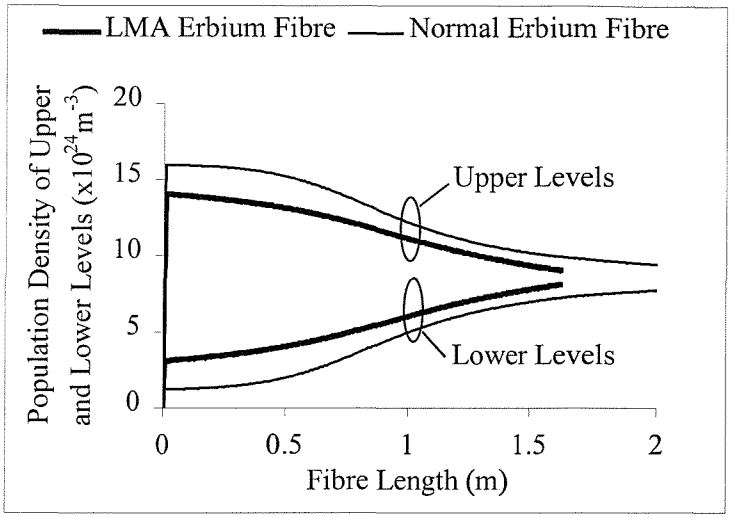

Figure 4-15 *– Variation of the population density of the upper and lower levels for both conventional and large mode area Erbium doped fibres along a length of fibre. The length of each fibre is optimised for equal pump absorption*

The lower population inversion density has the effect of suppressing the amplified spontaneous emission generated along the Erbium doped fibre, this is illustrated in Figure 4-16 which shows the build up of the amplified spontaneous emission for both the large mode area and normal Erbium doped fibres.

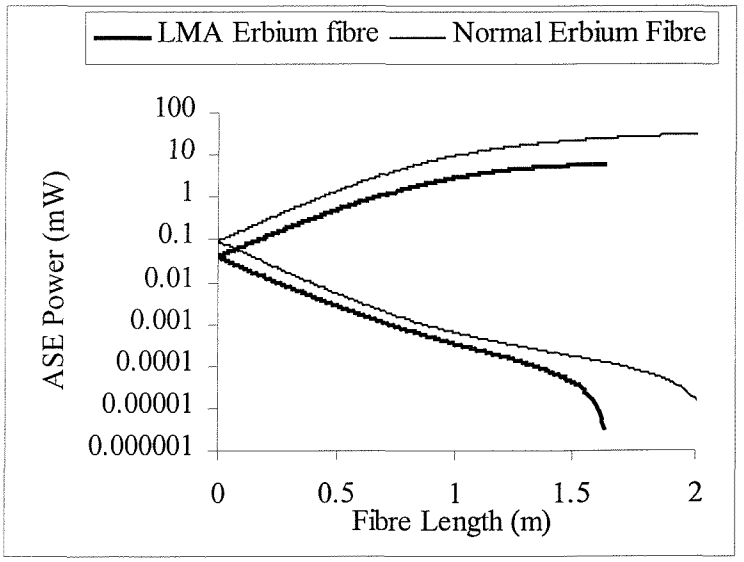

Figure 4-16 *– Variation of forward and backward ASE along a length of LMA and conventional Erbium doped fibre. The length of each fibre is optimised for equal pump absorption*

Although the lengths of the two fibres are optimised to have the same amount of absorbed pump power, the large mode area fibre generates only 6mW of ASE compared to the 30mW generated in the normal Erbium doped fibre. The energy depletion by the ASE places a limit on the amount of stored energy which is available to the Q-switched laser. This is clear from the results shown in Table 4-5. This table shows the modelled Q-switched performance using both the LMA and normal fibres at a fixed absorbed pump power.

Normal Erbium Doped Fibre	Large Mode Area Fibre
Peak Power = 757W	Peak Power = 2219W
Pulse Width = 40ns	Pulse Width = 35ns
Pulse Energy = 31μJ	Pulse Energy = 77μJ

***Table 4-5** – Table showing theoretical Q-Switched results for both normal and large mode area Erbium fibres at a fixed absorbed pump power*

The theoretical results for the LMA Erbium doped fibre show a twofold increase in the peak power extracted from the laser over that obtained using a standard Erbium doped fibre.

4.4 Conclusions

In this chapter a model for a Q-switched Erbium doped fibre laser has been developed. The model was developed by calculating the stored energy in a length of pumped fibre using a standard rate equation analysis and then modifying this to account for the presence of laser mirrors. These reflect amplified spontaneous emission into the cavity thus reducing further the stored energy. The magnitude of the population inversion (stored energy) is then used in a lumped element, rate equation approach to model the Q-switched behaviour.

The results from the model were used to show the variation in laser performance with both fibre length and repetition rate and to confirm that a large mode area fibre could be used to generate higher energy pulses.

4.5 References

[1] J.Armitage: 'Three-level fiber laser amplifier: A Theoretical model', *Applied Optics*, Vol.27, No.23, pp.4831-4836, (1988)

[2] E.Desurvire, C.R.Giles, J.R.Simpson and J.L.Zyskind: 'Efficient Erbium doped fibre amplifier at a 1.53μm wavelength with a high output power', *Optics Letters*, Vol. 14, No.22, pp.1266-1268, (1989)

[3] C.Giles and E.Desurvire: 'Propagation of Signal and Noise in Concatenated Erbium Doped fibre Optical Amplifiers', *Journal of Lightwave Technology*, Vol.9, No.2, pp.147-154, (1991)

[4] C.J.Gaeta, M.J.F.Digonnet and H.J.Shaw: 'Pulse Characteristics of Q-switched Fiber Lasers', *Journal of Lightwave Technology*, Vol.5, No.12, pp.1645-1651, (1987)

[5] A.Siegman: 'Lasers', *University Science Books*, ISBN 0-935702-11-5, (1986)

[6] M.N.Zervas and R.I.Laming: 'Efficient Erbium-Doped Fibre Amplifiers Incorporating an Optical Isolator', *IEEE Journal of Quantum Electronics*, Vol.31, No.3, pp.472-480, (1995)

[7] J.T.Verdeyen: 'Laser Electronics: Third Edition', *Prentice Hall*, ISBN 0-13-706666-X, (1995)

[8] R.S.Quimby, W.J.Miniscalco and B.Thompson: 'Quantitative characterization of clustering in Erbium doped silica glass fibres', *Fibre Laser sources and Amplifiers*, SPIE '93, Vol.2073, Paper 1, (1993)

[9] P.Roy and D.Pagnoux: 'Analysis and Optimisation of a Q-switched Erbium doped Fibre Laser Working with a Short rise time modulator', *Optical Fibre Technology*, Vol.2, pp.235-240, (1996)

[10] R.J.Beach: 'Optimisation of Quasi-Three level end-pumped Q-switched Lasers', *IEEE Journal of Quantum Electronics*, Vol.31, No.9, pp.1606-1613, (1995)

[11] C.D.Nabors: 'Q-switched Operation of Quasi-Three-Level Lasers', *IEEE Journal of Quantum Electronics*, Vol.30, No.12, pp.2896-2901, (1994)

[12] J.Nilsson and B.Jaskorzynska: 'Modelling and Optimisation of low-repetition-rate high-energy pulse amplification in cw-pumped Erbium doped Fibre Amplifiers', *Optics Letters*, Vol.18, No.24, pp.2099-2101, (1993)

Chapter Five

Experimental Investigation of Q-Switched Fibre Lasers

5.1 Introduction

This chapter describes the experimental work carried out with regards to Q-switched fibre laser sources for distributed sensing. It describes in detail the component requirements and the advantages and disadvantages of each component with respect to the different configurations of Q-switched fibre lasers. A number of Q-switched fibre lasers optimised for various applications requiring high pulse energies, narrow linewidth and short pulse duration are investigated.

5.2 Basic Design

The basic design for an Erbium doped fibre laser can be either an end-pumped Fabry-Perot configuration or, alternatively, a ring configuration. The simpler design of the Fabry-Perot configuration makes this preferable over the ring laser configuration. A basic Q-switched Erbium doped fibre laser utilising a Fabry-Perot cavity is shown in Figure 5-1. It consists of a 980nm pump laser, two mirrors which define the cavity and a Q-switch. The following section investigates each of these components in turn.

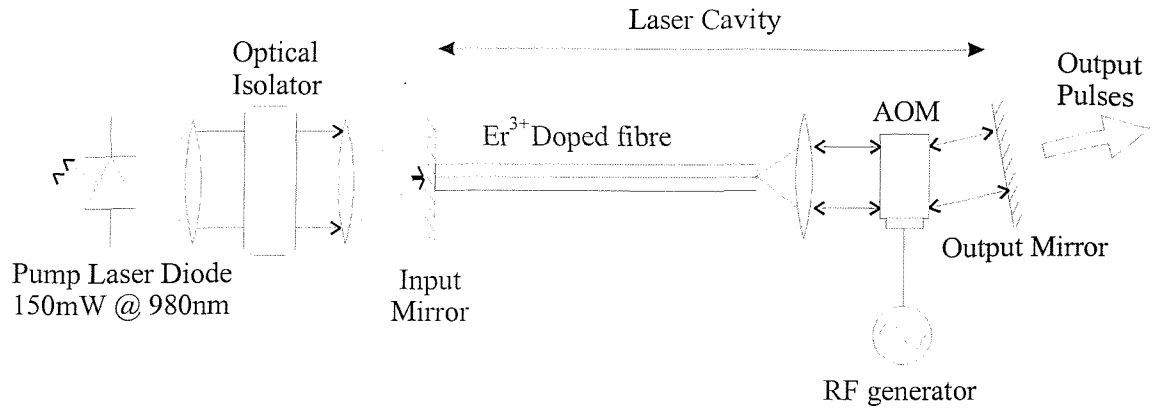

Figure 5-1 *– A schematic of a Q-switched Erbium doped fibre laser, using a bulk 980nm laser diode as the pump laser.*

5.3 Components

This section studies each of the laser components in turn and discusses the relative merits of possible alternatives for each component.

5.3.1 Pump Lasers

As discussed previously (section 2.2.2.1), for long range sensing applications, the wavelength of operation required for the Q-switched laser is 1.55μm. This limits the fibre dopant to an Erbium based system. The pump levels for the Erbium system have been widely explored in past publications [1][2][3]. In conclusion, these publications demonstrate that the most efficient pump wavelength for Erbium doped amplifiers and lasers is in the 980nm wavelength band.

At the start of this work (1994), 980nm laser diode technology was a rapidly developing technology, driven by the widespread success of the Erbium doped fibre amplifier for telecommunications applications. The following sections briefly summarise the advances of 980nm pump lasers and their effect on this research.

5.3.1.1 Bulk 980nm

The first 980nm pump laser used in this work was a 150mW device (Spectra Diode Labs, SDL-6572-H1) mounted in a bulk H1 can. The disadvantages of these first laser diodes are twofold. Firstly, the output beam of the diode is elliptical which limits the launch efficiency into a circular core; typically out of the 150mW available power only 90mW of this could be launched into the fibre. Methods of launching the light into the core using cylindrical lenses to compensate have been used but with limited success. Secondly, the laser diodes were sensitive to back reflections from the fibre end and therefore had to be used in conjunction with an optical isolator.

However, these bulk devices do have some advantages in a research and development environment, in situations which involve the use of non-standard fibre (i.e. large mode area fibre). In these cases, the alternative pigtailed laser diodes were unsuitable because of the mode mismatch which occurs between two dissimilar fibres. Another scenario in which bulk laser diodes are advantageous is for short cavity lasers. The WDM component needed to launch light from a pigtailed laser diode into the doped fibre can account for a major part of the cavity length. This is particularly the case when using Erbium/Ytterbium doped fibre which has a very short (~cms) absorption length at 980nm. The output characteristics of the bulk 980nm laser used in this work (SDL-6572-H1) are shown in Figure 5-2.

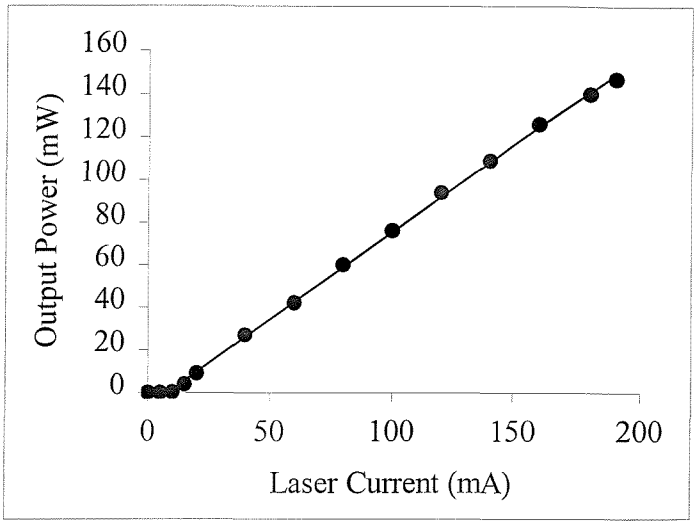

Figure 5-2 *– A plot showing the laser output power against drive current*

5.3.1.2 Pigtailed 980nm

Pigtailed 980nm laser diodes started to emerge onto the market at a reasonable price in early 1992 and offered increased in-fibre power. Modern fibre pigtailed laser diodes can provide in-excess of 165mW of 980nm into the fibre (Spectra Diode Labs, SDLO-2500-165), and are relatively immune to back reflections even in the absence of fibre isolators. Grating wavelength stabilised devices are available which can be operated without a cooler, thus reducing power consumption and the electronics needed to control the cooler, thus offering significant cost savings. Unless the application warrants the use of a bulk 980nm pump device, these pigtailed devices are ideal for pumping both Erbium amplifiers and lasers.

5.3.1.3 MOPA 980nm

A recent advance from the simple 980nm pump laser is the introduction of an additional semiconductor amplifier at 980nm. This is known as a MOPA configuration (Master Oscillator, Power Amplifier). A MOPA has significantly higher powers than conventional 980nm laser diodes, with bulk devices emitting powers in excess of 1Watt in a single transverse mode. Fibre pigtailed versions with minimum powers of 500mW are also available. The disadvantage of using MOPA configurations are twofold: firstly the high

cost, and secondly, the sensitivity of the devices to back-reflections. The amplifier stage before the chip can also act to amplify back reflections, which can build to high intensities and damage the mirrors of the laser oscillator. The reliability of these lasers is still questionable.

5.3.2 Mirrors

The laser cavity consists of two mirrors one of which will form the output coupling, the other will be a high reflector. Here we will discuss the relative merits of the most common types of fibre laser mirror.

5.3.2.1 Dielectric multi-layer coatings.

The usual method of providing a cavity end mirror involves placing the fibre in contact with a substrate coated with a dielectric film with the required characteristics. The coupling is usually unstable, suffers from poor repeatability and the surface is easily damaged by the fibre end. A better solution is to coat the end of the fibre directly. This can be achieved by first placing the fibre into a ferrule and then depositing the coating onto the end of the ferrule. This produces a much more stable configuration with the repeatability depending on the coating process. Although the cost for a coating run is expensive it is possible to simultaneously coat in excess of 100 ferrules in one batch, therefore the unit cost is significantly lower than buying bulk mirrors. One major problem using two bulk mirrors in a fibre laser geometry is that the output of the laser will not be in-fibre. The majority of fibre laser applications require the output to be in-fibre, the next sections investigate mirror configurations which are fibre compatible.

5.3.2.2 Bragg Gratings

The recent interest in photorefractive fibre Bragg gratings for dispersion compensation [4] and add/drop multiplexing for dense WDM communications [5] has decreased the price and increased the availability of these devices which are ideal for use as fibre laser mirrors. These devices consist of a periodic modulation in the refractive index of the core. This is

produced by exposing the core to an interference pattern created from a UV laser using either; a phase mask or the interference of two coherent beams. This periodic modulation produces a reflection when the Bragg criterion is met (5-1),

$$\lambda_B = 2 \cdot n \cdot \Lambda \qquad (5\text{-}1)$$

where λ_B is the Bragg wavelength at which maximum reflection occurs, n is the refractive index and Λ is the period of the index modulation.
The wavelength, reflectivity and bandwidth of the in-fibre gratings can be tailored to the specific application.

5.3.2.3 Sagnac Loop Mirrors

This device consists simply of two legs of a fused fibre coupler connected together, thus it is cheap, rugged and the coupling ratio can be tailored to produce the required reflectivity [6]. The relationship between the reflectivity, R, of the Sagnac loop mirror and the coupling factor, f, of the coupler is given by:

$$R = 4f \cdot (1 - f) \qquad (5\text{-}2)$$

Hence a 90/10 coupler will be equivalent to a 36% reflecting mirror. This formula however is only valid for small signal powers. At higher powers the coupling ratio becomes dependent upon the intensity of the light. This intensity dependence of the coupling ratio arises from the intensity dependence of the refractive index of the fibre. The intensity dependence of the refractive index leads importantly to an intensity dependent phase shift known as self-phase modulation.

Consider a coupler of length, L, with a coupling factor of f and incident power P_0. The reflectivity of the loop mirror is calculated by calculating the phase shifts acquired by the two counter-propagating waves and recombining them interferometrically back at the coupler. This results in an expression for the reflectivity of the coupler taking into account the non-linear phase shift generated by the intensity dependence of the refractive index:

$$R = 2f(1-f)(1+\cos((1-2f)\gamma P_0 L)) \qquad (5\text{-}3)$$

where γ is the non-linearity coefficient (5.135 $watt^{-1}$ km^{-1} [7]), P_0 is the incident power (watts) and L is the length of the loop. This effect is illustrated in Figure 5-3 which shows theoretically how the reflectivity of a Sagnac loop mirror made of a 90/10 coupler varies with power. The plot clearly illustrates that the reflectivity of the loop mirror falls from the 36% for small signals to 24% for a power of 150watts.

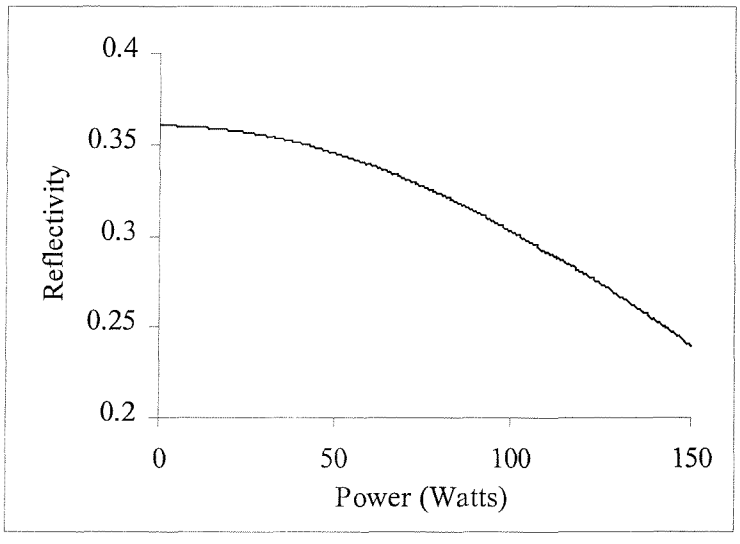

Figure 5-3 *– A theoretical plot showing the effect of SPM on the reflectivity of a Sagnac loop mirror of length 2metres*

In addition, due to self phase modulation, the reflectivity of the Sagnac loop mirror will vary over the pulse duration (see Figure 5-4).

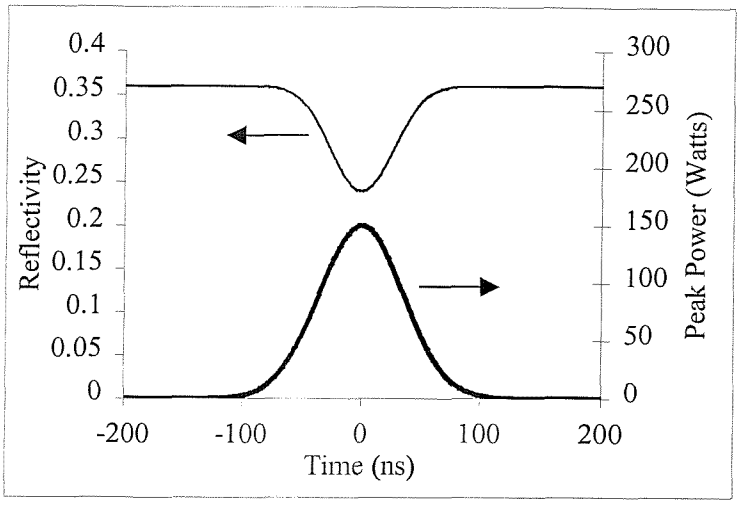

Figure 5-4 *– A theoretical plot showing a Gaussian pulse of peak power 150Watts and width 100ns with the reflectivity of a 2metre Sagnac loop mirror over the duration of the pulse*

At high pulse intensities or with long fibre loops, the effect of SPM becomes more apparent with the onset of a periodic structure when the phase difference approaches π. For a phase shift equal to π the reflectivity of the Sagnac loop is zero as illustrated in Figure 5-5.

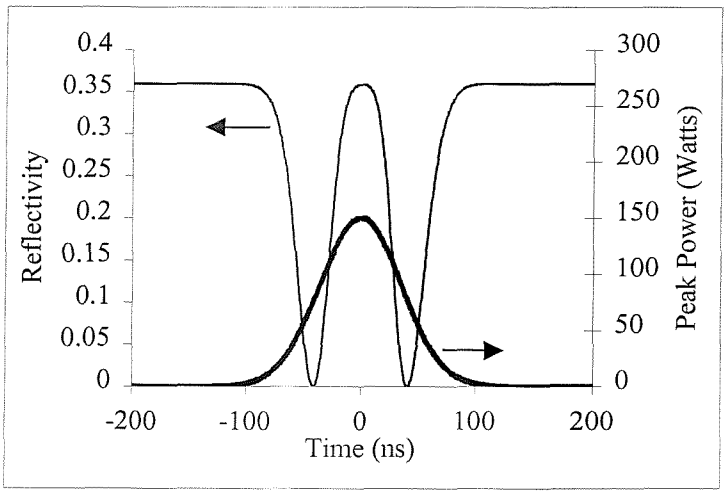

Figure 5-5 *- A theoretical plot showing a Gaussian pulse of peak power 150Watts and width 100ns with the reflectivity of a 10metre Sagnac loop mirror over the duration of the pulse.*

This large variation in the reflectivity of the Sagnac loop with intensity should be avoided to prevent pulse distortion. Therefore to implement a Sagnac loop mirror into a Q-switched laser system this effect has to be reduced to a minimum, this can be done by reducing the length of the loop, for example, a loop length of 200mm with a 90/10 coupler would exhibit a reduction in reflectivity from 36% to 35% at a power of 400Watts.

Provided these non-linear effects can be avoided, the Sagnac loop mirror offers an ideal, low cost, fibre compatible mirror.

5.3.3 Q-Switches

As discussed in section 3.3 there are only two methods of Q-switching which provide the required combination of high extinction ratio and fast rise time. The following paragraphs outline the characteristics of the devices used in this work.

5.3.3.1 Acousto-Optic

Throughout this program of research there have been continuous advances in acousto-optic modulator designs and specifications, including in-fibre acousto-optic modulators which offer faster rise times (<20ns) and increased convenience over the bulk devices. However, for the majority of the experiments carried out in this work, a bulk acousto-optic modulator was used which had the following specifications.

Type/Model	AA-GAS-25
Insertion Loss (dB)	0.1dB
Diffraction Efficiency	88%
Rise Time (ns)	100ns (from 10% to 90%)
RF Frequency (MHz)	110MHz
RF Drive Power	1Watt

***Table 5-1** – Acousto-Optic modulator specifications*

The plots below show the experimentally determined rise time and the diffraction efficiency of the acousto-optic modulator. The measurements were taken using a CW Erbium fibre laser to provide the 1.5μm light, which is then passed through the modulator. The rise time, from the 10% to 90% intensity values was measured to be 98ns with a diffraction efficiency of 80%. The rise time was measured using a 300μm InGaAs detector with a 50Ω resistance and a capacitance of 4.7pF.

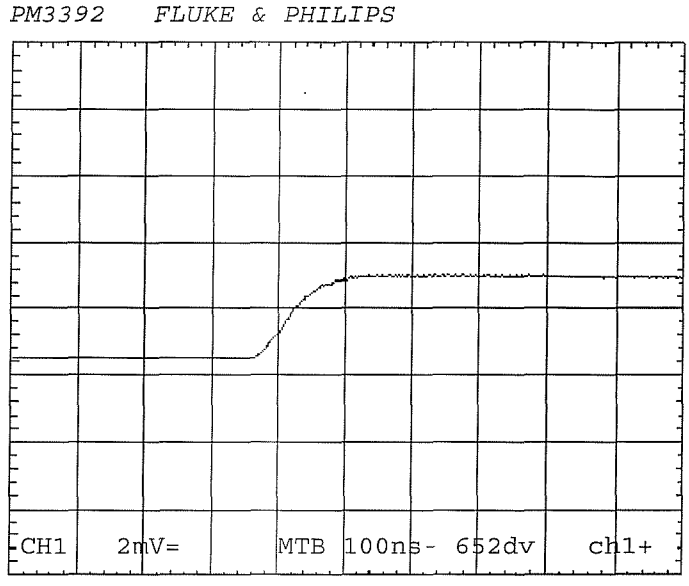

Figure 5-6 – *Rise time of the bulk AOM used experimentally*

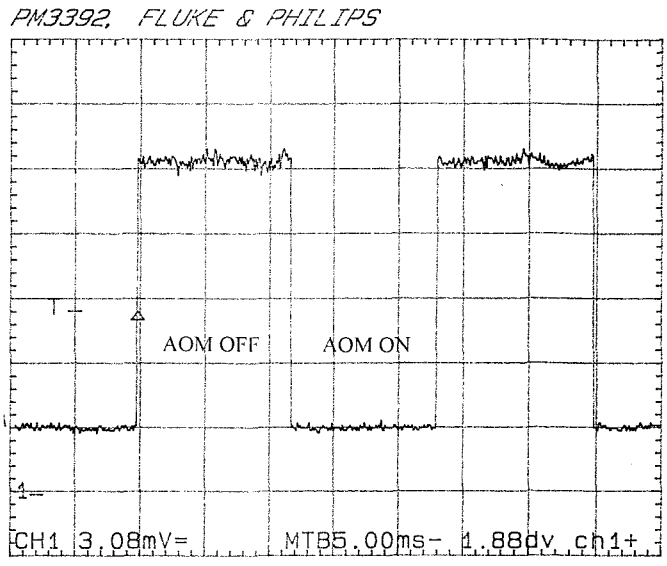

Figure 5-7 *– A plot showing the diffraction efficiency of the AOM. When the AOM is on, the intensity reduces to approximately 80% of it's value when off. Zero is indicated by '1-' in the lower left of the scope trace.*

5.3.3.2 Electro-Optic

Although acousto-optic modulators are becoming faster and more efficient, for the fastest switching times electro-optic modulators remain the only option. The electro-optic modulator used in this work was a Quantum technology Lithium Niobate based device, which has a rise time of 4ns, as illustrated in Figure 5-8. The problems presented by the use of the electro-optic modulator stem from the high voltages needed for its operation. For optimum Q-switched operation a voltage of 4.6kV is required, this introduces a large electrical noise spike on the detectors for the duration of the electrical pulse. Efforts to reduce this noise were attempted (i.e. proper insulation of the detectors and shielded cables) but with limited success. Other aspects of the electro-optic modulator that make it unsuitable for commercial applications are its high cost and limited repetition rate (1kHz).

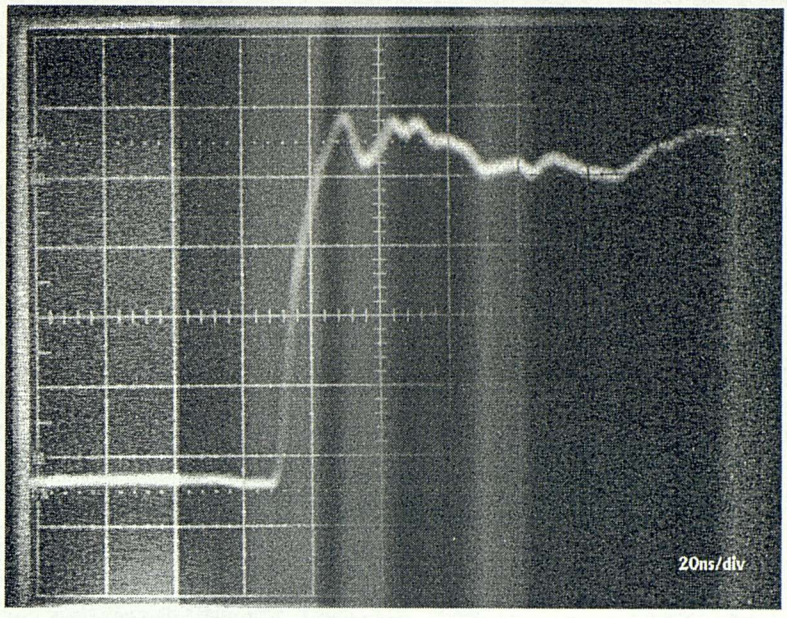

Figure 5-8 *- Rise time of the electro-optic modulator used experimentally*

5.3.4 Methods of reducing feedback from the fibre end

Due to the high gain of the Erbium fibre, the 4% reflection from the air/fibre interface is often sufficient to start lasing which depletes the population inversion. There are several methods of reducing this effect. Two different methods were attempted, 1) the addition of a cover slip to the fibre end, and 2) an angle polished fibre end.

5.3.4.1 Cover Slip

The purpose of a cover slip is to reduce the amount of light reflected back into the fibre, as illustrated in Figure 5-9.

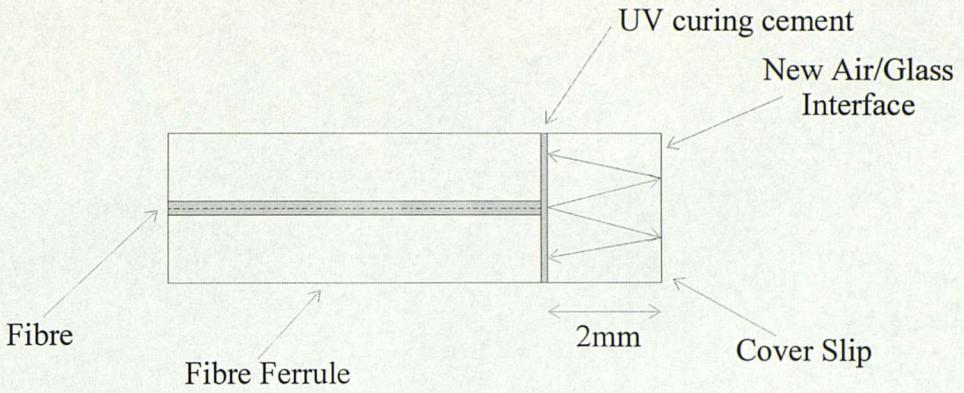

Figure 5-9 *– Schematic showing the use of a cover slip to reduce fibre end reflections*

This is achieved by bonding a small circular patch of glass, index matched to the core, onto the front face of a ferrule which holds the fibre (Figure 5-9). This has the effect of moving the air/glass interface away from the end of the fibre therefore reducing the amount of light reflected back down the fibre.

Using a cover slip in this manner, the Q-switched fibre laser produced pulses for a short duration (approx. 2-3 seconds) and then failed. Upon inspection of the cover slip, small black marks were seen within the UV curing cement which holds the cover slip in position. These were assumed to be formed due to the high power densities created by the Q-switched laser pulses adversely affecting the adhesive.

A similar method of removing the reflection from the end of the fibre is to physically bond the fibre to an intra-cavity GRIN lens, the air/fibre interface is therefore moved to the end of the GRIN lens in a similar manner to the operation of the cover slip. The bonding to the GRIN lens is not carried out with UV curing cement but instead by fusing the fibre to the lens using a low current arc [8].

5.3.4.2 Angled Polished Fibre End

This method requires that the end face of the fibre is polished/cleaved at an angle to prevent any reflected light re-entering a propagating mode of the fibre [9]. Figure 5-10 shows a schematic of a fibre end which is polished at an angle α.

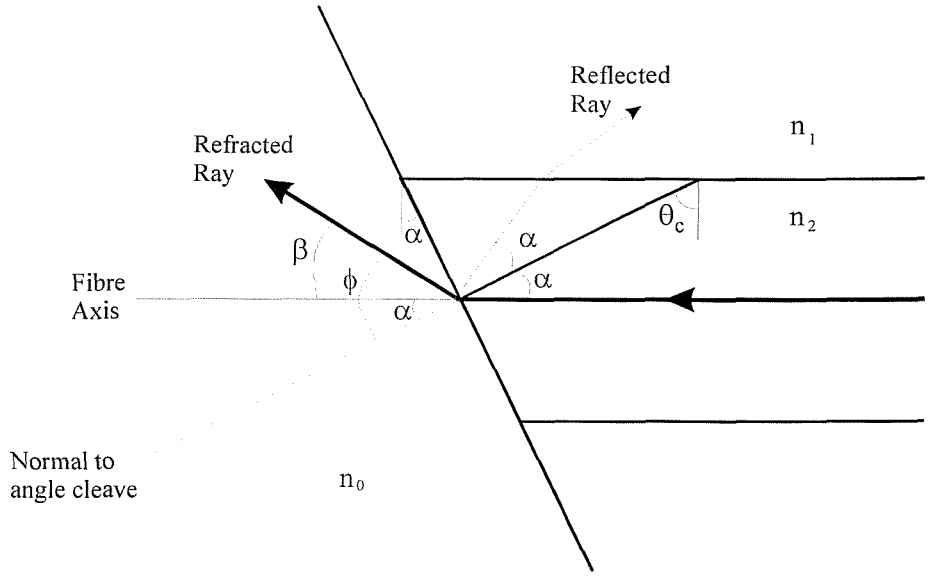

Figure 5-10 *– Schematic of an angle polished fibre end*

Figure 5-10 shows the propagation of a ray running parallel to the fibre axis, including the diffracted and reflected components at the core/air interface, it also shows the ray at the critical angle which defines the ray angles which will be propagated by total internal reflection. The minimum angle required to prevent any reflections from the fibre end entering a propagating mode of the fibre may be simply derived using Snell's law at the core/cladding interface and assuming $n_2 > n_1$. The critical angle is defined as:

$$\sin(\theta_c) = \frac{n_1}{n_2} \qquad (5\text{-}4)$$

And similarly at the core/air interface:

$$n_0 \sin\phi = n_2 \sin\alpha \qquad (5\text{-}5)$$

The critical angle can be written in terms of α as $\theta_c=\pi/2-\alpha$, substituting this into equation (5–3), we obtain the expression for α in terms of n_1 and n_2.

$$\cos(\alpha) = \frac{n_1}{n_2} \qquad (5\text{-}6)$$

Therefore if the core and cladding refractive indices are 1.51 and 1.5 respectively then α, the minimum polishing angle is 6.6°.

A disadvantage with angle polishing is that the beam exits the fibre at an angle which makes alignment more difficult. The angle at which the fibre needs to be angled for efficient coupling, β, is equal to $\phi-\alpha$. From equation (5-4) and assuming small angles such the $\sin(\theta)=\theta$ and $n_0=1$, we have $\phi=n_2\alpha$, and now subtracting α from each side we have:

$$\begin{aligned} \beta &= \phi - \alpha \\ &= n_2\alpha - \alpha \\ &= \alpha(n_2 - 1) \end{aligned} \qquad (5\text{-}7)$$

If n_2 is approximately 1.5 then $\beta=\alpha/2$, so therefore the fibre has to be angled at an angle half of the polishing angle, i.e. at least 3.3°.

The previous analysis only represents an approximation which is sufficient for most purposes. For a more accurate description, diffraction effects at the fibre/air interface must be included in the analysis [9].

5.4 Experimental Results from an Erbium doped Q-switched Fibre Laser

After introducing the components required for a Q-switched laser design, this section reports on the experimental investigation of the properties of Q-switched Erbium doped fibre lasers.

5.4.1 Experiment

The basic experimental arrangement for the Q-switched laser is shown in Figure 5-11 and consisted of a fibre pigtailed 980nm pump laser, providing 90mW of 980nm pump power through a WDM into the Erbium doped fibre (ND899, Table 5-2). On one end of the Erbium doped fibre there was a highly reflecting mirror (R=99% at 1500-1550nm) which formed one end of the laser cavity whilst at the other end the light from the fibre was focussed through a bulk acousto-optic modulator operating in first order, on to an output mirror with a 25% reflectivity at 1500-1550nm, which formed the other end of the laser cavity. The starting cavity length was 4.6m which was made up of a length of 3m of Erbium doped fibre.

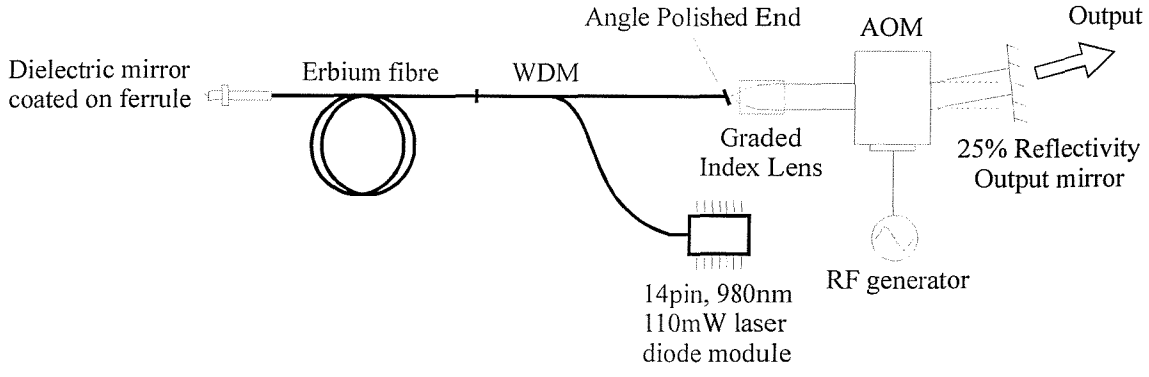

Figure 5-11 *- Schematic showing the Q-switched fibre laser configuration used to monitor performance changes with fibre length*

The Erbium doped fibre was angle polished to reduce the 4% Fresnel end reflection which because of the high gain of the Erbium doped fibre could cause laser action to take place between the high reflectivity mirror and the end-reflection.

Fibre Number	ND0899
Numerical Aperture	0.17
Cut-off Wavelength	940nm
Erbium Concentration	800ppm

Table 5-2 *– ND899 Erbium doped fibre specifications*

5.4.2 Results

During the course of this research a number of Q-switched lasers have been constructed with a wide variation of parameters to optimise different characteristics (e.g. high peak power or short pulse width). The results obtained and presented in this section are those using the Q-switched configuration described previously (section 5.4.1) but are compared wherever appropriate with results from other configurations in order to enhance the results and clearly illustrate the trends in design.

5.4.2.1 Variation of Peak power and Pulse width with Fibre Length

The variation of peak power and pulse width with fibre length can be considered as one of the most important trends to understand because it has a major effect on the performance of the Q-switched laser. Figure 5-12 shows the variation of peak power and pulse width with fibre length for two sets of data corresponding to the two different configurations which are summarised in Table 5-3. The two configurations differ in three main aspects, with configuration 2 having a lower launched pump power, higher output mirror reflectivity and shorter cavity length.

	Configuration 1 as described in the previous section	Alternative Configuration 2
AOM mode of operation	First Order	First Order
AOM type	Bulk AOM (5.3.3.1)	Bulk AOM (5.3.3.1)
Pump Laser	Pigtailed 980nm (5.3.1.2) Launched Pump 90mW	Bulk 980nm (5.3.1.1) Launched Pump 37mW
Output Mirror reflectivity	25%	50%
Cavity Length (excluding the Erbium doped fibre)	1.6metres	0.65metres

Table 5-3 *- Table showing the parameters of the two Q-switched laser configurations which are used to obtain the results shown in Figure 5-12*

Looking initially at the results obtained from Configuration 1, it can be seen that there exists an optimum Erbium doped fibre length to achieve maximum peak output power, away from which the peak power falls off rapidly (Figure 5-12). The initial increase in peak power with Erbium fibre length is due to the increase in the magnitude of the stored energy in the fibre. Beyond the optimum fibre length (determined by the available pump power and the saturation of the gain by ASE) a drop in peak power occurs due to re-absorption of the signal from the unpumped sections of fibre.

The variation of the pulse width with Erbium fibre length is also shown in Figure 5-12, again an optimum fibre length exists at which the pulse width is a minimum. For fibre lengths shorter that this optimum length an increase in pulse width is observed. This increase is attributed to the lower round trip gain of the cavity; i.e. more round-trips are required for the pulse to build-up and to deplete the inversion to below threshold. For Erbium fibre lengths longer than the optimum length an increase in pulse width is again observed, this is attributed to the increase in round trip time.

As the Erbium length increases past the optimum length, a sudden shift in wavelength is observed from 1530nm to 1560nm (shaded area). This change in operating wavelength is due to the preferential absorption/loss at the shorter 1530nm wavelengths by unpumped lengths of fibre [10][11]. A detailed investigation into the variation of operating wavelength with cavity parameters is carried out in section 5.4.2.3.

The results obtained demonstrate the importance of optimising the length of Erbium fibre for the available pump power, a discrepancy of 25% of the optimum length can cause dramatic swings in the peak power.

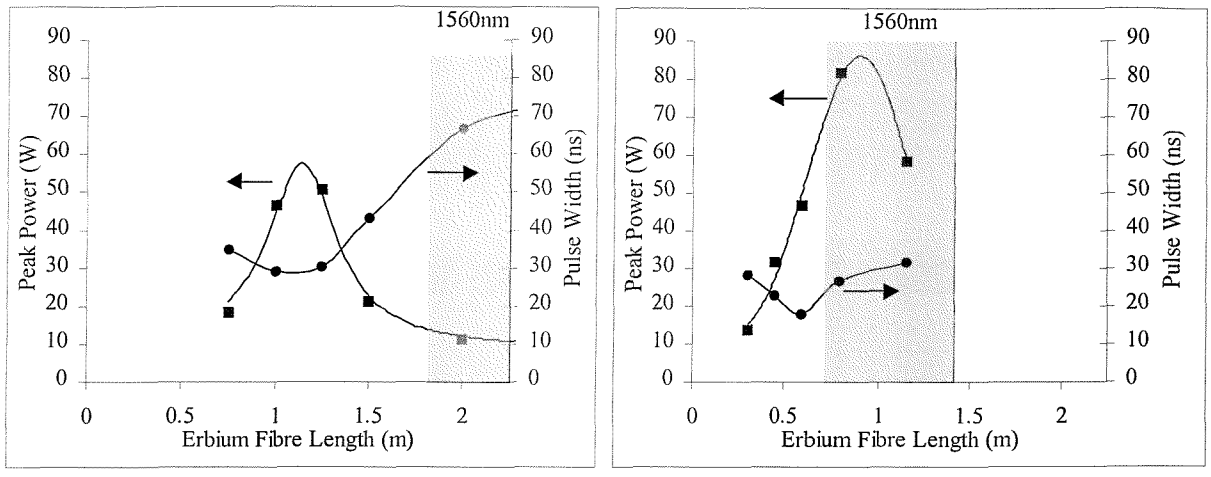

Configuration 1 *Configuration 2*

***Figure 5-12** - Plot showing the variation of peak power and pulse width with Erbium fibre length for two laser configurations*

The higher peak powers observed using configuration 2 can be attributed to two main factors:

1) For a given Erbium fibre length, the Erbium doped fibre occupies a larger percentage of the overall cavity length in configuration 2 than it does in configuration 1. This leads to the observed shorter pulses and higher peak powers.
2) The higher mirror reflectivity in configuration 2 coupled with the high intra-cavity losses due to operation of the AOM in first order can also explain the higher peak powers. This is theoretically modelled in section 4.3.3..

The results obtained experimentally (Figure 5-12) show good correlation with the trends explored theoretically in Chapter 4 (Figure 4-12).

5.4.2.2 Variation of Peak Power and Pulse Width with Repetition Rate

The variation of peak power and pulse width was measured as a function of repetition rate and the results are shown in Figure 5-13. These results were obtained using two arbitrary Erbium fibre lengths (80cms and 115cms). The peak power starts to decrease at a repetition rate of above approximately 1kHz, this decrease corresponds to a lifetime of 1ms for the Erbium ions. This is not consistent with the measured lifetime of Erbium ions of 10-12ms [12]. The lifetime appears shorter in a fibre laser/amplifier due to the presence of ASE which effectively shortens the lifetime of the ions in the metastable level.

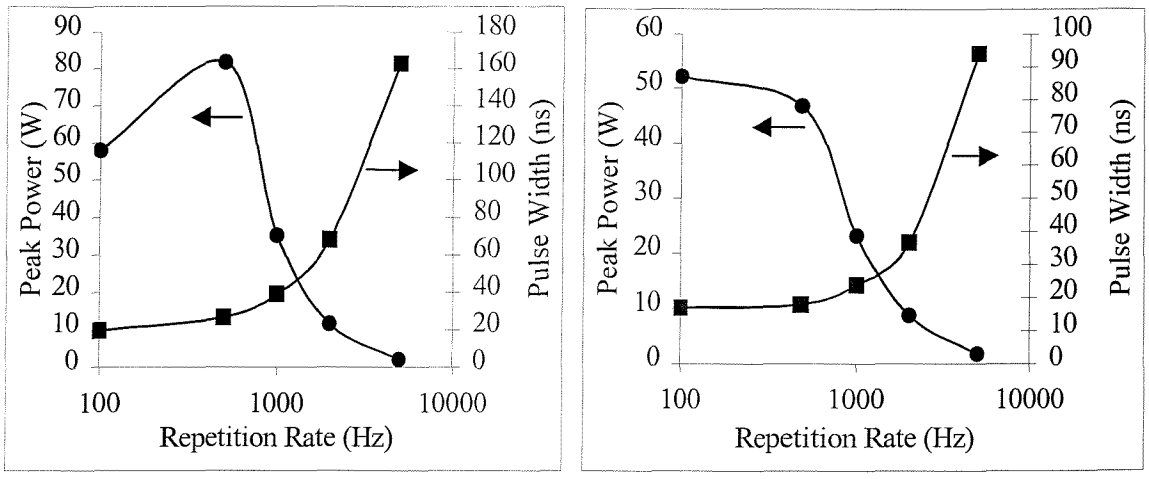

(a) Fibre Length 80cms (b) Fibre Length 115cms

Figure 5-13 *- Plots of Peak Power and Pulse Width as a function of repetition rate for two different fibre lengths (results obtained using Configuration 2)*

5.4.2.3 Variation of Lasing Wavelength for both CW and Q-switched operation

The gain profile of Erbium fibre covers the wavelength range 1520-1570nm allowing a laser to operate within this region depending upon the cavity configuration. The fibre length and pump power are critical parameters in a three level laser when determining the wavelength of operation. A laser with a long Erbium fibre length will operate at a longer wavelength due to the preferential re-absorption of the shorter wavelengths in the un-pumped section of fibre. This is illustrated in Figure 5-14 which shows the variation in spectral output of four

fibre lasers under CW operation with different Erbium fibre lengths (0.75m, 1.25m, 2m and 3m). Increasing the length of the Erbium fibre causes the wavelength of operation to shift to longer wavelengths.

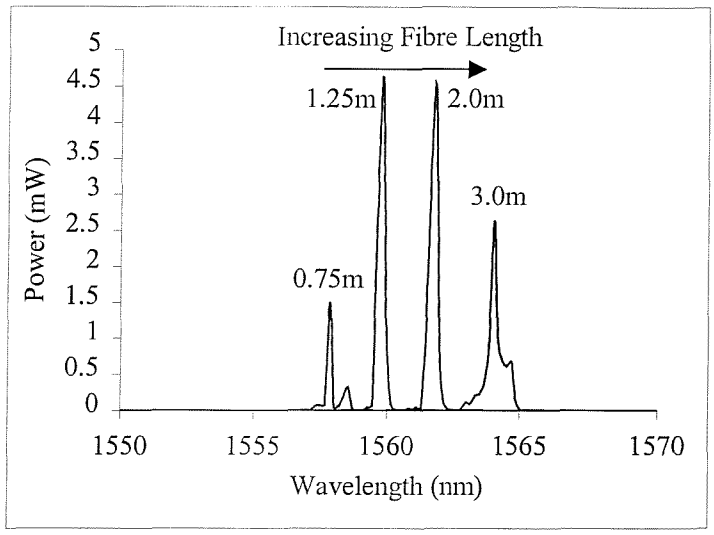

Figure 5-14 *– Variation in spectral output of CW Erbium doped fibre lasers for different fibre lengths (0.75m, 1.25m, 2m and 3m)*

Unlike CW fibre lasers, Q-switched fibre lasers generally operate at the shorter wavelength of 1.53μm. This can be explained by considering the cavity when it is in the high loss state, i.e. when there is no feedback from one of the mirrors. In this state there is no population inversion depletion due to an intra-cavity signal and therefore a higher population inversion can be generated within the fibre. This higher population inversion promotes operation at the shorter wavelengths.

However the operating wavelength of the Q-switched laser is dependent on a number of other parameters including the repetition rate and cavity losses. If an acousto-optic modulator is used the cavity losses will depend on the mode of operation i.e. zero or first order.

Operating the laser in first order mode increases the cavity loss by a factor equal to the diffraction efficiency squared over operation in zero order. This increase in loss causes the

laser to operate at 1530nm due to the higher gain at this wavelength. Operating the laser in the lower loss zero order causes the laser to operate at 1560nm (Figure 5-15).

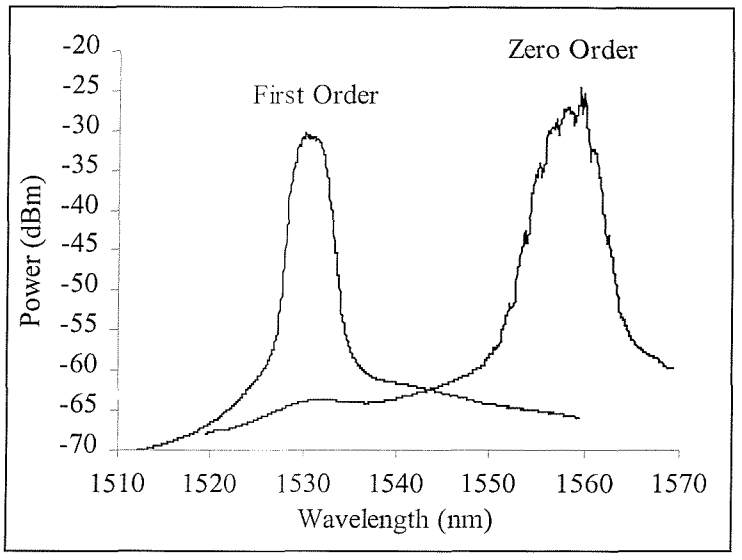

Figure 5-15 *– Plot showing the wavelength spectrum of the laser operating in either zero or first order mode (Erbium fibre length – 450mm)*

A laser operating in first order can also be forced to operate at 1560nm by increasing the length of the fibre beyond its optimum length or providing more gain so that the laser will again operate at the longer wavelength, as demonstrated experimentally from Figure 5-16.

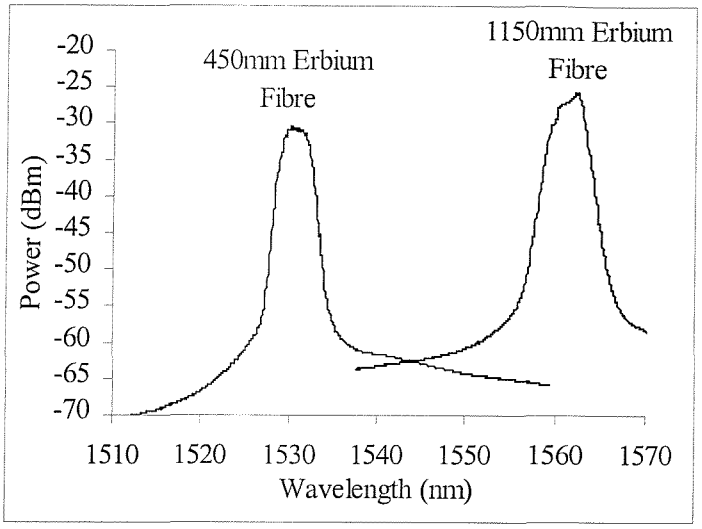

Figure 5-16 *– Variation in lasing wavelength for two Q-switched lasers with different lengths of Erbium doped fibre (First order operation)*

Finally one other factor which affects the operating wavelength of the Q-switched laser is the repetition rate. As discussed in section 5.4.2.2 the lifetime of the Erbium ions is approximately 1ms which corresponds to a maximum operating repetition rate of 1kHz. Beyond this rate the population inversion doesn't fully recover and this is manifested as a reduction in peak power and a shift to longer wavelengths.

The operating wavelength for the Q-switched fibre laser is important for the commercial sensing applications for which the device is to be used. A laser operating at 1530nm would generate the temperature dependent anti-stokes Raman signal in the wavelength region 1430-1440nm, where the fibre loss is higher because of absorption by OH^- ions. If the laser operates at 1560nm then the anti-Stokes signal occurs at higher wavelengths where the loss due to the OH^- ions is reduced. A stable wavelength operation in the 1560nm band is therefore necessary.

5.4.3 Conclusions

The section has discussed some of the basic design considerations in producing a high power, short pulse Q-switched fibre laser. The importance of fibre length on Q-switched peak power and pulse width as well as operating wavelength has been emphasised and experimentally verified. These experiments were carried out in the early stages of design and show the trends in laser performance with parameters such as repetition rate etc, and do not show the highest powers obtained. Subsequent optimisation (e.g. alignment, fibre length etc.) of the laser resulted in a Q-switched laser producing 140Watt, 25ns pulses at a repetition rate of 500Hz for 90mW of pump power and represented the highest peak power obtained from this compact diode pumped system.

5.5 Erbium/Ytterbium doped Q-switched Fibre Lasers

In an attempt to produce high power, short pulses at 1.56μm, an Erbium/Ytterbium based system was investigated. The details of the Erbium/Ytterbium co-doping has been described in section 3.2.2, but to summarise, the addition of the Ytterbium increases the pump absorption which results in a shorter fibre length for a given absorbed pump power [13][14] [15].

5.5.1 Experiment

Figure 5-17 shows the schematic of the Erbium/Ytterbium Q-switched fibre laser. Essentially the arrangement consisted of an end pumped Fabry-Perot cavity with an intra-cavity acousto-optic Q-switching element.

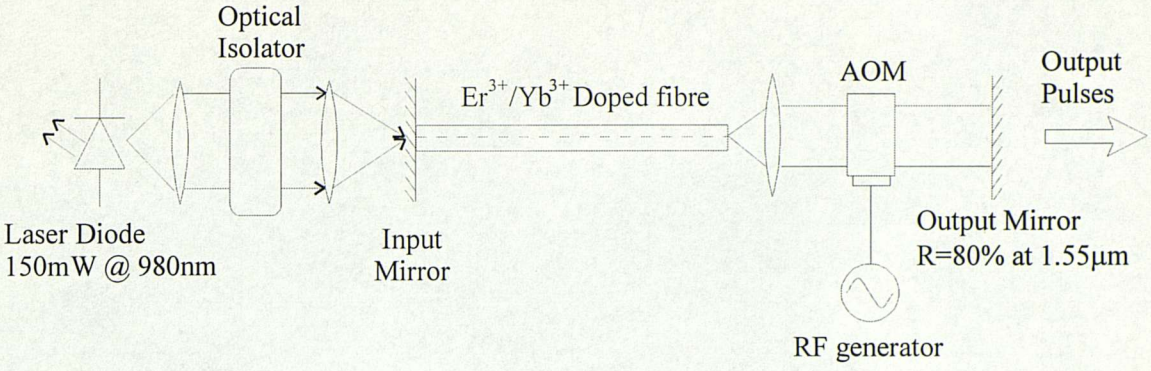

***Figure 5-17** – Schematic of Erbium/Ytterbium doped Q-switched fibre laser*

The laser was pumped with the bulk 980nm laser diode described in section 5.3.1.1 and provided 45mW of launched pump power. The parameters of the fibre used in this experiment are shown in Table 5-4.

Fibre Number	ND0950
Numerical Aperture	0.17
Cut-off Wavelength	1.3μm
Erbium Concentration	780ppm
Ytterbium/Erbium ratio	20:1

***Table 5-4** – ND950 Erbium/Ytterbium doped fibre specifications*

A length of fibre between 50-100mm was found to absorb sufficient pump to reach the lasing threshold. A length longer than 100mm was insufficiently pumped and a length shorter than 50mm did not provide enough gain to overcome the losses of the modulator. The low round trip gain of the Erbium/Ytterbium fibre has three main consequences for the design of the laser cavity:

1) It was not necessary to angle polish the end of the fibre, as because of the short lengths of fibre there was not sufficient round trip gain to initiate lasing from the 4% Fresnel reflection.
2) Zero order operation of the acousto-optic modulator could be used effectively because the diffraction efficiency of the modulator was sufficient to suppress lasing action when

in the low Q/high loss state.

3) High reflectivity cavity mirrors (80% and 99%) had to be used to reduce the laser threshold.

5.5.2 Results

5.5.2.1 CW operation of the Erbium/Ytterbium fibre laser

The laser was constructed with an output mirror with a reflectivity of 80% providing feedback into the laser cavity. Figure 5-18 shows the laser output power as a function of estimated launched pump power.

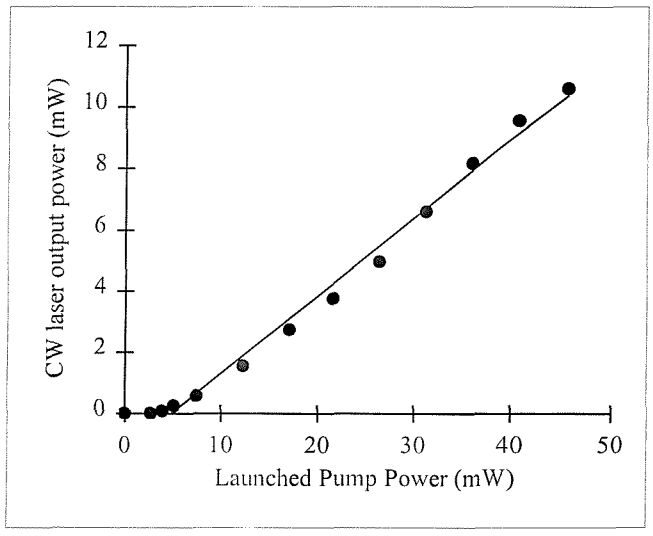

Figure 5-18 *– Plot of launched Pump power against laser output power*

A CW power of 10.6mW at a wavelength of 1535nm was demonstrated for a launched pump power of 45mW, this corresponds to a launched slope efficiency of 26%. The pump power required to reach threshold was 2.5mW.

5.5.2.2 Q-switched operation of the Erbium/Ytterbium fibre laser

The laser was Q-switched using an acousto-optic modulator which was operated in zero-order. A output peak power of 58Watts with a pulse width of 15ns were found at a repetition rate of 500Hz. The launched pump power required to reach threshold was 4.5mW. Figure 5-19 illustrates the variation of peak power and pulse width with repetition rate for the Erbium/Ytterbium Q-switched fibre laser.

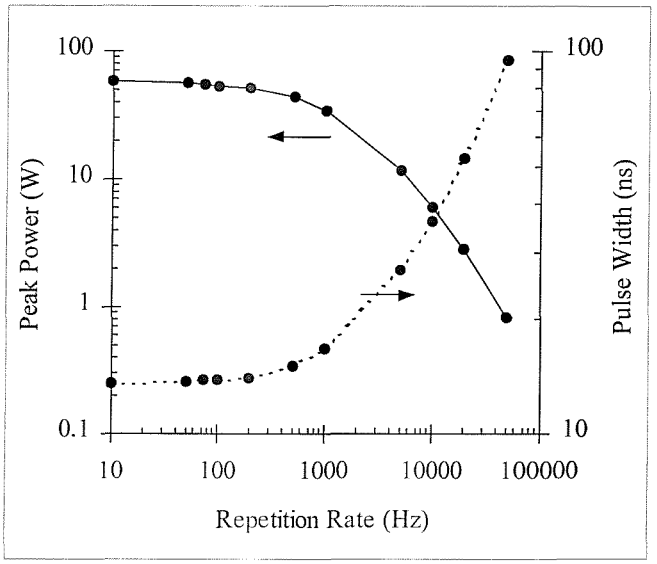

***Figure 5-19** – Variation of Peak Power and Pulse Width with repetition rate for Erbium/Ytterbium Q-switched fibre laser*

The fall-off of the peak power with increasing repetition rate is a result of the finite recovery time of the population inversion, which is directly related to the lifetime of the metastable level, typically 10-12ms for the Erbium ion. The lifetime of the metastable level is effectively reduced by the presence of amplified spontaneous emission in the cavity, which depletes the upper laser level, analogous to the collision process in gas lasers which shorten the lifetime of the gas molecules. In section 5.4.2.2 we reported that the effective lifetime of the Erbium ions in a Q-switched laser is reduced to 1ms. Therefore, a repetition rate greater than 1kHz causes a reduction in peak power. Figure 5-19 shows that the addition of Ytterbium allows high peak powers to be maintained at higher repetition rates. Pump light absorbed by the Ytterbium ions is transferred to the adjacent Erbium ions by a fast

cross-relaxation process; hence the Erbium ions experience a higher pump intensity than in the absence of the Ytterbium. It has been reported previously [16] that by pumping the laser harder, higher peak powers can be achieved at higher repetition rates. This is illustrated in Figure 5-19 which shows a peak power of 1watt and pulse width of 95ns at a repetition rate of 50kHz, similar performance was achieved at 5kHz for the Erbium only fibre. This ability of Erbium/Ytterbium co-doped Q-switched lasers to operate at higher repetition rates makes them suitable for application which require high repetition rates (i.e. laser range finding)

5.5.3 Conclusions

We have produced for the first time a diode pumped Q-switched Erbium/Ytterbium co-doped fibre laser which produces high power, short pulses of 58Watts, 15ns at a repetition rate of 500Hz. It was found that the addition of Ytterbium to the gain medium increased the effective pump rate of the Erbium ions, which has the effect of maintaining the high peak powers at higher repetition rates.

5.6 Electro-Optically Q-switched Fibre Lasers

In the last section a co-doped Erbium/Ytterbium fibre was used in conjunction with an AOM to generate shorter pulses from a Q-switched fibre laser. This section explores using an electro-optic modulator (EOM) as a Q-switching element. Electro-optic modulators generally have faster rise times (<10ns) and lower insertion losses than acousto-optic modulators and therefore an increase in performance for the Q-switched fibre laser can be expected.

5.6.1 Experiment

A similar configuration to that used previously is used in this experiment with the acousto-optic modulator replaced with an electro-optic modulator (Figure 5-20).

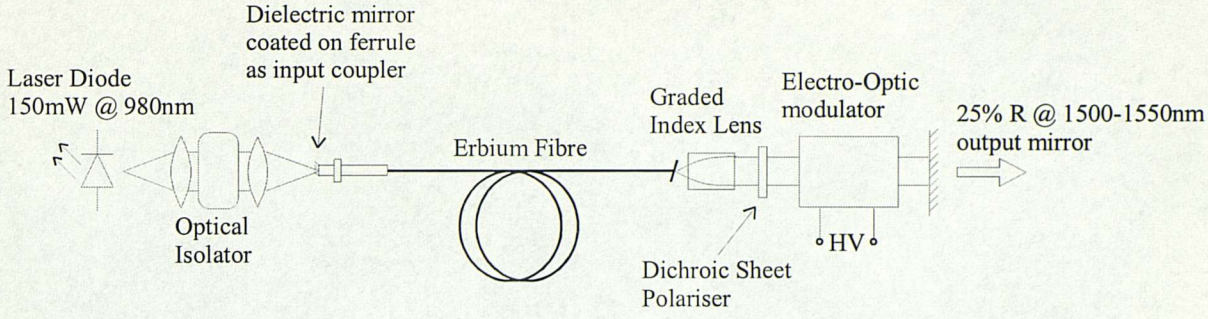

Figure 5-20 *- Schematic of Electro-optically Q-switched fibre laser*

An optimised length of Erbium doped fibre (ND899), 80cms in length was used as the gain medium and was pumped with a bulk 150mW laser diode operating at 980nm (Section 5.3.1.1). The light from the pump laser diode was focussed into the Erbium doped fibre through a dichroic mirror which was coated onto the end of a ferrule containing the fibre. The dielectric coating had a reflectivity of 99% at 1550-1550nm and a 95% transmission at 980nm. The light from the fibre end was then focussed using a graded index lens through a dichroic sheet polariser and the EOM [17] onto an output mirror with a 25% reflectivity at 1500-1550nm. In order to produce an efficient fibre laser the polarisation must be maintained during each round trip of the cavity. If the fibre significantly alters the otherwise linearly polarised light on each round trip then the laser threshold will increase and the efficiency will be reduced.

5.6.2 Results

5.6.2.1 CW operation of single polarisation fibre laser

Theoretically, a perfectly round, straight, strain free fibre can be modelled by two degenerate modes of propagation with equal propagation coefficients, $\beta_x=\beta_y$. Any polarisation state injected into the fibre would therefore remain unchanged. In a practical single mode fibre there exists two fixed non-degenerate orthogonal, phase independent polarisation eigenmodes, these are formed due to imperfections such as thermal stresses and core asymmetry in the fibre. These two modes propagate with different phase velocities and observe different refractive indices, n_x and n_y. The difference between the effective refractive indices is called the fibre birefringence, $B_f=n_y-n_x$. These orthogonal eigenmodes

are coincident with the birefringent axes of the fibre. In order to confirm the existence and find the angular position of the two orthogonal fibre axes, the system was operated in CW operation with an intra-cavity polariser. The polariser was rotated through 180° and measurements of output power were taken at 10° intervals. Figure 5-21 shows the results, two optimum orthogonal polarisation's are clearly indicated.

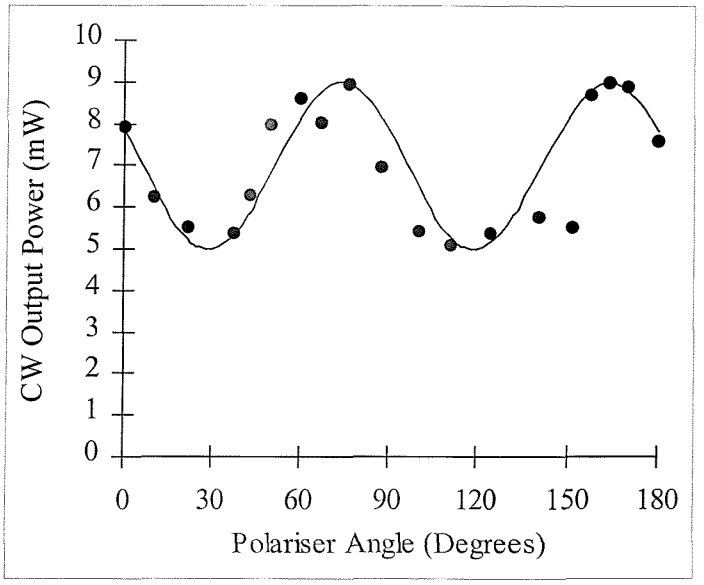

Figure 5-21 *- Variation of CW output power with intra-cavity polariser angle*

When the polariser is aligned with the x-eigenmode, the y-eigenmode is strongly attenuated and the laser is forced to operate in the x-mode only, similarly when the polariser is aligned to the y-mode, the x-mode is attenuated. When the polariser is mis-aligned from one of these birefringent axes, it introduces a loss to both of the polarisation eigenmodes, this additional loss causes a decrease in laser efficiency and an increase in the laser threshold. When the polariser is aligned at 45° to the principle axis, a power of 5mW is recorded, hence the loss introduced by the polariser is not sufficient to prevent laser action.

Therefore in order for efficient Q-switched operation of the laser the polariser must be orientated with one of the eigenmodes of the fibre.

Measurements of CW output power against launched pump power were taken with the polariser aligned to each eigenmode and also in the absence of the polariser. Figure 5-22 shows the results obtained for these three configurations.

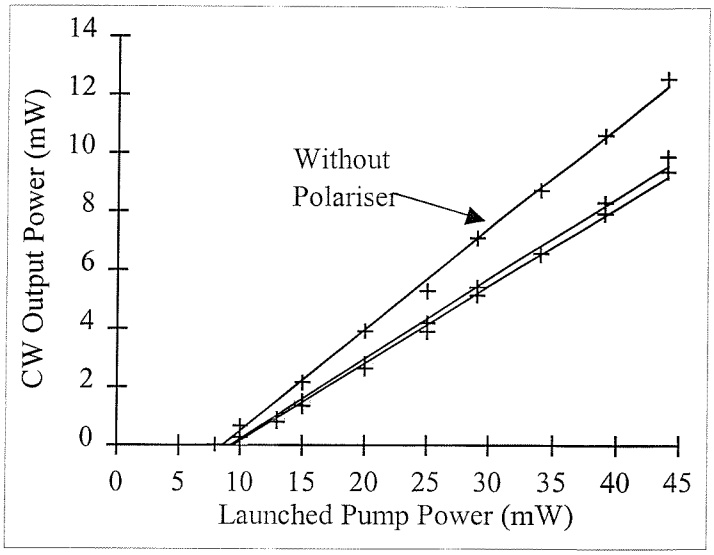

Figure 5-22 *- CW Output power against launched pump power with intra-cavity polariser orientated parallel to each eigenmode, and in the absence of a polariser*

With the polariser in the cavity and aligned to a polarisation eigenmode, a maximum CW output power of 9.5mW was obtained with a launched slope efficiency of 28% and a threshold of 8mW of launched pump power. Figure 5-22 shows a small variation in the characteristics for the two pump polarisation orientations, this is thought to be due to the orientation of the pump polarisation and the polarisation anisotropy present in rare earth doped fibres [18][19]. In the absence of the polariser a maximum CW output power of 12mW was obtained with a launched slope efficiency of 35% and a threshold of 7mW launched power.

So to conclude, for efficient Q-switching operation with an electro-optic modulator, the polariser must be aligned with the birefringent axis of the fibre (Figure 5-21). The results obtained after fulfilling this criterion are discussed in the next section.

5.6.2.2 Q-switched operation using an electro-optic modulator

An applied voltage of 4.6kV was applied to the electro-optic modulator which was sufficient to convert the linearly polarised light to circular polarised light and in conjunction with a sheet polariser was sufficient to prevent CW lasing. On operation of the Q-switched laser, pulses within the Q-switched pulse envelope were observed at a frequency corresponding to

the round trip time of the cavity. Figure 5-23 shows the results which were obtained with the laser operating at a repetition rate of 200Hz. Repetition rates in excess of 1kHz were not possible with this Pockels cell although it is possible to buy additional driver modules to increase the repetition rate to 100kHz.

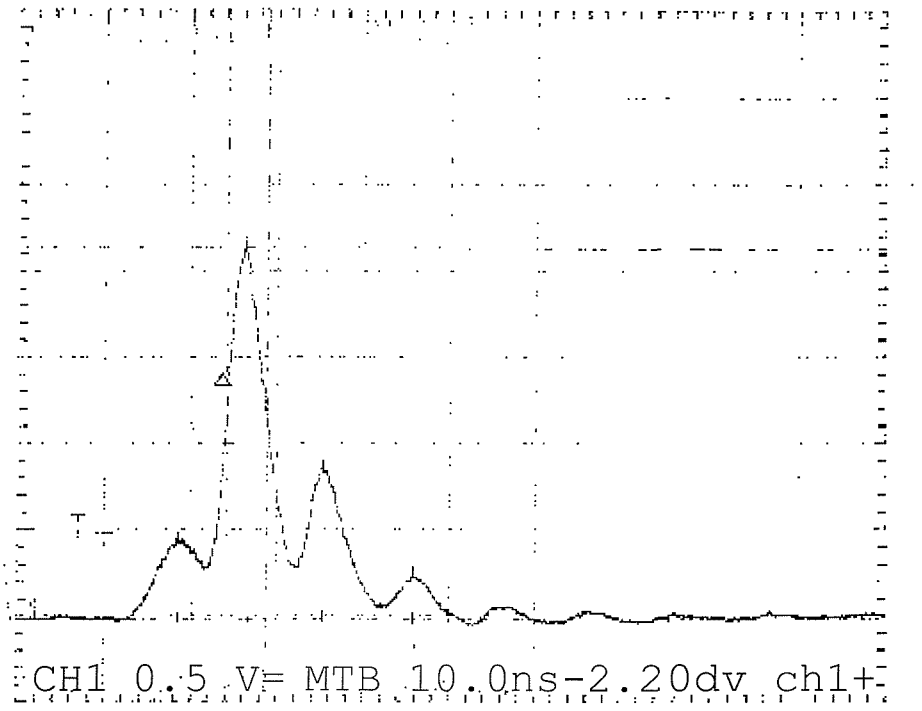

Figure 5-23 *- Output Pulse from the electro-optically Q-switched Erbium doped fibre laser*

Figure 5-23 clearly shows the pulse structure within the Q-switched pulse envelope. It consists of four pulses which are separated by 10ns, the round trip time. The largest of these pulses has a peak power of 540Watts and a pulse width of 4ns, the Q-switched envelope has a width of 10ns. These results represent the highest peak powers observed in a diode pumped Q-switched Erbium doped fibre laser.

The observed structure on the pulse was stable and did not vary with time although changes in the position of the output mirror caused the position of the peaks to change. In previous publications [20], the structure on the pulse has been attributed to self-mode locking caused by the effect of self-phase modulation. This relies on the intensity dependence of the

refractive index to spectrally broaden the pulse so that individual longitudinal modes overlap and couple together to self-mode lock [20][21][22].

This self-mode locking would therefore require high power densities within the cavity in order to achieve the required spectral broadening to couple adjacent modes together. However experimentally this explanation is flawed due to the fact that the pulsed effect is also observed at low peak powers. Further doubt is cast upon this self-phase modulation explanation when the results in section 5.7 are considered. A large mode area fibre is used to produce peak powers in excess of 4kW but no self-pulsing is observed on the Q-switched laser pulse. Further investigation into the observed pulsed behaviour is carried out in a later section.

5.6.2.3 Investigation into self-pulsing Q-switched fibre lasers

Other than the higher powers achieved in using a electro-optic modulator, in excess of 500Watts compare to the 140Watts achieved in previous configurations the only other significant change in the configuration is the decrease in the rise time of the modulator, from 100ns (acousto-optic modulator) to 4ns.

An alternative explanation to self-mode locking is the possibility that the pulsed operation stems from the build-up of ASE coupled with gain depletion at high pulse powers. Consider the Q-switched laser in the high loss state, feedback of the ASE which would initiate the start of the Q-switched pulse is prevented by the modulator. If the cavity is instantaneously switched from a high loss to a low loss state then the small ASE signal is reflected from a mirror back into the cavity. If the signal is such that the laser amplifier is in the small signal regime then after one round trip time, the intensity of the signal at the modulator is equal to the initial ASE power multiplied by the round trip gain. On each round trip the power increases step-wise until gain saturation occurs and the signal starts to be depleted resulting in a pulsed behaviour.

However if the switching time is slow compared to the round-trip time of the cavity then this effect is smoothed out and the pulsed behaviour is not observed.
To investigate this hypothesis a Q-switched fibre laser was constructed with a long round-trip time (8metres = 80ns) and an acousto-optic modulator which had a fast rise time (20ns) compared with the round-trip time. An acousto-optic modulator was used instead of the electro-optic modulator because of the ability to adjust its rise time by applying an appropriate filter to the RF generator input.

Figure 5-24 shows three experimentally observed pulses for different modulator switching times. For the 375ns switching time the self-pulsation is no longer apparent, for the intermediate 115ns switching time, the smoothing effect caused by the slower switching speed is clearly visible and with the unfiltered signal to the RF generator giving rise to the 22ns switching time, the pulsed operation becomes more evident.

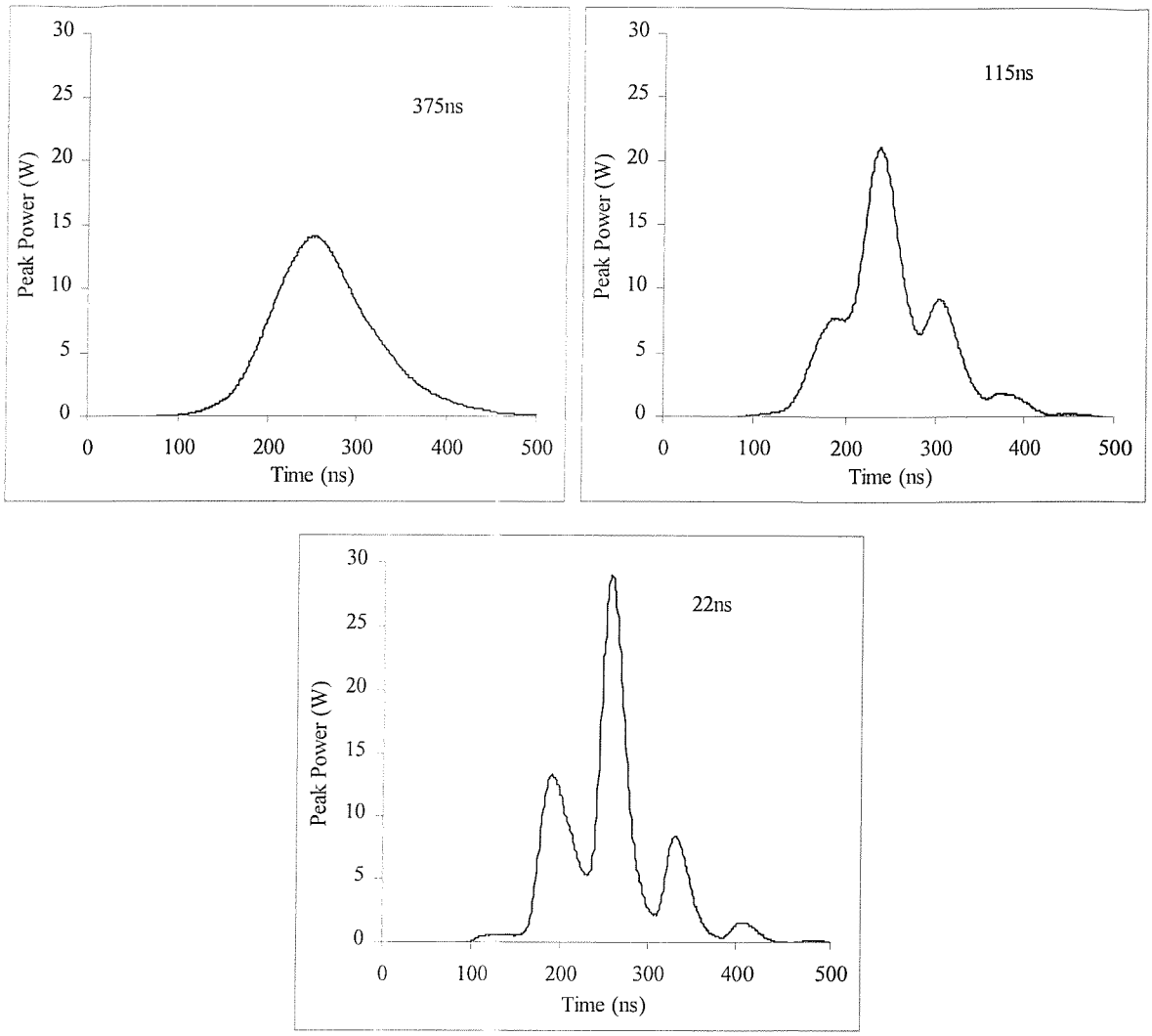

Figure 5-24 *- Q-switched pulses observed with different modulator switching times*

Figure 5-25 shows a Q-switched pulse displayed on a log plot. In order to obtain the measurements of the low powers at the start of the pulse, the pulse was truncated to avoid saturation of the detector. This was achieved by reducing the opening time of the switch to cut off the pulse prematurely.

The results clearly show the stepwise build-up of the ASE at the initial leading edge of the pulse. At high powers gain depletion at the trailing edge of each step initiates the build-up to the pulsed behaviour which was previously incorrectly attributed to self-phase modulation.

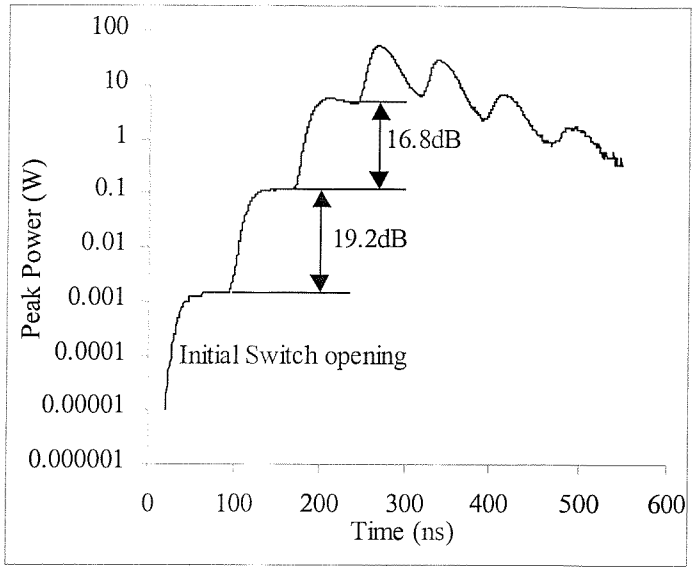

Figure 5-25 *- Experimental results showing the build-up of the Q-switched pulse from the initial ASE*

5.6.3 Conclusions

By careful optimisation of fibre length, mirror reflectivity and modulator performance, a diode pumped Erbium doped Q-switched fibre laser producing pulses of 540watts and 10ns duration has been demonstated. This represents the highest peak power reported to date from a diode pumped system. In using an electro-optic modulator with a fast 4ns switching time, a consistent theory for the self-pulsing observed in Q-switched fibre lasers has been proposed and experimentally verified. The self-pulsation which occurs within the envelope of Q-switched fibre lasers with a frequency equal to the round-trip time has previously been attributed to self-phase modulation leading to self-mode locking. In this chapter we have proved that the pulsation is generated when using a modulator with a switching time fast compared to the round-trip time of the cavity. A stepwise build-up of ASE then occurs and in conjunction with gain depletion at high powers initiates the pulsed behaviour.

5.7 Large Mode Area Erbium doped Q-switched Fibre Lasers

Section 3.2.3 describes a method of increasing the amount of stored energy in a length of Erbium doped fibre for a fixed absorbed pump power. This involves increasing the mode area of the fibre whilst maintaining single mode operation [23][24]. A large mode area fibre has two principal advantages:

1) For a given absorbed pump power, increasing the mode area reduces the amplified spontaneous emission. The reduction in ASE enables an increase in stored energy to be obtained.
2) The increased mode area increases the threshold for non-linear Raman and Brillouin effects. These occur at high powers and cause the pulse energy to be shifted into longer wavelengths.

The effect of substituting normal Erbium doped fibre with large mode area fibre has been modelled and for a fixed absorbed pump power the large mode area fibre shows a twofold increase in the energy extracted from the laser (section 4.3.4). This section describes experimentally the first operation of a Q-switched fibre laser using a novel large mode area fibre geometry.

Initially to illustrate the increase in the mode fibre area and to confirm that the fibre still propagates with a single transverse mode, the far field patterns for both a conventional and large mode area fibre were measured.

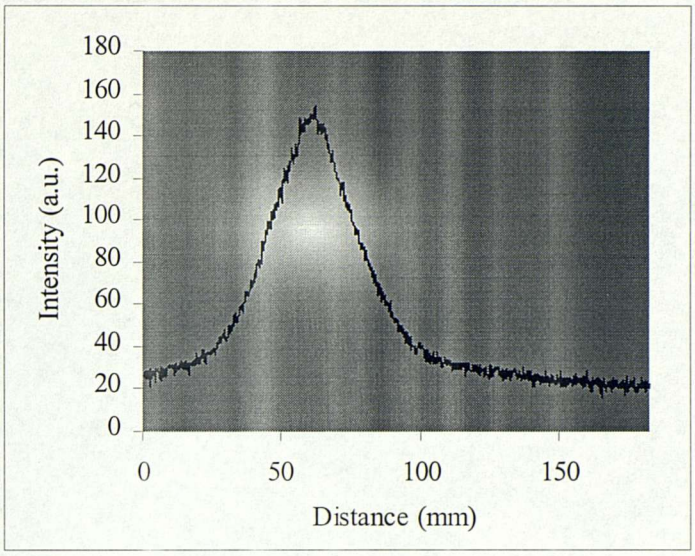

Figure 5-26 – *Far Field Diameter of a conventional Erbium doped fibre*

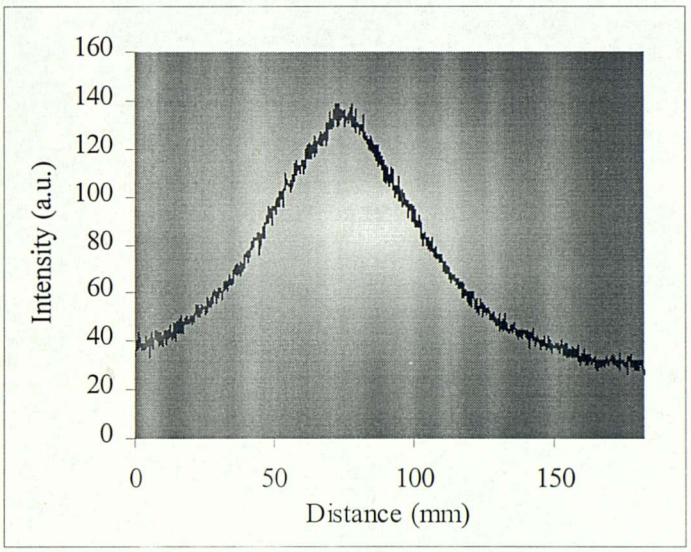

Figure 5-27 – *Far Field Diameter of a Large Mode area Erbium doped fibre*

The results shown in Figure 5-26 and Figure 5-27 were obtained using a Germanium infra-red Vidicon camera to view the far-field patterns on a screen position 220mm from the fibre end. A silicon filter was placed at the fibre end to remove any residual 980nm pump light. The measured far field diameters (full width at half height) for the conventional and LMA fibres were 67.7mm and 35.5mm respectively. Using a simple trigonometric

approach, and measuring the distance between the fibre end and the screen and the far-field diameters, the N.A. for the conventional and LMA fibres was determined to be 0.15 and 0.08 respectively. These values agreed with preform measurements for both fibres. It is also clear from the mode profiles that the signal is propagating in a single transverse mode in the LMA fibre.

5.7.1 Experiment

The experimental arrangement is shown in Figure 5-28.

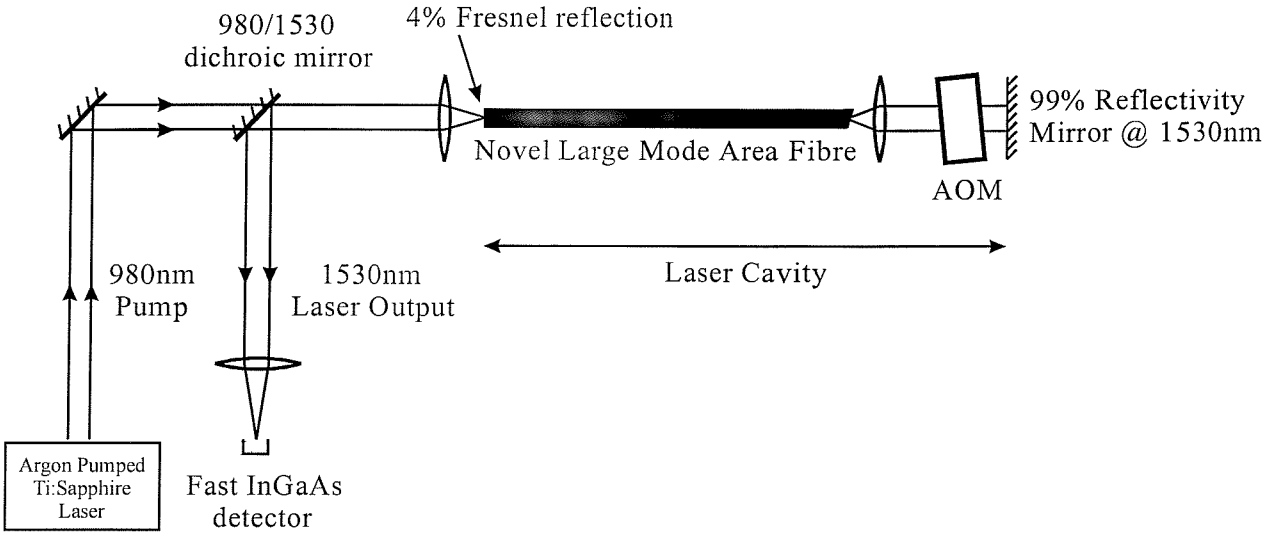

Figure 5-28 *– Schematic of experimental arrangement for a Large mode area Q-switched fibre laser*

An Argon pumped Ti-Sapphire is used as the pump source with up to 1.2Watts of output power at 980nm. This pump was launched into the large mode area fibre through a dichroic mirror at 45° to the fibre axis, this mirror was also used to obtain the output. The specifications of the large mode area fibre used in the experiment are shown in Table 5-5.

Fibre Number	ND1036
Numerical Aperture	0.08
Core Radius	7.3μm
Erbium Concentration	4000ppm

Table 5-5 *– ND1036 Large Mode Area fibre specifications*

The near end of the fibre was cleaved perpendicular to the axis of the fibre and formed one mirror of the laser cavity. The far end of the fibre was polished at an angle of 16° to prevent the fibre lasing from the 4% Fresnel reflection. The length of fibre used in this study was 630mm and was optimised for the available launched pump power of 600mW. The output from the far end of the fibre was focused using an anti-reflection coated graded index lens through an acousto-optic modulator and onto a highly reflecting mirror, 99% at 1500-1550nm. A silicon filter was placed between the end of the fibre and the modulator to filter out any residual 980nm pump light. This was needed because the high residual pump powers generated heating effects in the modulator which caused a gradual thermal misalignment.

5.7.2 Results

In the CW configuration the laser produced over 200mW of CW power with an absorbed slope efficiency of 39% which, with respect to the quantum efficiency, is 62%. The plot of CW output power against absorbed pump power is shown in Figure 5-29. The absorbed pump power is measured by taking the difference between the launched pump (assuming a launch efficiency of 50%) and the residual pump power.

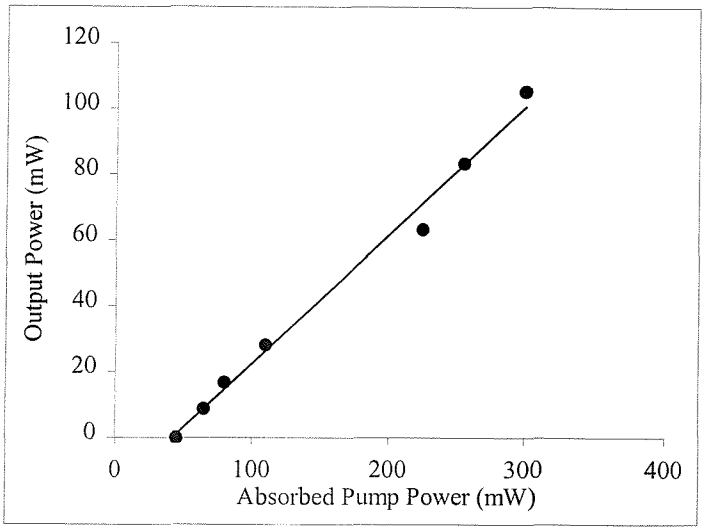

Figure 5-29 *– A plot of CW output power of the large mode area fibre laser against absorbed pump power (Absorbed Slope Efficiency, 39%).*

To produce the Q-switched laser the modulator was operated in zero order. This provided the best results because of the high diffraction efficiency of the modulator (80%). Using this configuration, peak powers in excess of 4kW with associated pulse widths of 11ns were obtained at a repetition rate of <1kHz. A typical pulse is shown in Figure 5-30, the pulse energy is in excess of 50μJ. This represents the highest peak power and pulse energy from a Q-switched fibre laser to date.

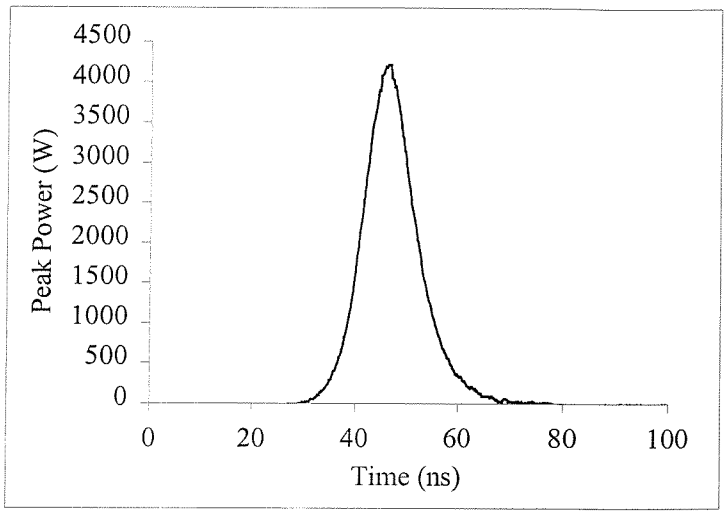

Figure 5-30 – *Typical High Power Pulse from the large mode area Q-switched fibre laser*

The variation of peak power and pulse width with repetition rate is shown in Figure 5-31 and shows the typical behaviour of an Erbium doped Q-switched fibre laser.

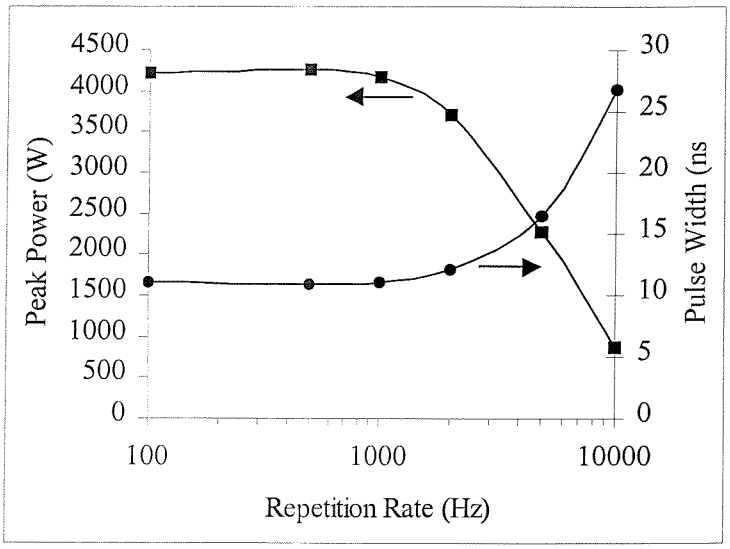

Figure 5-31 – *Output Peak Power and Pulse Width of the large mode area Q-switched fibre laser as a function of repetition rate*

The variation of pulse energy with estimated launched pump power is shown in Figure 5-32, the launched pump power was calculated assuming a launch efficiency of 50%. The increase

in pulse energy with launched pump power shows a saturation effect at high pump powers. This is caused by gain saturation and can be explained by the increase in the ASE signal at higher pump powers which limits the available gain and subsequently the pulse energy [16]. For an estimated launched pump power of 600mW the measured output pulse energy was 50μJ. The previously reported maximum output pulse energy obtained from a Q-switched Erbium doped fibre laser was 6μJ [25].

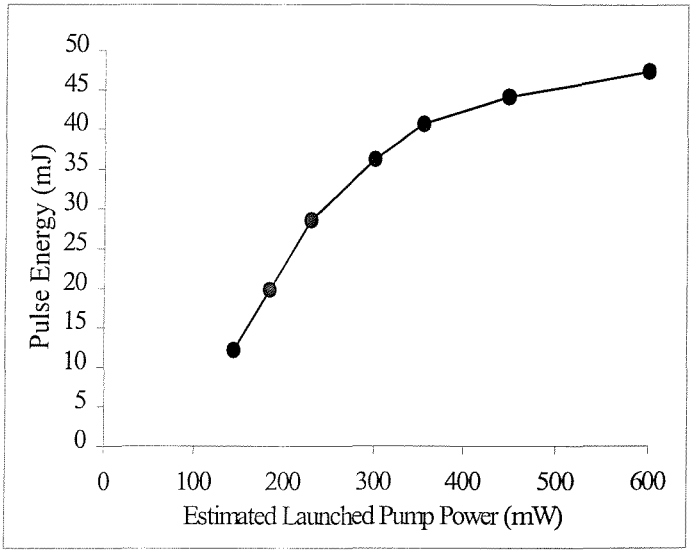

Figure 5-32 – *Output Pulse Energy as a function of Launched Pump Power*

5.7.3 Conclusions

In conclusion, by using a novel fibre geometry a large increase in the maximum pulse energy obtained for a Q-switched fibre laser has been obtained. The continuing optimisation of the large mode area fibre with respect to dopant concentration and core radius for laser power amplifiers should result in pulse energies exceeding 100μJ to be obtained.

5.8 Narrow Linewidth Erbium doped Q-switched Fibre Lasers

Advances in fabrication techniques of in-fibre Bragg gratings has enabled the linewidth of such devices to be reduced to <16pm at 1550nm. It is the narrow linewidth of such gratings in conjunction with the high power, short pulses obtainable from Q-switched fibre lasers which makes this technology suitable for Brillouin distributed temperature sensing. The use of a narrow in-fibre Bragg grating as an output coupler of a Q-switched fibre laser causes the laser to operate with a linewidth and wavelength determined by the grating.

5.8.1 Experiment

Figure 5-33 shows a schematic diagram of the experimental arrangement used to produce the narrow-linewidth Q-switched fibre laser.

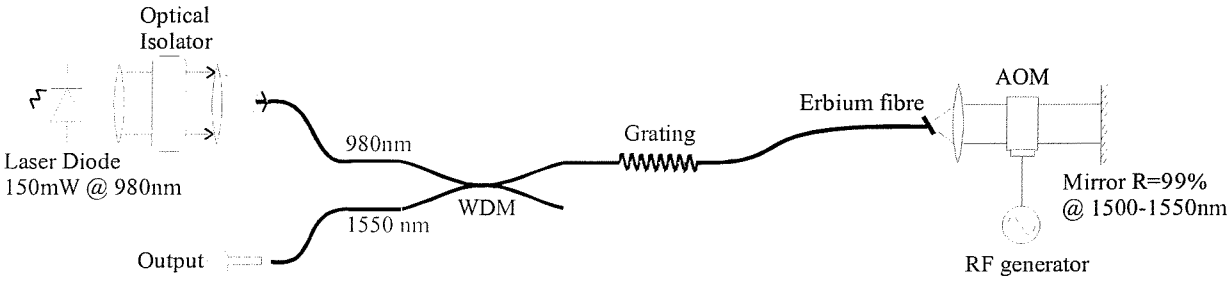

Figure 5-33 *- Schematic of Narrow Linewidth Q-switched Erbium doped Fibre Laser*

The Erbium doped fibre is pumped with a 150mW, 980nm bulk laser diode (Section 5.3.1.1). A WDM is used to couple the pump light through the grating into the Erbium doped fibre. Early fibre gratings had to be hydrogenated to increase the photosensitivity of the fibre in order to write the grating. This had the unfortunate side effect of increasing the absorption at 980nm, the pump could not therefore be transmitted through the grating. In early experiments therefore the grating was placed at the other end of the WDM which had the effect of increasing substantially the fibre cavity length. This problem was solved by doping the fibre with Boron or Aluminium which increased the photosensitivity of the fibre without the adverse effects caused by hydrogenation. The grating in this experiment and all further gratings were fabricated using a moving

fibre/phase mask method [26] rather than the early interferometric methods [27]. The grating specifications are shown in Table 5-6.

Reflectivity	60%
Linewidth	<2GHz
Wavelength	1530.2nm

Table 5-6 – *A table showing the grating specifications used in this experiment*

A 600mm length of Erbium doped fibre (ND899) was used as the gain medium (See Table 5-2 for specifications). The length of fibre was optimised for maximum output peak power in zero-order Q-switched operation at a repetition rate of 500Hz. The fibre was terminated with a 17° angle polished end to prevent any feedback from the Fresnel reflections which would cause CW lasing. The output from the fibre end was focused using a graded index lens through the acousto-optic modulator (See section 5.3.3.1 for specifications) onto a plane high reflecting (99% at 1500-1550nm) mirror. The total length of the laser cavity between the mirror and the grating was 1.22m.

5.8.2 Results

Under CW conditions in the absence of the AOM, the laser had an output power of 7.1mW with a threshold pump power of 6.6mW, the corresponding slope efficiency was 17% of the launched pump power (Figure 5-34). This low value for the slope efficiency (Er^{3+}/Yb^{3+} - 26%, Er^{3+} - 25%) was due to the 1530nm wavelength of the grating. At this wavelength there is not sufficient pump power available to bleach the 1530nm transition and hence a decrease in slope efficiency is observed [10].

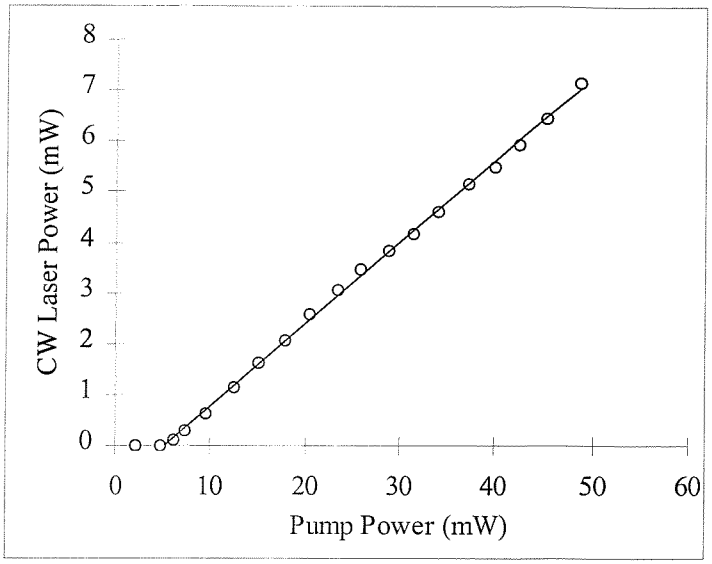

Figure 5-34 *- CW Output Power against Pump Power for the Narrow Linewidth Q-switched fibre laser*

Under Q-switched operation the acousto optic modulator was operated in zero order mode; in this configuration the feedback into the laser is provided by the undeflected zero order beam. At a repetition rate of 500Hz, a peak power of 102.5Watts and a pulse width of 17.7ns was obtained for 50mW of launched pump power. The variation of peak power and pulse width with repetition rate is shown in Figure 5-35 and is typical of an Erbium doped Q-switched fibre laser.

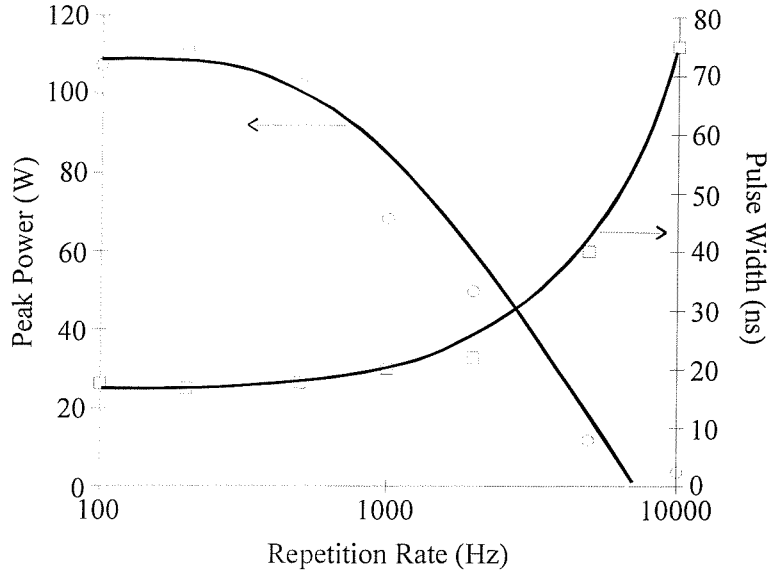

Figure 5-35 *- A plot of Peak Power and Pulse Width against Repetition Rate for a Narrow Linewidth Q-switched Fibre Laser*

5.8.2.1 Measurement of the Q-switched Laser Linewidth

To measure the linewidth of the laser a scanning Fabry-Perot interferometer was used to interrogate the signal. The mirror spacing of the Fabry-Perot was adjusted to 50mm which corresponds to a free spectral range (FSR) of 3GHz. The laser was initially operated under CW conditions and the output from the Fabry-Perot is shown in Figure 5-36. The scanning Fabry-Perot operates by applying a ramp voltage to one of the mirrors causing the interferometer to be scanned across a number of fringes. The results are shown in Figure 5-36 where the Fabry-Perot is scanned over five FSR's. The distance between adjacent peaks is determined by the mirror spacing and was set to 3GHz. By decreasing the slope of the ramp voltage applied to the Fabry-Perot the spectrum can be examined more closely to reveal the axial mode structure (Figure 5-36).

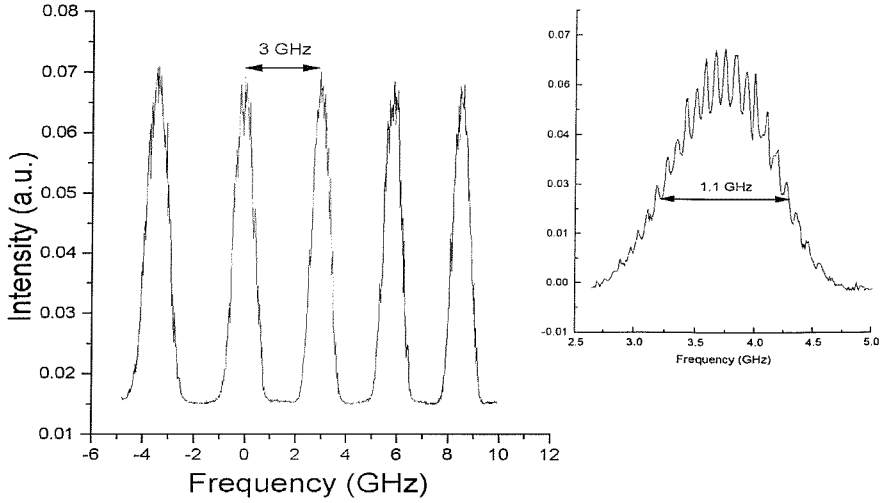

Figure 5-36 *- Plot of the output from the scanning Fabry-Perot showing the spectrum of the CW narrow linewidth laser*

The inset to Figure 5-36 clearly shows the axial mode structure of the spectrum, the period of the structure being equal to the round trip frequency of the laser cavity.

Measuring the spectrum of the Q-switched laser is slightly more difficult, because the scanning of the Fabry-Perot is not synchronised with the pulses from the laser. In order to measure the spectrum of the Q-switched laser two methods were used:

1) The envelope function of the digital scope was used, this picks out the pulse as and when it passes through the interferometer so over a number of minutes a trace is built-up of the spectrum
2) The Fabry-Perot was scanned manually over the spectrum and the intensity of the pulse was plotted as a function of applied voltage to the Fabry-Perot.

These two techniques were carried out and the results were found to be in agreement. Figure 5-37 shows the results from the envelope method. A linewidth of 1.3GHz was measured for the Q-switched pulse and 1.1GHz for the CW case.

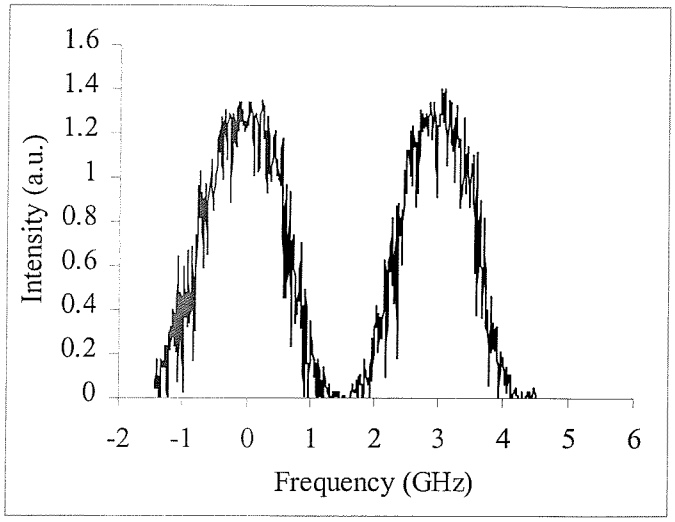

Figure 5-37 *- Plot of the output from the Fabry-Perot showing the spectrum of the Q-switched fibre laser*

5.8.2.2 Thermal Stability of the Narrow Linewidth Laser

One important consideration when using a grating in a fibre laser is the thermal stability of the laser wavelength. In order to measure the temperature sensitivity of the laser wavelength, the grating was mounted on a thermo-electric cooler (TEC) along with a calibrated thermistor. The centre wavelength of the laser was measured as a function of grating temperature using an optical spectrum analyser with a resolution of 0.1nm. The results of grating temperature against laser wavelength are shown in Figure 5-38.

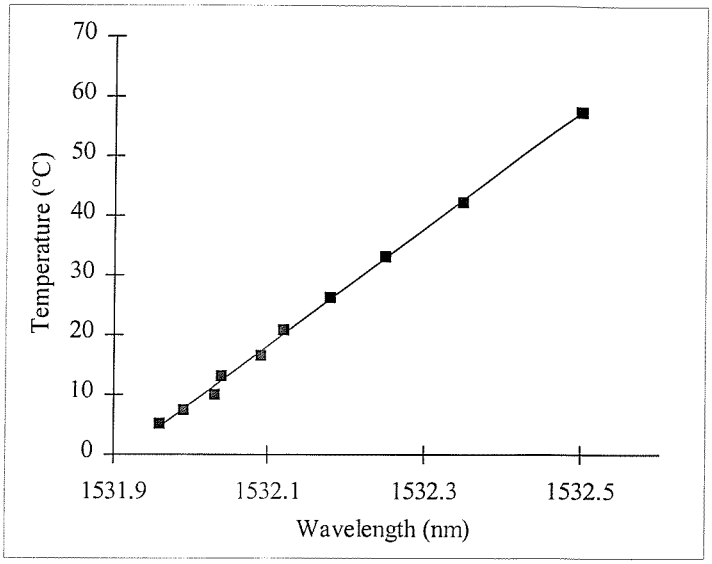

Figure 5-38 *- Plot of CW Laser wavelength against grating temperature*

The temperature sensitivity was measured to be 0.01nm/°C, which at 1530nm relates to a frequency dependence of 1.25GHz/°C. As we shall see in the next chapter, this temperature dependence of the laser wavelength becomes important when locking the centre wavelength to the transfer function of an interferometer as is the case in Brillouin temperature sensing.

5.8.3 Conclusions

The recent advances in fibre Bragg grating technology has enabled a narrow linewidth Q-switched Erbium doped fibre laser to be developed which produces pulses that fulfil the criteria for Brillouin distributed temperature sensing. Peak powers in excess of 100Watts with pulse widths of 18ns have been produced which have a spectral linewidth of less than 2GHz. This makes the source ideal for Brillouin temperature sensing which requires a source with a linewidth of less than 10GHz in order to be able to spectrally resolve the Brillouin signal from the Rayleigh. The next chapter explains fully the subject of distributed Brillouin temperature sensing.

5.9 Conclusions

In this chapter aspects of Q-switched Erbium doped fibre laser design have been covered with an aim to increase the understanding of Q-switched laser dynamics and to ultimately provide devices which fulfil the specifications required by both Raman and Brillouin temperature sensors. It has been demonstrated that an Erbium doped Q-switched fibre laser can produced the high power, short duration pulses required for Raman based temperature sensing as set out in section 2.2.2.1. Similarly the advances in fibre Bragg grating technology has lead to the development of a narrow linewidth Q-switched laser suitable for Brillouin based temperature sensing (section 2.3.2.1.).

In addition a number of advances have been made in other areas. The highest peak power obtained from a Q-switched Erbium doped fibre laser has been demonstrated using a novel large mode area fibre whilst the use of an electro-optic modulator with a fast (4ns) rise time produced a pulsed effect within the Q-switched envelope. This effect had previously been attributed to self-phase modulation whilst this work demonstrated it to be caused when the switching time of the modulator is fast compared to the round-trip time of the cavity, the step-wise build up of the ASE coupled with gain saturation generates the pulsed effect.

5.10 References

[1] R.I..Laming, M.C.Farries, P.R.Morkel, L.Reekie, D.N.Payne, P.L.Scrivener, F.Fontana and A.Righetti: 'Efficient Pump wavelengths of Erbium doped fibre optical amplifer', *Electronics Letters*, Vol.25, No.1, pp.12-14, (1989)

[2] A.Lidgard, D.J.Digiovanni and P.C.Becker: 'A Comparative Study of an Erbium doped fibre amplifier pumped at 811nm and 980nm', *IEEE Journal of Quantum Electronics*, Vol.28, No.1, pp.43-47, (1992)

[3] R.I.Laming, S.B.Poole and E.J.Tarbox: 'Pump excited-state absorption in Erbium doped fibres', *Optics Letters*, Vol.13, No.12, pp.1084-1086, (1988)

[4] W.H.Loh, R.I.Laming, Y.Gu, M.N.Zervas, M.J.Cole and T.Widdowson: '10cm chirped fibre Bragg grating for dispersion compensation at 10Gbit/s over 400km of non-dispersion shifted fibre', *Electronics Letters*, Vol.31, No.25, pp.2203-2204, (1995)

[5] L.Dong, P.Hua, T.A.Birks, L.Reekie and P.St J.Russell: 'Add/drop filters for wavelength division multiplexing optical fibre systems using a Bragg grating assisted mismatched coupler', *IEEE Photonics technology Letters*, Vol.8, pp.1656-1658, (1996)

[6] N.J.Doran and D.Wood: 'Non-linear optical loop mirror', *Optics Letters*, Vol.13, No.1, pp.56-58, (1988)

[7] G.P.Agrawal: 'Non-linear Fibre Optics: Second Edition', *Academic Press*, ISBN. 0-12-045142-5

[8] F.Seguin and T.Oleskevich: 'Diode pumped Q-switched Fibre Laser', *Optical Engineering*, Vol.32, No.9, pp.2036-2041, (1993)

[9] R.Ulrich and S.C.Rashleigh: 'Beam to Fibre coupling with low standing wave ratio', *Applied Optics*, Vol.19, No.14, pp.2453-2456, (1980)

[10] W.L.Barnes, P.R.Morkel, L.Reekie and D.N.Payne: 'High quantum efficiency Er^{3+} fibre lasers pumped at 980nm', *Optics Letters*, Vol.14, No.18, pp.1002-1004, (1989)

[11] C.G.Atkins, J.F.Massicott, J.R.Armitage, R.Wyatt, B.J.Ainslie and S.P.Craig-Ryan: 'High-Gain, Broad Spectral Bandwidth Erbium doped fibre amplifier pumped near 1.5μm', *Electronics Letters*, Vol.25, No.14, pp.910-911, (1989)

[12] M.J.F.Digonnet: 'Optical Fibre Lasers and Amplifiers', *Dekker Publishing*, (1993)

[13] J.E.Townsend, W.L.Barnes, K.P.Jedrzejewski and S.G.Grubb: 'Yb^{3+} sensitised Er^{3+}doped silica optical fibre with ultra-high transfer efficiency and Gain', *Electronics Letters*, Vol.27, No.21, pp.1958-1959, (1991)

[14] D.C.Hanna, R.M.Percival, I.R.Perry, R.G.Smart and A.C.Tropper: 'Efficient operation of and Yb sensitised Er fibre laser pumped in the 0.8μm region', *Electronics Letters*, Vol.24, No.17, pp.1068-1069, (1988)

[15] E.Tanguy, J.P.Pochelle, G.Feugnet, C.Larat, M.Schwarz, A.Brun and P.Georges: 'Mechanically Q-switched co-doped Er/Yb glass laser under Ti/Sapphire and laser diode pumping', *Electronics Letters*, Vol.31, No.6, pp.458-459, (1995)

[16] P.Myslinski, J.Chrostowski, J.A.Koningstein and J.R.Simpson: 'High Power Q-switched Erbium doped Fibre Laser', *IEEE Journal of Quantum Electronics*, Vol.28, No.1, pp.371-377, (1992)

[17] HVP-5LP-F Pockels cell Driver and LN-9 Q-switch: Quantum Technology, 108 Commerce Street, 32746-6212, Florida, USA

[18] J.T.Lin: 'Polarisation effects in Fibre Lasers' *University of Southampton*, Thesis (1990)

[19] J.T.Lin, P.R.Morkel, L.Reekie and D.N.Payne: 'Polarisation effects in fibre lasers', *European Conference on Optical Communications ECOC*, Helsinski, pp.109-112 (1987)

[20] P.Myslinski, J.Chrostowski, J.A.K.Koningstein and J.R.Simpson: 'Self-mode locking in a Q-switched Erbium doped fibre laser', *Applied Optics*, Vol.32, No.3, pp.385-407, (1993)

[21] M.C.Farries, P.R.Morkel and J.E.Townsend: 'The properties of the Samarium Fibre Laser', *Fibre Laser Sources and Amplifiers ed. Digonnet*, ISBN 0-82-478785-4

[22] W.L.Barnes, P.R.Morkel, M.Farries, L.Reekie and D.N.Payne: 'Q-switching in Fibre Lasers', *Fibre Laser Sources and Amplifiers*, ed. Digonnet, ISBN 0-82-478785-4

[23] J.Nilsson and B.Jaskorzynska: 'Modelling and Optimisation of low repetition rate high energy pulse amplification in CW pumped Erbium doped fibre amplifiers', *Optics Letters*, Vol.18, No.24, pp.2099-2101, (1993)

[24] D.Taverner, D.J.Richardson, L.Dong, J.E.Caplan, K.Williams and R.V.Penty: '158μJ pulses from a single transverse mode large mode-area EDFA', *Optics Letters,* Vol.26, No.6, pp.378-380, (1997)

[25] A.Chandonnet and G.Larose: 'High-Power Q-switched Erbium fibre laser using an all-fibre Intensity Modulator', *Optical Engineering*, Vol.32, No.9, pp.2031-2035, (1993)

[26] M.J.Cole, W.H.Loh, R.I.Laming, M.N.Zervas and S.Barcelos: 'Moving fibre/phase mask-scanning beam technique for enhanced flexibility in producing fibre gratings with a uniform phase mask', *Electronics Letters*, Vol.31, No.13, pp.1488-1489, (1995)

[27] K.O.Hill, Y.Fujii, D.C.Johnson and B.S.Kawasaki: 'Photosensitivity in optical fibre waveguides: Application to reflection filter fabrication', *Applied Physics Letters*, Vol.32, No.10, pp.647-649, (1978)

[28] D.B.Mortimore: 'Fibre Loop Reflectors', *IEEE Journal of Lightwave Technology*, Vol.6, No.7, pp.1217-1224, (1988)

[29] R.A.Betts, T.Tjugiarto, Y.L.Xue and P.L.Chu: 'Nonlinear Refractive Index in Erbium doped Optical Fibre: Theory and Experiment', *IEEE Journal of Quantum Electronics*, Vol.27, No.4, pp.908-913, (1991)

Chapter Six

Brillouin Distributed Temperature Sensing

6.1 Introduction

As described in section 2.3 the method used to determine the temperature profile along a length of optical fibre is to measure the intensity of the Brillouin backscattered signal. This chapter explores both the source and detection requirements for such a Brillouin based temperature sensor and highlights the problems which have been overcome in the final design in addition to the results achieved.

Before considering the individual components of the Brillouin DTS, let us examine in more detail one of the major obstacles which had to be overcome to achieve the required temperature resolution, i.e. coherent Rayleigh noise.

6.2 Introduction to Coherent Rayleigh Noise

Coherent noise on Rayleigh backscattered light is a well known problem in the field of coherent optical time domain reflectometry (C-OTDR). To explain the origin of CRN, consider the fibre to be made up of a large number of scatter elements (fluctuations in refractive index, and fibre composition etc.) which have a random spacing. Light scattered from these elements interferes with each other to generate random spatial intensity fluctuations on the backscattered trace. These fluctuations are known as coherent Rayleigh noise. The correlation between the backscattered elements can be altered by either using a source with a large bandwidth or by averaging over a large number of different frequencies, this technique is called frequency shift averaging (FSAV) [1]. It has been shown that the intensity fluctuations on the Rayleigh backscattered signal is reduced proportional to the square root of the number of independent frequency averages taken [2].

For Brillouin temperature sensing we need both a narrow linewidth source to generate the Brillouin backscattered light and a method of carrying out the technique of frequency shift averaging, in order to generate a Rayleigh signal with a reduced CRN component. One method to achieve this would be to use two sources, a narrow linewidth source and a broadband source. The broadband source would have the effect of simultaneously generating a wide range of frequencies which would then average out the coherent interference effects which cause the CRN. Obviously this method requires the use of two sources, and broadband high power pulsed sources are still difficult to obtain. A recently published paper which addresses the problem of CRN in Brillouin based temperature sensors used an ASE source with a 3dB linewidth of 5nm. This reduced the CRN by a factor of between 5 and 6 and hence increased the temperature resolution accordingly [3].

6.2.1 Experimental verification of Coherent Rayleigh Noise

Using the narrow linewidth Q-switched fibre laser with a linewidth of approximately 2GHz the Rayleigh backscattered traces in Figure 6-1 were obtained. Each trace was obtained independently and each trace was obtained with 16384 averages. The traces have been separated for clarity but from visual inspection it is clear that there is a high degree of coherence between each trace. Further averaging will not reduce this noise.

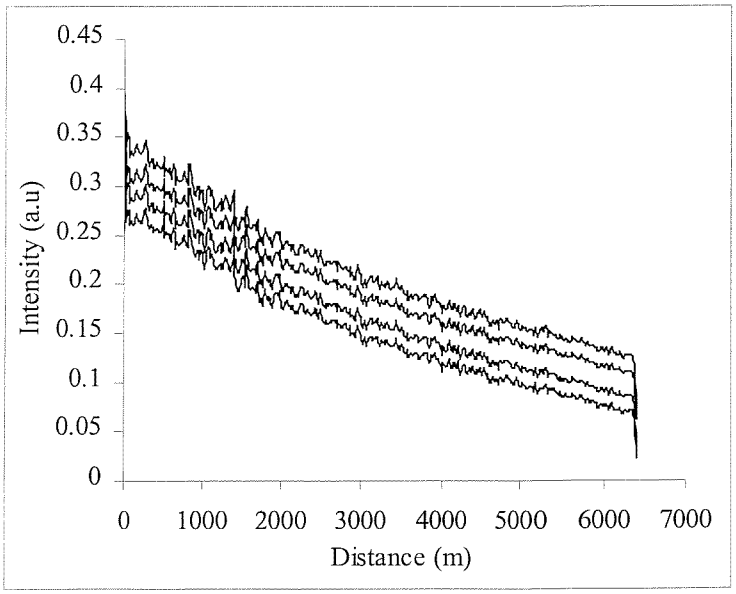

Figure 6-1 *- Four Independent Rayleigh traces obtained with a narrow linewidth source at the same wavelength*

Figure 6-2 shows the average of the above four traces and a value for the r.m.s. coherent Rayleigh noise. An r.m.s. value of 2.5% coherent noise on the signal was obtained, which relates to a 2.5% error on the Landau-Placzek ratio. This in turn corresponds to a temperature resolution of ±8.3°C assuming a temperature sensitivity of 0.3%/K [4][5]. For the temperature resolution to be improved, the coherent noise clearly has to be reduced.

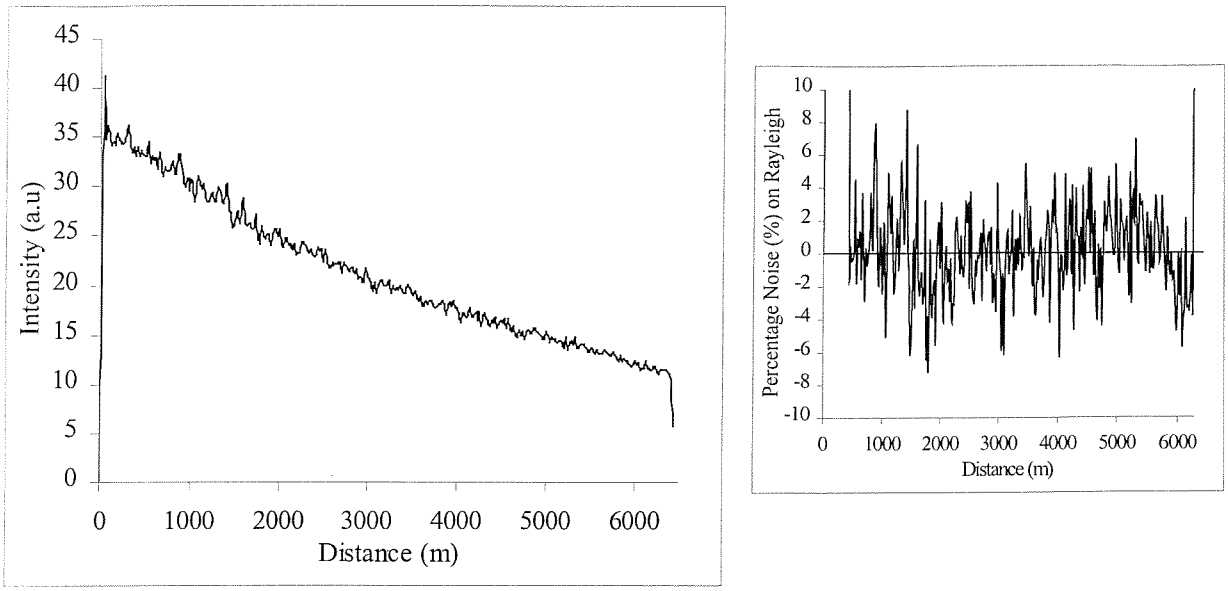

Figure 6-2 *- Rayleigh signal and inset showing the % noise on the signal*

As described earlier, a method of reducing this noise is to scan the source over many different wavelengths, a process of frequency shift averaging (FSAV). The next section describes how the Q-switched laser was modified to accommodate this technique.

6.2.2 Reduction of Coherent Rayleigh Noise

In section 5.8.2.2 it was reported that changing the temperature of the grating could vary the operating wavelength of the laser. However if the wavelength is to be swept over 5nm or more, then the temperature change required to produce such a wavelength shift would be approximately 500°C. Such a high temperature variation is not a practical proposition. An alternative method of changing the wavelength of the laser is to apply a strain to the grating. To measure the variation of grating wavelength as a function of strain, the grating was held

securely at each end and a strain was applied. Figure 6-3 shows how the wavelength varied with applied strain.

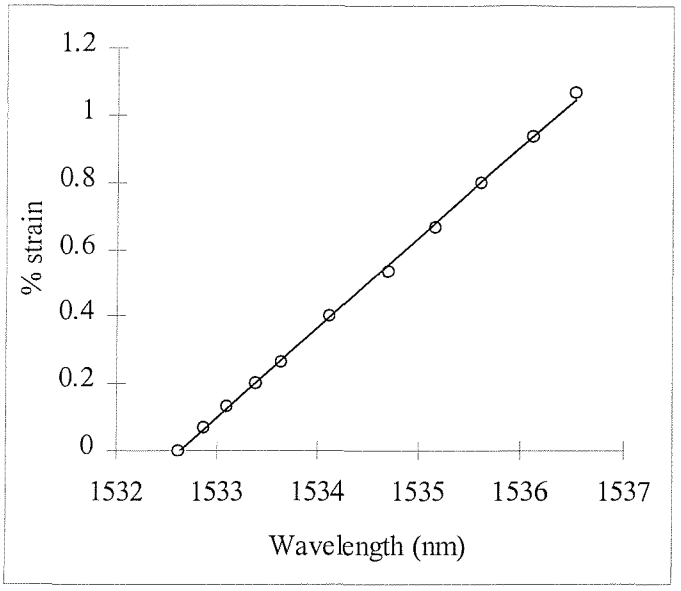

Figure 6-3 *- Plot showing the shift in centre wavelength of the grating as a function of applied strain*

A strain of just over 1% of the grating or a 0.8mm extension of 75mm of fibre produced a wavelength shift of 4nm. An experiment was carried out where the Rayleigh backscattered trace was taken at five discrete wavelengths with a 1nm separation. Figure 6-4 shows the results. The Rayleigh backscattered trace was taken at every 1nm wavelength shift, and by close inspection of Figure 6-4 it can be seen that the degree of correlation which existed in Figure 6-1 is reduced.

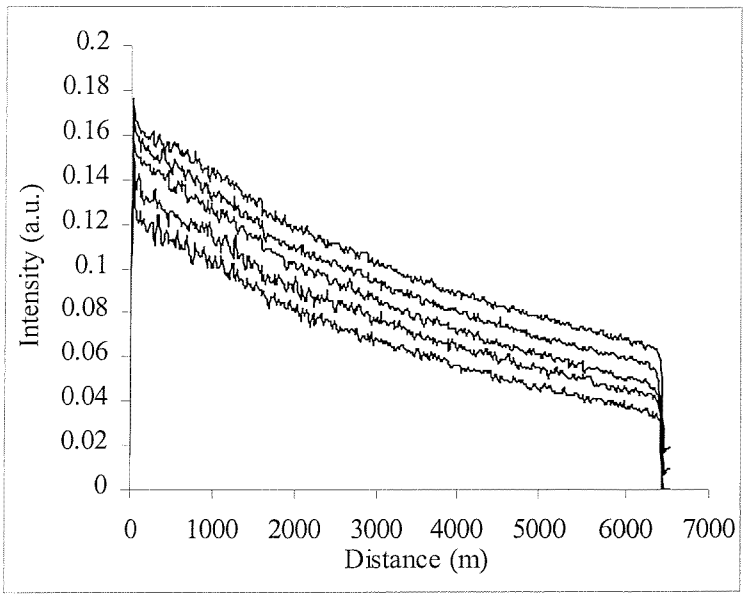

Figure 6-4 *- Uncorrelated Rayleigh traces at five different wavelengths with a 1nm separation*

By averaging traces over a range of discrete wavelengths the magnitude of the coherent Rayleigh noise is therefore reduced. Figure 6-5 represents a cumulative average of the coherent Rayleigh noise as summed over a number of discrete wavelengths. It has been shown previously [2] that the intensity of the fluctuations decreases in proportion to the number of discrete, independent backscattered traces. This is in good agreement with these results.

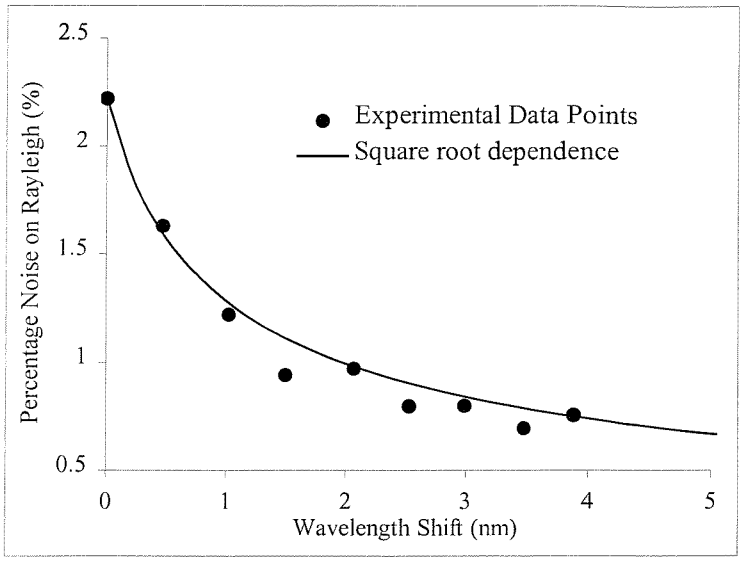

Figure 6-5 *- Cumulative average of Rayleigh backscattered traces for discrete wavelengths separated by 0.5nm*

The coherent Rayleigh noise was reduced to a value of 0.7% by taking the cumulative average of 9 measurements separated in wavelength by 0.5nm. To further decrease the noise on the Rayleigh the source was continuously scanned over the 5nm. This reduced the coherent noise to a level of just 0.4% which corresponds to a temperature resolution of 1.4°C. The Rayleigh plot is shown in Figure 6-6.

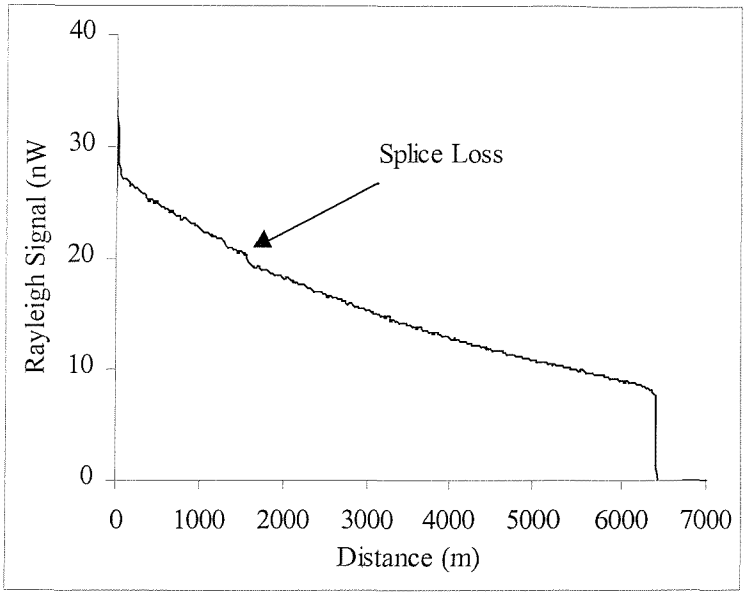

Figure 6-6 *- Rayleigh Backscattered trace with the source wavelength continuously scanned over 5nm*

In Figure 6-6 the splice losses in the sensing fibre are clearly visible whereas previously, see Figure 6-4, they were obscured by the coherent Rayleigh noise.

6.2.3 Conclusion

In conclusion we have reduced the coherent Rayleigh noise by scanning the wavelength of the Q-switched laser, this was done by an applied strain to the grating which shifts the operating wavelength. The final section in this chapter investigates the Brillouin distributed temperature sensor as a whole system, Q-switched fibre laser, Mach-Zehnder and detection and averaging.

6.3 Components for Brillouin DTS Systems

There are two main components which make up the Brillouin distributed temperature sensor, these are the source and the detection systems.

6.3.1 Source considerations for Brillouin DTS

The source is the major component of the DTS system and therefore needs to be reliable, cheap to produce and able to fulfil the high power, short pulse, narrow linewidth requirements discussed in chapter 2. The narrow linewidth Q-switched fibre laser discussed in the previous chapter is an ideal source for this application, with the additional benefit, highlighted in the previous section of being able to reduce the CRN on the Rayleigh signal by straining the grating.

6.3.2 Detection of the Brillouin signal

Another practical aspect of the Brillouin DTS system which has to be examined is the separation of the Brillouin and Rayleigh signals in the detection system. The two signals as we have seen are separated by approximately 10GHz, with such a small frequency separation the two signals cannot be separated using conventional dichroic filters as is the case in the Raman based DTS. In early experiments the Brillouin Stokes or anti-Stokes were separated from the Rayleigh using a bulk Fabry-Perot interferometer [4]. Bulk Fabry-Perot interferometers are in general, large and expensive devices, not at all suitable for a commercial instrument. They also introduce a large loss into the system a typical loss through the Fabry-Perot is approximately 10dB. Attempting to overcome the loss by using an EDFA to amplify the backscattered signal has been demonstrated but suffers from degradation of the signal due to the presence of ASE [6]. A Fabry-Perot does however have a high rejection ratio of in excess of 30dB which makes it a suitable filter to reject the Rayleigh from the Brillouin. Another simple type of interferometer, which offers a simple, cheap and effective means of separating the two signals has been developed based on the Mach-Zehnder interferometer [7].

6.3.2.1 Mach-Zehnder Interferometer

An illustration of an all-fibre Mach-Zehnder interferometer is shown in Figure 6-7.

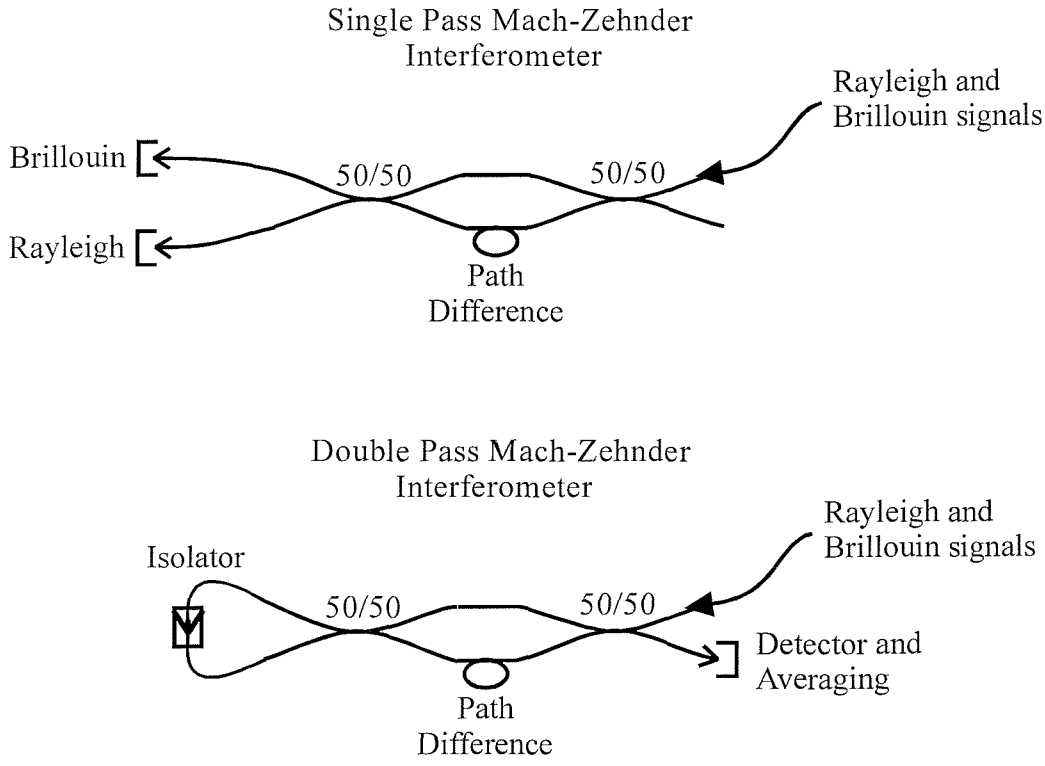

***Figure 6-7** -Schematic of both, (a) Single pass and (b) Double pass Mach-Zehnder Interferometers*

The interferometer consists of two 50/50 couplers connected together as shown, with a path imbalance in one arm of the interferometer [8][9]. Two configurations were developed the first was the single pass configuration which separated the Rayleigh and Brillouin signals into separate arms. The Rayleigh signal could be measured in one arm whilst both the anti-Stokes and Stokes Brillouin signals were detected in the other arm. Using this configuration both the Rayleigh and Brillouin signals can be measured simultaneously and the LPR can be calculated by simply dividing one signal by the other. This device offers low insertion loss (<1dB) and a rejection of the Rayleigh from the Brillouin signals of 17dB. Assuming the spontaneous Brillouin anti-stokes and stokes signals are 1/60 the intensity of the Rayleigh signal then 37% of the signal in the Brillouin arm will be due to Rayleigh

contamination. To overcome this relatively low rejection of the Rayleigh signal from the Brillouin a double pass configuration [10] was used.

The double pass configuration had a measured rejection ratio of 27dB which relates to a 5.6% contamination of the Brillouin signal with Rayleigh. The importance of reducing the Rayleigh signal from the Brillouin is to reduce the noise and therefore increase the temperature resolution. As discussed previously the predominant noise source is coherent Rayleigh noise which exists on the Rayleigh signal and cannot be reduced by further averaging. The coherent Rayleigh noise has been measured to be 2.5% of the Rayleigh signal which if there is a 5.6% contamination of the Brillouin signal by the Rayleigh relates to a 0.14% noise (0.5°C) on the Brillouin signal. It is this which is the limiting factor on the temperature resolution of the device.

The double pass configuration was achieved by passing the Brillouin arm back though the Mach-Zehnder, an isolator was used to prevent the Rayleigh signal from going back down the sensing fibre. In the basic configuration shown in Figure 6-7 only the Brillouin signal could be measured, to simultaneous monitor both the Rayleigh and Brillouin a 95/5 tap coupler was placed in the Rayleigh arm, so as the monitor the Rayleigh.

In the design of the Mach-Zehnder it is the path imbalance between the arms of the Mach-Zehnder that determines the free spectral range. The FSR is give by the equation:

$$d = \frac{c}{n \cdot (\Delta \upsilon)_{FSR}}$$

where d, is the path imbalance between the two fibre arms, n, is the refractive index, and $(\Delta\upsilon)_{FSR}$ is the free spectral range of the device (approximately 22GHz) . A path imbalance of 9.1mm gives the required FSR of 22GHz. Figure 6-8 shows the transmission of a double and single pass Mach-Zehnder interferometers. The transfer function, F(ν), for the single and double pass configuration is given by equation (6-1), where n=1 for a single pass and n=2 for the double pass. It can be seen that the double pass Mach-Zehnder has a narrower transmission window. This is beneficial as it allows a decrease in tolerance on the path

imbalance due to the flatter profile between the transmission peaks, a difference of 1mm or so will not affect the rejection of the Rayleigh from the Brillouin arms.

$$F(\nu) = \left[\frac{1}{2}\cdot\left[1+\cos\left(\frac{2\cdot\pi\cdot\nu}{FSR}\right)\right]\right]^{n} \qquad (6\text{-}1)$$

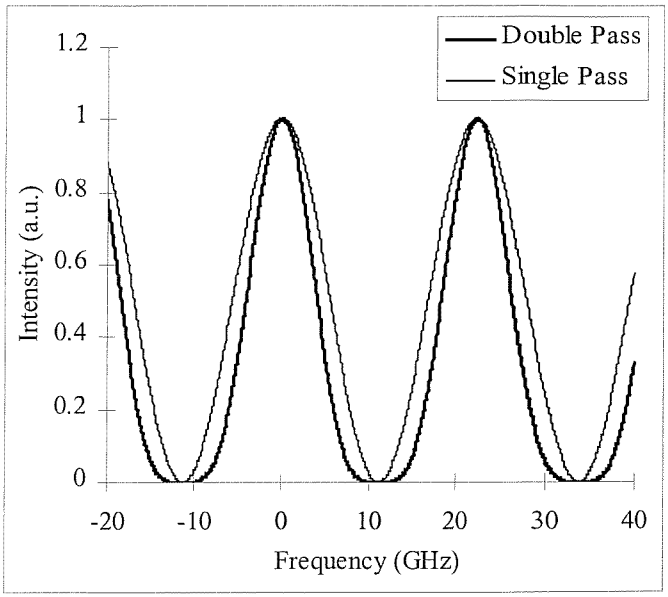

Figure 6-8 *- Plot showing the transfer functions of both the single pass and double pass Mach-Zehnder interferometer*

The Mach-Zehnder device was thermally insulated from the environment to produce sufficient stability in the short term i.e. over the time of the measurements.

6.4 Distributed Temperature Sensor - Experiment and Results

A schematic of the final design of the distributed temperature sensor is shown in Figure 6-9. The design consists of the narrow linewidth Q-switched laser, which provides both narrow linewidth and quasi-broadband source, and a Mach-Zehnder interferometer which separates the Rayleigh and Brillouin.

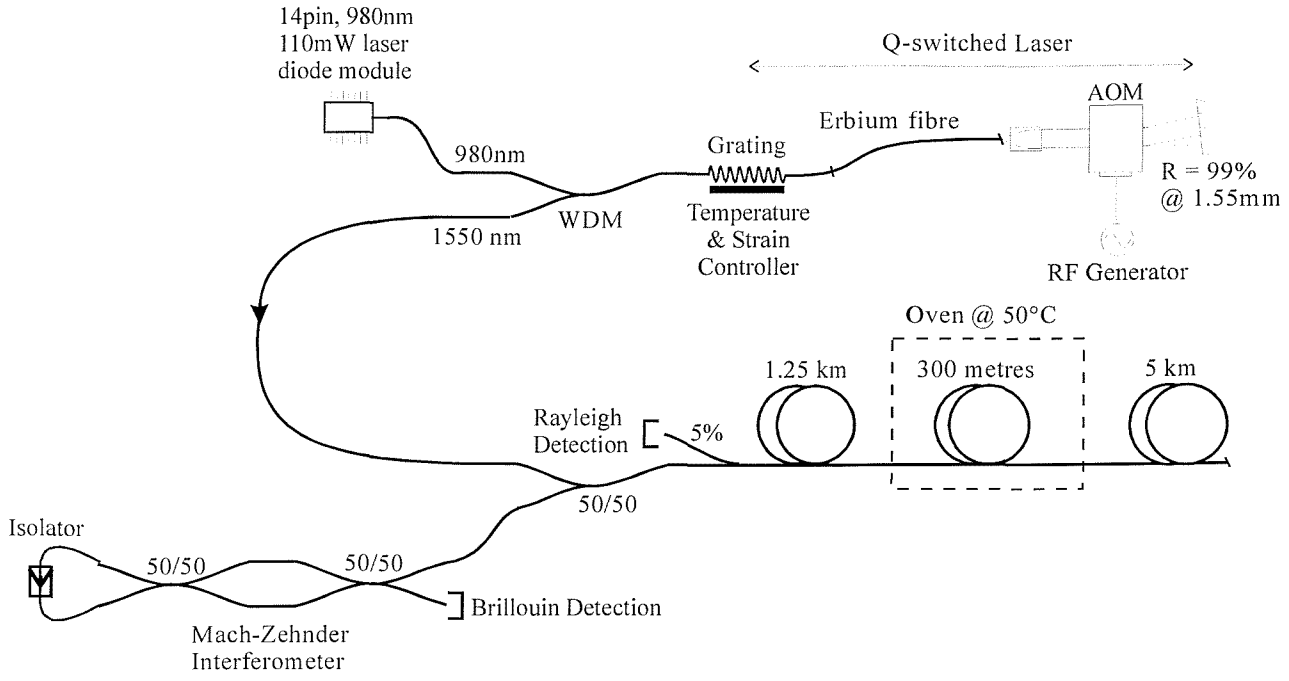

***Figure 6-9** - Brillouin Distributed Temperature Sensor*

The Rayleigh backscattered light is obtained by tapping off 5% of the signal before it reaches the Mach-Zehnder interferometer. By scanning the wavelength of the laser over 5nm, the coherent Rayleigh noise is reduced to a level where a less than 1.5°C temperature resolution can be obtained. The laser wavelength is then fixed and the grating is tuned using the temperature controller to obtain maximum throughput of the Brillouin from the Mach-Zehnder. The Rayleigh signal is only used as a reference to remove variations in localised attenuation from the Brillouin signal, therefore it is not necessary to continuously monitor the Rayleigh signal. The Brillouin signal obtained from the output of the Mach-Zehnder is shown in Figure 6-10. The sensing fibre is split into three sections with only the centre 300m section heated to 50°C, where a clear increase in signal can be observed.

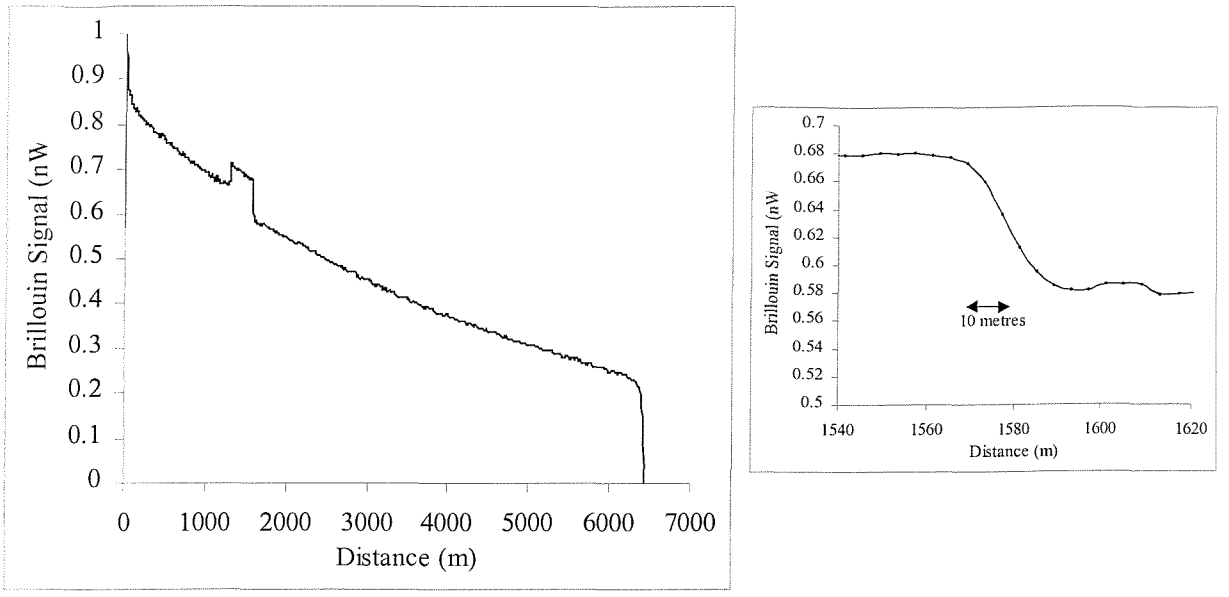

Figure 6-10 *- Brillouin Signal from sensing fibre with the interface between the heated and unheated section of the fibre expanded to demonstrated system spatial resolution*

The Landau-Placzek ratio is defined as the Rayleigh divided by the total Brillouin signal (Stokes and anti-Stokes components). The division of the Rayleigh by the Brillouin removes any dependence on local attenuation changes such as splice and bend losses. The Landau-Placzek ratio is shown in Figure 6-11.

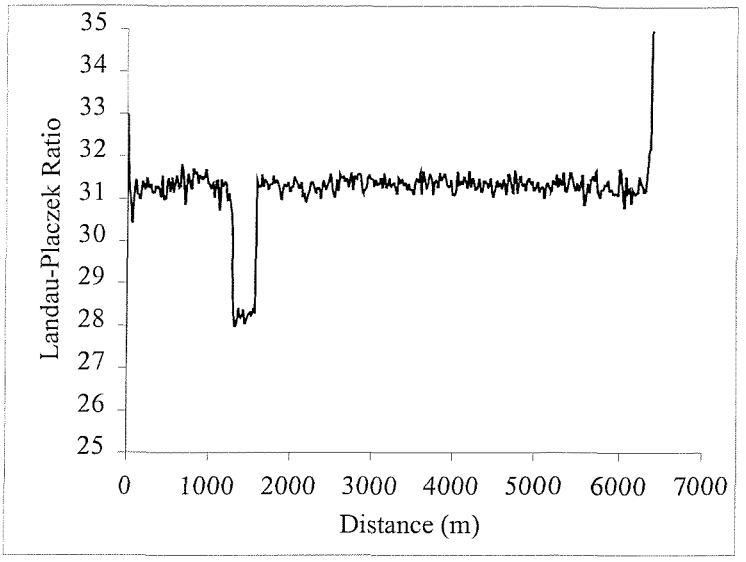

Figure 6-11 *- Landau-Placzek ratio of a 6km length of fibre, a central 300m length is heated to 50°C*

As Figure 6-11 shows the Landau-Placzek ratio (LPR) is independent of any local variations in attenuation, as either side of the heated section there is a splice loss which has no effect on the Landau-Placzek ratio but which can be seen on the Rayleigh plot (Figure 6-6). The centre section is heated to a temperature of 50°C and this is shown as a decrease in the LPR. The sensor developed has a spatial resolution of 10metres and a temperature resolution of 1.4°C over a range of 6.5km.

6.5 Conclusions

In conclusion, using a narrow linewidth Q-switched fibre laser and the all-fibre Mach-Zehnder interferometer, a low cost, single ended distributed temperature sensor has been demonstrated that is suitable for commercial development. The predominant noise source has been identified as coherent Rayleigh noise and a method of reducing this noise using a technique of frequency shift averaged has been demonstrated using the Q-switched laser.

6.6 References

[1] K.Shimizu, T.Horiguchi and Y.Koyamada: 'Characteristics and Reduction of Coherent Fading Noise in Rayleigh Backscattering Measurement for Optical Fibers and Components', *Journal of Lightwave Technology*, Vol.10, No.7, pp.982-987, (1992)

[2] J.P.King, D.F.Smith, K.Richards, P.Timson, R.E.Epworth and S.Wright: 'Development of a Coherent OTDR Instrument', *Journal of Lightwave Technology*, Vol.LT-5, No.4, pp.616-624, (1987)

[3] P.C.Wait and T.P.Newson: 'Reduction of coherent noise in the Landau-Placzek ratio method for distributed fibre optic temperature sensing', *Optics Communications*, Vol.131, pp.285-289, (1996)

[4] P.C.Wait and T.P.Newson: 'Landau-Placzek ratio applied to Distributed Fibre Sensing', *Optics Communication*, Vol.122, pp.141-146, (1996)

[5] J.Schroeder, R.Mohr, P.B.Macedo and C.J.Montrose: 'Rayleigh and Brillouin scattering in K_20-SiO_2 glasses', *Journal of American Ceramic Society*, Vol.56, No.10, pp.131, (1973)

[6] T.R.Parker, M.Farhadiroushan, V.A.Handerek and A.J.Rogers: 'A Fully Distributed Simultaneous Strain and Temperature Sensor using Spontaneous Brillouin Backscatter', *IEEE Photonics Technology Letters*, Vol.9, No.7, pp.979-981, (1997)

[7] K.De Souza, G.P.Lees, P.C.Wait and T.P.Newson: 'A diode pumped Landau-Placzek based distributed temperature sensor utilising an all-fibre Mach-Zehnder interferometer', *Electronics Letters*, Vol.32, No.23, pp.2174-2175, (1996)

[8] C.A.Millar, D.Harvey and P.Urquhart: 'Fibre Reflection Mach-Zehnder Interferometer', *Optics Communications*, Vol.70, No.4, pp.304-308, (1989)

[9] G.Dickinson, D.A.Chapman and D.A.Gorham: 'Properties of the fibre reflection Mach-Zehnder interferometer with identical couplers', *Optics Letters*, Vol.17, No.17, pp.1192-1194, (1992)

[10] K.De Souza, P.C.Wait and T.P.Newson: 'Double-pass configured fibre Mach-Zehnder interferometric optical filter for distributed fibre sensing', *Electronics Letters*, Vol.33, No.25, pp.2148-2149, (1997)

Chapter Seven

1.64μm pulse Generation and Amplification

7.1 Introduction

The successful construction of a number of high-powered Q-switched lasers allowed a number of experiments exploiting Raman gain in fibres. This chapter describes alternative applications for Q-switched Erbium doped fibre lasers, namely the generation of higher order Raman wavelengths, and the amplification of pulsed signals in the 1.64μm wavelength region. The high powers (>100watt) available in Q-switched fibre lasers, combined with the long interaction lengths due to the waveguiding nature of optical fibre, enables the generation of multiple orders of Stokes wavelengths. This Raman gain at the Stokes wavelengths can provide the means both to generate high power sources and to amplify existing signals in the wavelength range 1640-1680nm. The interest in wavelengths in the 1.6μm region is for live maintenance of fibre optic telecommunications links i.e. monitoring the fibre for defects whilst the fibre is being used for telecommunications. An optical time domain reflectometry (OTDR) technique is used to monitor the fibre attenuation. In an OTDR system, a short pulse of light is transmitted down the sensing fibre and the Rayleigh backscattered light is detected. The intensity of the backscattered light provides a measure of the loss in the fibre and the time between launching the light pulse into the fibre and obtaining the backscattered signal provides a continuous measure of distance in the fibre. Another possible application is as a source for Distributed Temperature Sensing (DTS) based on Raman scattering. This relies on the OTDR technique but the anti-Stokes Raman signal is detected rather than the Rayleigh. If the pump is at 1.64μm then the weak temperature dependent anti-Stokes Raman signal will be generated in the low loss window at 1.53μm. The weak backscattered signal is therefore generated where the fibre loss is at it's lowest. This chapter investigates both the generation of light in the 1.6μm band for OTDR and DTS applications and the amplification of such signals.

7.2 Introduction to 1.64μm Pulse Generation

Although 1.6μm sources have an application in monitoring live transmission lines for defects and as a source for DTS systems, the production of OTDR systems at this wavelength was limited because of the low power of available semiconductor laser diodes at this wavelength. For high resolution, high dynamic range OTDR, high peak power, short pulses are required, typical of those emitted from Q-switched laser sources. However the production of a Q-switched fibre laser at the 1.64μm wavelength is not possible because of the lack of a suitable gain medium. Recently [1][2] a high power 1662nm pulsed source was generated from a low power laser diode which was amplified using a 1546nm pulse from another laser diode which was amplified to 1.4watts using an EDFA. This produced an output power of 200mW and pulse widths of 100ns at a wavelength of 1662nm. In this chapter we report a simple method of producing pulses in the 1.6μm band using the process of stimulated Raman generation.

7.2.1 Theory of 1.64μm Pulse Generation

To generate the light in the 1.6μm wavelength band it is necessary to stimulate the first order Raman light using the Q-switched laser and a length of single mode telecommunications grade fibre [3][4]. By sending an intense pulse of light down the fibre from the Q-switched laser, the Raman Stokes wavelengths are generated co-propagating with the forward travelling pulse with the maximum intensity occurring at a wavelength shift of 440cm^{-1} wavenumbers. These Raman wavelengths build up by a process of stimulated Raman generation until the pump pulse is depleted. The generated first order Raman wavelength can also go on to generate further multiple orders of Raman wavelengths in the 1.7μm and 1.8μm regions each separated by 440cm^{-1} wavenumbers. The generation of subsequent Raman orders is detrimental as it takes power from the required 1.6μm band and shifts it to higher wavelengths. The threshold for stimulated Raman generation is defined in equation (2-2) and is inversely proportional to the fibre effective length. Therefore for long lengths of fibre (30km) the threshold for Raman generation is calculated to be as low as 620mW for a 100ns pulse width (see section 2.2.2.1). If a high power pump pulse of 100W is launched into such a length of fibre, this will generate many Raman orders which will

have the effect of depleting the required first order 1.6μm Raman band. To produce just the first order Raman in the 1.6μm band the length of the fibre needs to be optimised. The experiment was carried out using three lengths of fibre 300m, 600m, and 1360m and the Raman threshold and output were investigated.

7.2.2 Experiment

The experimental arrangement is shown in Figure 7-1.

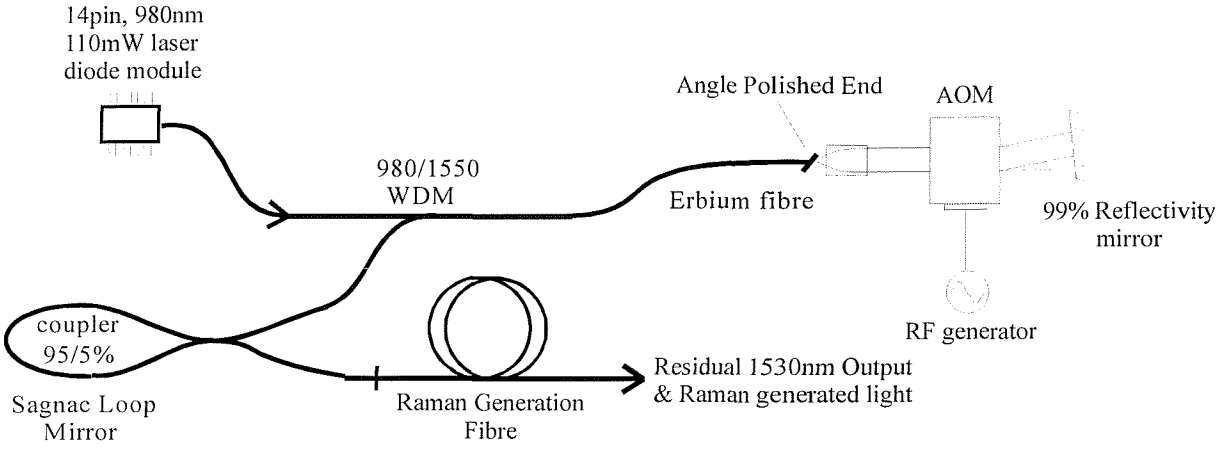

***Figure 7-1** - Schematic of Raman Generation Experiment*

The experiment consists of a Q-switched fibre laser which generates high power pulses of light at 1530nm. The Q-switched laser discussed in section 5.4 was modified to include a Sagnac loop mirror as the output coupler [5]. Using the loop mirror instead of conventional bulk mirrors has the major advantage of making the Q-switched laser fibre compatible and allows direct splicing onto the Raman generation fibre.

The Q-switched laser was operated in first order with a peak power of 96W and a pulse width of 20ns. These pulses were launched into a length of single-mode fibre to generate the Raman Stokes shifted wavelengths. Results showing the power of the launched pulse and the generated Raman and residual pump were collected for three different lengths of fibre, 300m, 600m and 1360m.

7.2.3 Results and Conclusion

The 96watt, 20ns pulse which was launched into the Raman generation fibre is shown in Figure 7-2. The residual 1.53μm pump and the generated 1.64μm Raman signal for the 300m, 600m and 1360m lengths of fibre are shown in Figure 7-3 and the results are tabulated in Table 7-1.

Fibre Length (m)	Output power at 1.64μm, (3dB bandwidth of 25nm)	Threshold power at 1.53μm for generation of Stokes at 1.64μm
300	8.4	32
600	7.7	22
1360	5.4	13

Table 7-1 *- Table showing Raman output power and Threshold powers for the generation of Raman for three lengths of fibre*

The generated Raman signal was filtered from the residual 1.53μm pump using a bandpass filter centred at 1.64μm with a 3dB bandwidth of 25nm, similarly the 1.53μm residual pump was separated from the Raman signal using a filter centred at 1.53μm.

Figure 7-3a shows the Raman output and residual pump for the 300m length of fibre. The transfer of energy from the pump to the Raman causes the observed depletion of the pump signal at powers in excess of 32Watts. An undistorted Raman signal with a centre wavelength of 1.64μm, a peak power of 8Watts and a pulse width of 10ns was generated.

The results in Figure 7-3b were obtained with 600m of fibre. The depletion observed on the residual pump power occurs at a lower power of 22Watts, indicating a decrease of the Raman threshold caused by the longer fibre length. A distortion of the Raman signal is also evident and is attributed to the generation of further Raman Stokes orders. This generation of further Stokes orders becomes more pronounced with the 1360m length of fibre as shown in Figure 7-3c. In conclusion the higher threshold obtained by using a short length of fibre to generate the Raman, coupled with the high peak powers from the Q-switched laser, enabled a 1.64μm pulsed source to be produced with peak powers in excess of 8watts, a pulse width of 10ns and an optical bandwidth of 25nm.

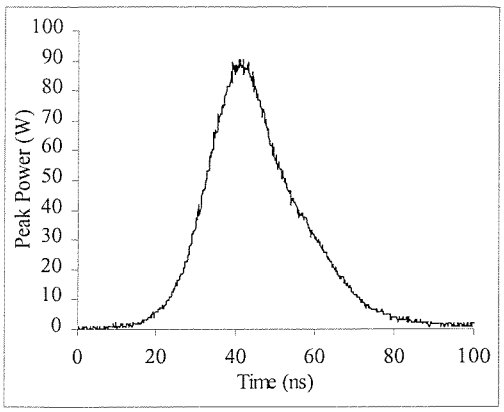

Figure 7-2 *- 1.53μm pulse from Q-switched laser*

a)

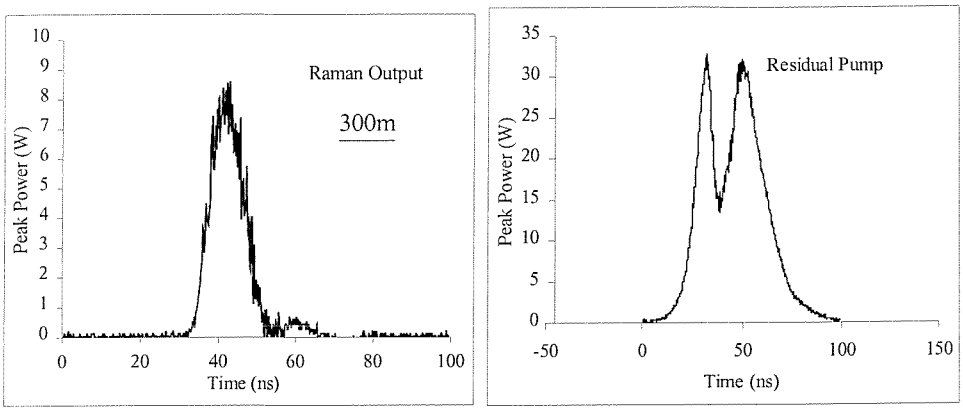

b)

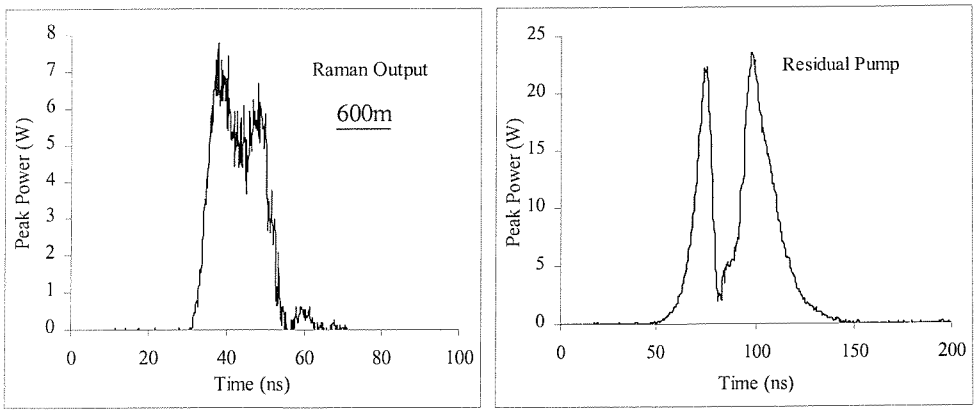

c)

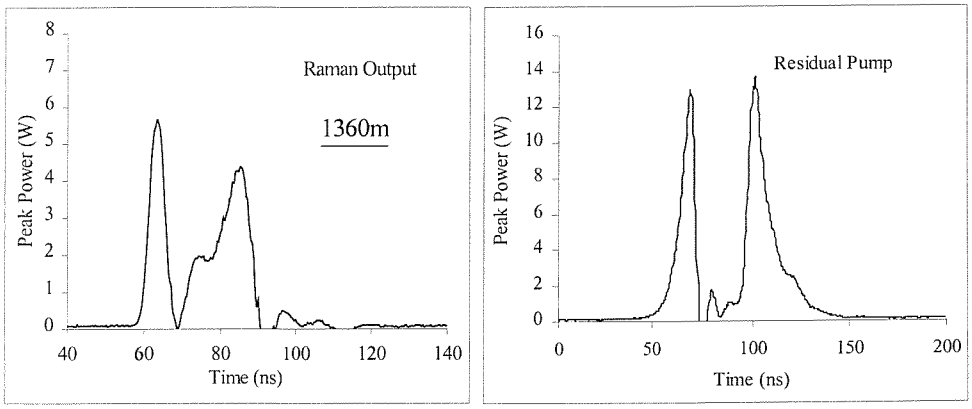

Figure 7-3 *- Plots showing Residual 1.53μm pump and Raman output from (a) 300metres, (b) 600metres and (c) 1360metres of fibre*

7.3 Introduction to 1.64μm Pulse Amplification

The previous section utilised Raman gain to generate Raman Stokes shifted wavelengths for 1.64μm OTDR and DTS applications. In this section the possibility of using Raman gain to increase the dynamic range of such a system is investigated. The proposed technique combines the use of a Q-switched Erbium doped fibre laser operating at 1.53μm both to generate 1.64μm pulses and pump the fibre under test to provide additional Raman amplification. Raman amplification occurs when the 1.53μm and 1.64μm pulses overlap and this occurs at a position determined by the dispersion within the fibre and the initial separation of the two pulses. By delaying the pump pulse with respect to the OTDR pulse, amplification of the latter may be delayed by tens of kilometres. This technique operates with both the Raman pump pulse and the OTDR pulse just below their respective stimulated Raman thresholds at the front end of the fibre under test. The amplification of the signal pulse allows a greater pulse energy to be achieved some distance down the test fibre thus increasing the dynamic range of the system. The amount of energy available to amplify the OTDR pulse is governed by (i) the peak intensity of the pump which is determined by the stimulated Raman threshold and (ii) the pulse width. This may be considerably larger than the OTDR pulse width, which is determined by the system spatial resolution.

7.3.1 Experiment

A Q-switched Erbium doped fibre laser, as shown in Figure 7-1, produced 125watt, 28ns pulses at a repetition rate of 800Hz. Each of these pulses was divided into two, using a 90/10 coupler (Figure 7-4).

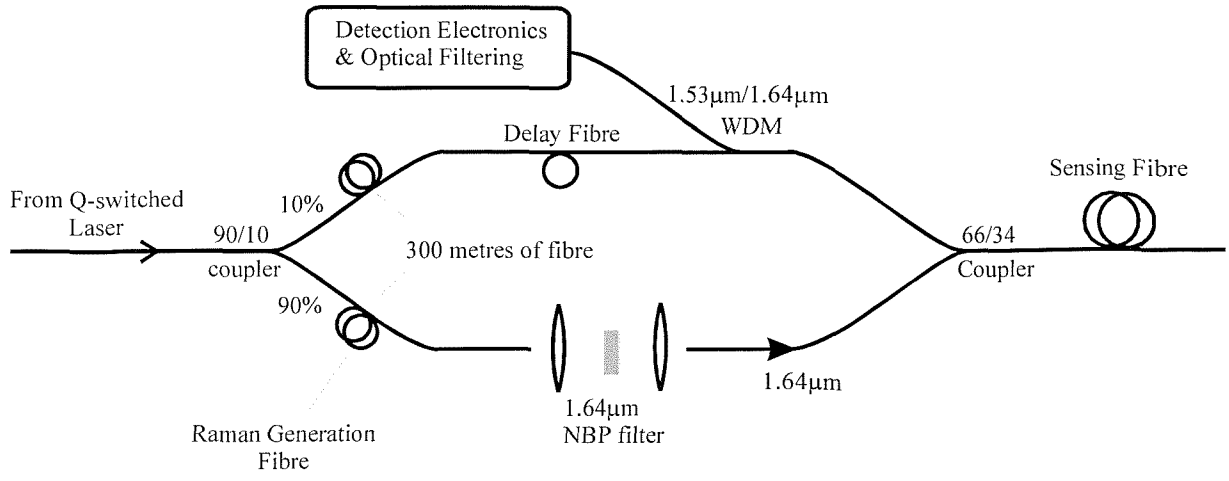

Figure 7-4 *- Schematic of experiment for delayed Raman amplification of 1.64μm OTDR signals*

The light in the 90% arm was used to generate the 1.64μm light by a process of stimulated Raman scattering along a 300m length of fibre as described previously. This 1.64μm light was separated from the residual light by a narrow-band pass filter centred at 1.64μm. This produced a 1.64μm pulse with a peak power of 1watt, a pulse width of 18ns and a 3dB optical bandwidth of 25nm. This pulse was then recombined with the 1.53μm pulse travelling in the 10% arm using a 66/34 coupler which, because of the high power of the 1.65μm signal is biased in favour of the backscattered signal. A delay is introduced between the two pulses entering the fibre by adjusting the length of fibre on the 10% arm of the coupler. The two wavelengths are in the anomalous dispersion regime and therefore the shorter 1.53μm wavelength travels faster than the 1.64μm wavelength. The delay is adjusted so that the 1.53μm pulse falls just behind the 1.64μm pulse. The initial starting positions of both of the pulses is shown in Figure 7-5 with a delay of 35ns between the peaks of the two pulses.

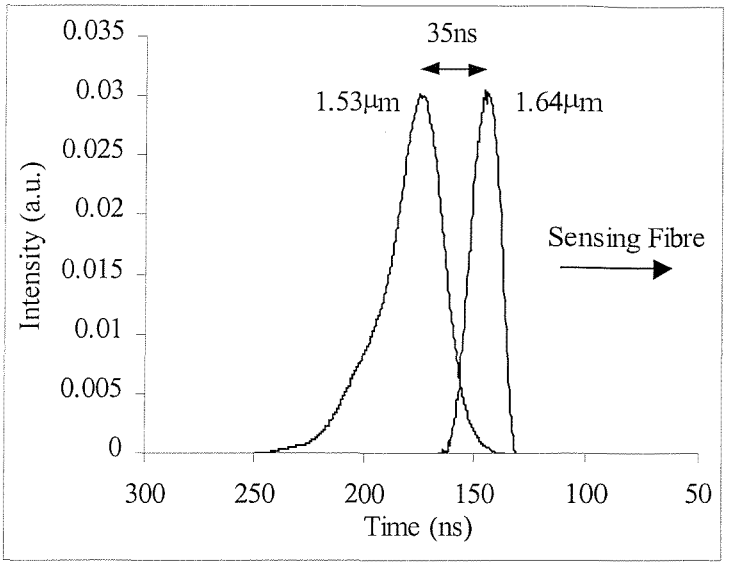

Figure 7-5 *- Schematic showing the separation of the 1.55μm and 1.64μm pulses at the start of the sensing fibre*

Assuming the dispersion of the fibre to be 17ps/nm.km, then the peaks of the two pulses will overlap at a distance of approximately 20km down the fibre. When the two pulses travel along the fibre under test, the 1.53μm pulse passes through the 1.64μm signal pulse amplifying it through a process of Raman amplification.

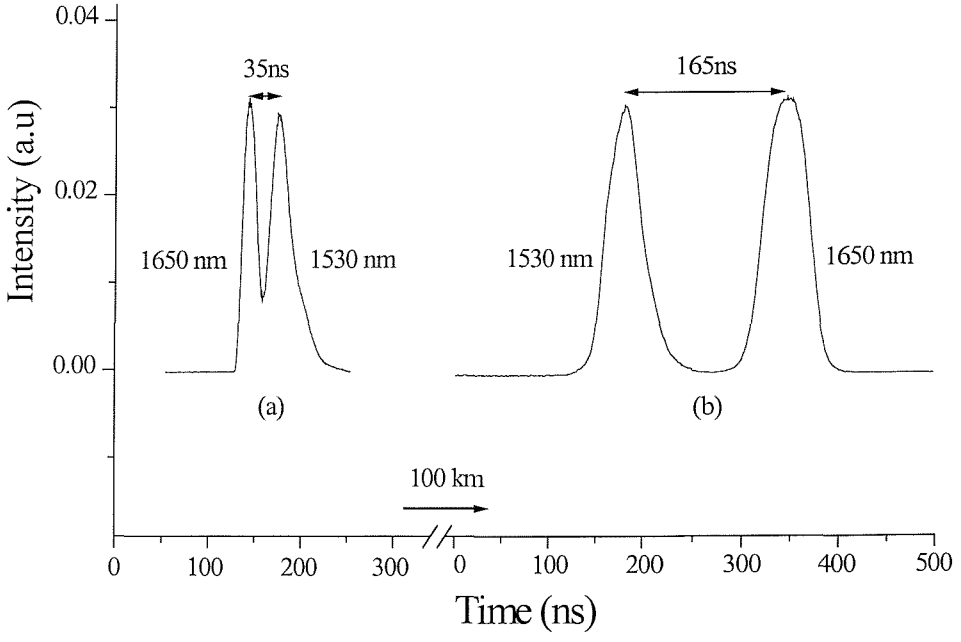

Figure 7-6 *- Plot showing the relative positions of the two pulses at the start and end of the sensing fibre*

Figure 7-6 shows the 1.53μm and 1.64μm pulses at the start and end of a 100km length of fibre. Due to the fibre dispersion the 1.53μm pulse has passed through the 1.64μm pulse and relative to this pulse has travelled a total of 200ns further, using this value and the length of the test fibre the dispersion parameter was calculated to be 17ps/nm.km, which confirms the initial assumption.

7.3.2 Results

Figure 7-7 shows the results obtained from the 1.65μm OTDR without any pulsed amplification, the range of such a system is just over 80km with the splice losses visible up to this length.

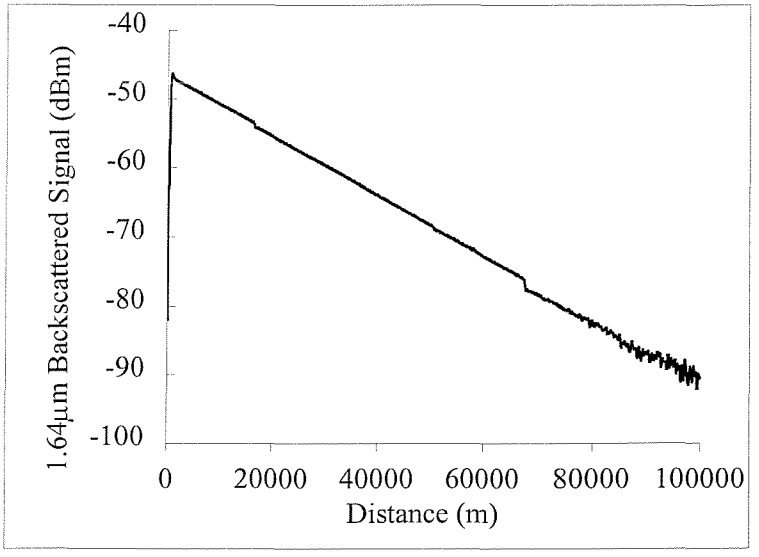

***Figure** 7-7 - 1.64μm OTDR trace with no Raman amplification*

With the pulsed amplification the results are shown in Figure 7-8. The range can now be extended to over 100km with a similar noise level to that at 80km with no pulse amplification.

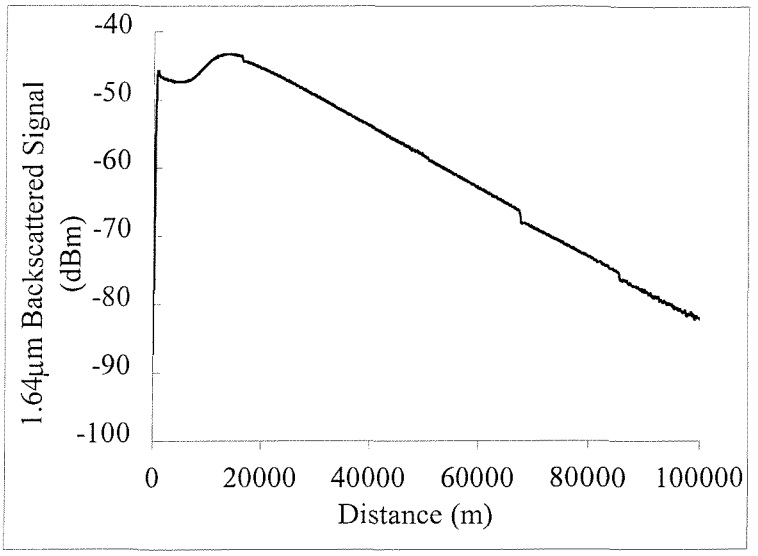

***Figure 7-8** - 1.64µm OTDR trace with Delayed Raman Amplification*

Figure 7-9 shows the evolution of this amplified OTDR signal as a function of pump pulse power. The pump power is increased up to a maximum of 5watts in 1watt increments. There is a reduction in the rate of increase of net gain with increasing peak pump power levels. This is attributed to the saturation of the Raman amplification process caused by the generation of further orders of Stokes shifted wavelengths.

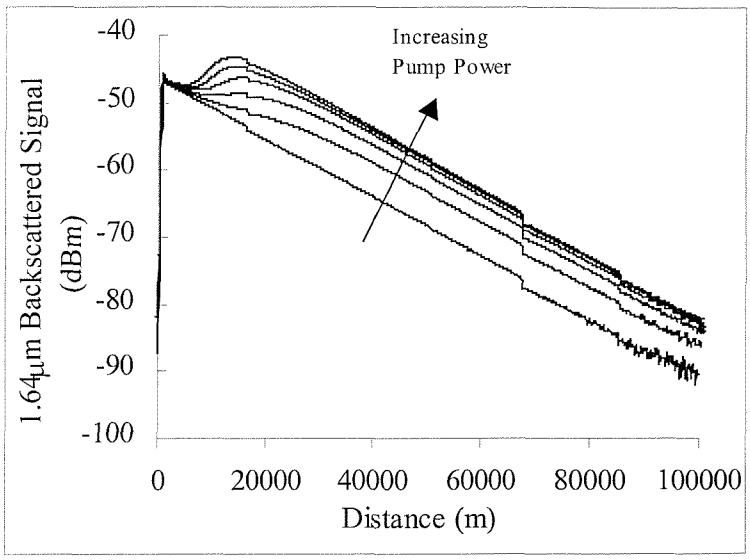

Figure 7-9 *- Variation of 1.64μm OTDR signal with increasing 1.53μm pump signals in 1watt increments for a fixed 1.64μm signal of 850mW*

The saturation of the amplification process is illustrated in Figure 7-10. The plot shows the net amplification of the 1.65μm OTDR signal for a range of 1.53μm pump powers.

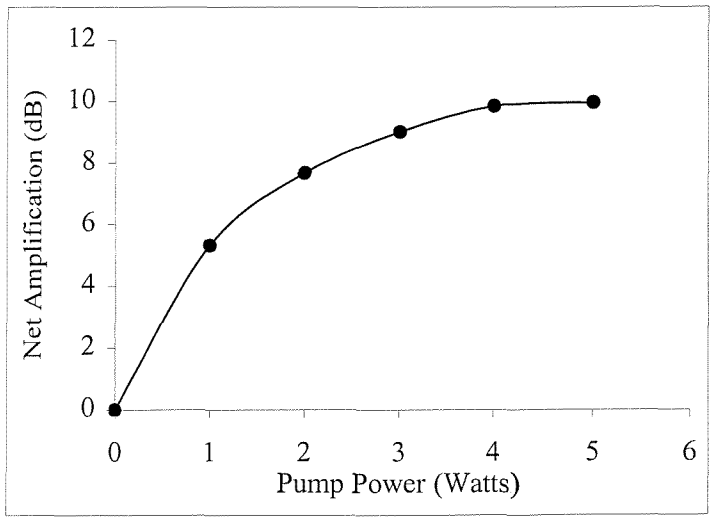

Figure 7-10 *- Net amplification of the 1.65μm OTDR signal for pump powers up to 5 Watts*

The following plot (Figure 7-11) shows the variation of the OTDR signal with increasing signal powers.

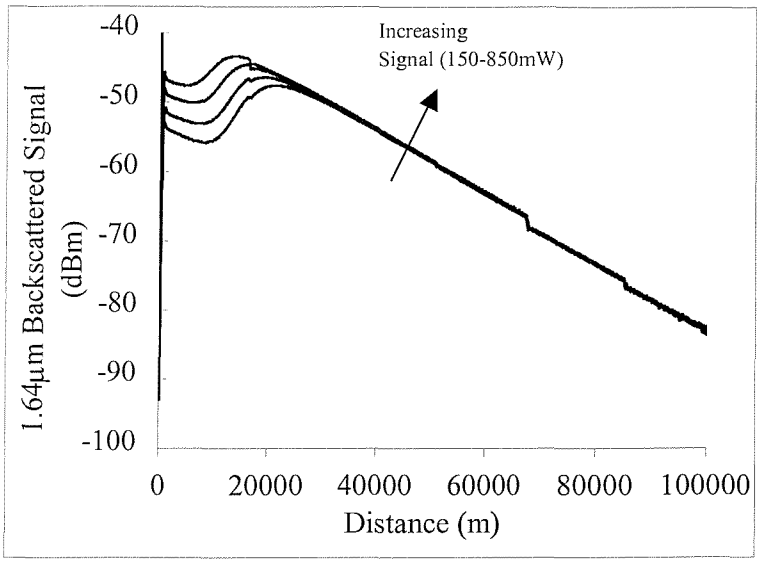

***Figure** 7-11 - Variation of 1.64μm OTDR signal with increasing signal powers (150, 300, 560 and 850mW) with a fixed pump power of 5.4watts*

The interesting point to note about these results are that by increasing the signal power no further increase in dynamic range is obtained, this again is attributed to the generation of further orders of Stokes wavelengths which limit the magnitude of the 1.64μm OTDR signal.

7.4 Conclusions

Through a process of delayed Raman amplification and the utilisation of a high power Q-switched Erbium fibre laser, a novel technique of increasing the dynamic range of 1.65μm OTDR has been demonstrated. By means of fibre dispersion a 1.53μm pulse passes through a 1.65μm pulse at a delayed position down the sensing fibre this results in amplification of the 1.65μm pulse. Furthermore, the amplification is achieved without significant noise penalty as a result of the directionality of the amplification process. This technique is therefore ideal for increasing the range of OTDR backscattered measurements. However this technique may be employed for other applications of distributed measurements, such as distributed strain and temperature sensing based on Raman and Brillouin scattering. As the limiting threshold value of probe pulse occurs some distance down the sensing fibre, increases in sensor range are expected.

7.5 References

[1] T. Horiguchi, T. Sato and Y. Koyamada, 'Stimulated Raman Amplification of 1.6μm Band Pulsed Light in Optical Fibres', *IEEE Photonics Technology Letters*, Vol.4, No.1, pp. 64-66, (1992)

[2] T. Sato, T. Horiguchi, Y. Koyamada and I. Sankawa: 'A 1.6μm Band OTDR Using a Synchronous Raman Fibre Amplifier', *IEEE Photonics Technology Letters*, Vol.4, No.8, pp. 923-924, (1992)

[3] Govind P. Agrawal: 'Nonlinear Fibre Optics - Second Edition', *Academic Press*, ISBN 0-12-045142-5, Chapter 8 - Stimulated Raman Scattering

[4] J. Auyeung and A. Yariv: 'Spontaneous and Stimulated Raman Scattering in Long Low Loss Fibers', *IEEE J. Quantum Electronics*, QE-14, No.5, pp. 347-352, May (1978)

[5] N. J. Doran and D. Wood: 'Nonlinear-optical loop mirror', *Optics Letters*, Vol.13, No.1,pp. 56-58, January (1988)

Chapter Eight

Summary of Thesis and Conclusions

8.1 Introduction

This thesis presented a theoretical and experimental examination of Q-switched Erbium doped fibre laser devices. A computer model was developed to obtain information on trends in performance of the Q-switched laser when various parameters are altered. The starting point for the model was to obtain information on the pump absorption and the population inversion in the fibre. This was achieved using a standard rate equation model for three level amplifier systems. The model provided a quantitative value for the energy stored in the amplifier medium which could then be used, along with the cavity losses, to model the Q-switched pulse characteristics of the fibre laser. Using an amplifier model to calculate the stored energy in the medium allows ASE effects to be modelled. In this work, the basic amplifier model was adapted to take into account the depletion of the stored energy by the reflection of ASE from a highly reflecting mirror on one end of the amplifier. It is this arrangement which is found in a Q-switched laser, and the reflection of the ASE back into the cavity from such a mirror was found to reduce the stored energy by 27%, with a corresponding decrease in performance.

Armed with the results from the computer model, a number of different experimental configurations were explored resulting in a number of novel findings. An Erbium doped Q-switched laser was initially developed for use as a source for Raman based distributed temperature sensing. The final device design has now been implemented in a commercial sensing device, the York Sensors DTS-800 ULR system. The Q-switched Erbium doped fibre laser had a peak power in excess of 100Watts output with a 20ns pulse width, ideal for long range distributed temperature sensing. The design was later improved to incorporate

the advances in 980nm pump laser diodes from bulk devices to fibre pigtailed pump sources, this improved the long-term stability and reliability of the device.

In order to produce shorter pulse widths, the Erbium fibre was replaced with Erbium/Ytterbium fibre. This had the effect of substantially reducing the cavity length from a 1.2metre long Erbium doped laser to a cavity less than 20cms in length. The addition of the Ytterbium offers an alternative route to pumping the Erbium ions. The Ytterbium ions absorb the pump light and then, by a process of cross-relaxation between the adjacent Ytterbium and Erbium ions, allows the energy to be transferred. The pulse width generated by this laser was 15ns and although short was not as short as expected. The larger than expected pulse width was attributed to the larger number of round trips required for the Q-switched pulse to build-up. The large number of round trips were due to a lower round trip gain caused by the shorter length of fibre. This however represents the highest peak power (58watts) from a diode pumped Q-switched Erbium/Ytterbium fibre laser.

In a further bid to obtain shorter pulses from a Q-switched fibre laser, a faster modulator was utilised. The acousto-optic modulator was exchanged for a faster electro-optic modulator or Pockels cell, the model used in this work had a switching time of 4ns. The results obtained represented the highest peak powers obtained from a diode pumped Q-switched Erbium doped fibre laser with a peak power of 540Watts and pulse width of 12.5ns. However an unusual phenomenon was observed within the Q-switched envelope which manifested itself as a stable pulsed structure with a frequency equal to the round trip time of the cavity. It had been suggested in previous publications that this pulsed behaviour was due to mode coupling enhanced by the effect of self-phase modulation [1]. Self-phase modulation occurs because of the non-linear intensity dependence of the refractive index and we would therefore expect this effect only to occur at high peak powers. However, the wide range of experimental configurations carried out in this work has led us to believe that the pulsed behaviour observed is in fact caused when the switching time of the modulator is fast compared to the round trip time of the cavity. A step-wise build up of ASE is then observed which when coupled with gain depletion causes the aforementioned pulsed behaviour. This observation was backed up by an experiment in which the temporal behaviour of the laser was investigated as a function of modulator switching time. It was

found that if the switching time is slow compared to the cavity round trip time, the pulsation could be reduced and finally eliminated.

Further evidence that the self-phase modulation theory was incorrect was provided with the advent of a novel large mode area fibre type. The large mode area fibre improves the energy storage within the fibre by reducing the amplified spontaneous emission (ASE), for a given absorbed pump power, and by increasing the threshold at which non-linear Raman and Brillouin effects occur. Using this large mode area fibre, the highest peak powers ever emitted from a Q-switched fibre laser were demonstrated, i.e. a peak power of 4kW and a pulse width of 10ns. With these high peak powers the laser would be an ideal candidate for the proposed self-mode locking through self-phase modulation. However a single pulse was observed and not the pulsed behaviour proposed in the self-mode locking theory. This strengthened the theory proposed in this work that the pulsed behaviour is due to a combination of ASE build up and gain saturation. Since this work, the large mode area fibre has been utilised to produce 0.5mJ pulses. These advances were achieved by further optimisation of the core radius and dopant concentration [2].

Finally, and most importantly from a Brillouin sensing perspective, the development of fibre Bragg gratings enabled a narrow linewidth Erbium doped Q-switched fibre laser to be produced. The high peak power (>100Watts), short pulse (<20ns) characteristics combined with a linewidth of less than 2GHz matched exactly the requirements for distributed temperature sensing using spontaneous Brillouin scattering. Additionally the use of an in-fibre Bragg grating instead of a bulk output mirror has the advantage of generating an output which is compatible with other fibre components. This was the first demonstration of a Q-switched Erbium doped fibre laser incorporating a fibre Bragg grating and it provided a cost effective source with all the requirements for Brillouin distributed temperature sensing.

The narrow linewidth Q-switched fibre laser in conjunction with a double pass Mach-Zehnder interferometer had been developed to demonstrate a commercially viable Brillouin distributed temperature sensor. During the development of the sensing system, the Q-switched laser displayed another useful property; the ability to scan the lasing wavelength over a 5nm range. It was this property which led to an increased temperature resolution by

reducing the dominant coherent Rayleigh noise using the technique of frequency shift averaging. The noise on the Rayleigh signal was reduced from 2.2% to 0.42% by scanning the wavelength of the laser continuously over 5nm. This corresponds to a temperature resolution of 1.4°C. In this thesis a Brillouin distributed temperature sensor with a spatial resolution of 10metres, temperature resolution of 1.4°C and range of 6.5km has been demonstrated. Since this work, an increase in performance has been achieved by using a high performance averaging and low noise APD signal detection. The current sensing system performance has a spatial resolution of 3.5metres, temperature resolution of 1.4°C but with an increase in range to 16km. It is the aim of York Sensors to replace current Raman based long range sensors with the technology developed in this work.

In the final chapter a novel method for increasing the dynamic range of 1.65μm ODTR systems was demonstrated along with the construction of a high power source at 1.65μm by using Raman amplification. If the high peak powers from a Q-switched laser are launched into a length of fibre, gain occurs at the Raman shifted wavelength. Using this principle, this work demonstrates a pulsed source at 1.65μm with 8watts peak power and 10ns pulse width. This represents the highest peak powers achieved at 1.65μm from a diode pumped fibre laser system.

The Q-switched laser technology was also used to increase the dynamic range of 1.65μm OTDR which is increasingly used to detect faults on live 1.53μm transmission systems. The technique utilises delayed Raman amplification of the 1.65μm signal pulse by a co-propagating 1.53μm pump pulse. Amplification occurs when the two pulses overlap. The position of this overlap being determined by the initial delay between the pulses and the fibre dispersion. An increase in dynamic range of 17.5dB was observed and the 1.65μm OTDR range was extended to in excess of 100km.

8.2 Future Work

In terms of future work regarding Q-switched Erbium doped fibre lasers, the spectral properties of the pulse are as at the this time unexplored. Spectral filtering of the Q-switched pulse using a narrow fibre grating is envisaged as a method of producing shorter pulses (1-5ns) from a conventional Q-switched fibre laser.

The work on the Brillouin distributed temperature sensor is based on the premise of expanding the technology to provide a fully distributed temperature and strain sensor for commercial exploitation. This will involve measuring both the intensity variation of the Brillouin signal, as demonstrated in this work, and the frequency variation. With this information both the temperature and strain can be resolved. Work is currently in progress to produce fibre laser sources that have a sufficiently narrow linewidth, ~50MHz, to be used for Brillouin distributed strain sensing.

8.3 Conclusion

This thesis has researched the field of Q-switched fibre lasers and the exploitation of Q-switched fibre laser technology for use in distributed sensing applications. The ease with which the Q-switched sources developed in this work have been integrated into commercial sensing systems provides evidence of their importance in this field.

8.4 References

[1] P.Myslinski, J.Chrostowski, J.A.K.Koningstein and J.R.Simpson: 'Self-mode locking in a Q-switched erbium doped fibre laser', *Applied Optics*, Vol.32, No.3, pp.385-407, (1993)

[2] D.J.Richardson, P.Britton, D.Taverner: "Diode pumped, high energy, single transverse mode Q-switch fibre laser", *Electronics Letters,* Vol.33, No.23, pp.1955-1956, (1997)

Authors Publications (1995-Present)

1995

'980nm diode pumped Er/Yb doped Q-switched fibre laser'
Electronics Letters, Vol.31, No.21, pp.1836-1837, (1995)
G.P.Lees, A.Leach, A.Hartog and T.P.Newson

1996

'A Narrow linewidth, High Power, Q-switched Erbium doped fibre laser'
CLEO/Europe, Hamburg, Paper CMM3 (1996)
G.P.Lees, M.J.Cole and T.P.Newson

'A diode pumped Landau-Placzek based distributed temperature sensor utilising an all-fibre Mach-Zehnder Interferometer.'
Electronics Letters, Vol.32, No.23, pp. 2174-2175, (1996)
K.De Souza, G.P.Lees, P.C.Wait and T.P.Newson

'A Diode Pumped High Power simultaneously Q-switched and mode locked Erbium doped fibre laser.'
Electronics Letters, Vol.32, No.4, pp.332-333, (1996)
G.P.Lees and T.P.Newson

'A Narrow linewidth Q-switched Erbium Doped Fibre Laser'
Electronics Letters, Vol.32, No.14, pp.1299-1300, (1996)
G.P.Lees, M.J.Cole and T.P.Newson

'1.64 μm pulsed source for a Distributed optical fibre Raman Temperature Sensor'
Electronics Letters, Vol.32, No.19, pp.1809-1810, (1996)
G.P.Lees, A.Leach, A.Hartog and T.P.Newson

1997

'2kW Peak Power Q-switched Erbium Doped Fibre Laser'
Advanced Solid State Lasers (ASSL), Florida, Paper No. ME10 (1997)
G.P.Lees, D.Taverner, D.J.Richardson, L.Dong and T.P.Newson

'A Q-switched Erbium Doped Fibre Laser utilising a novel large mode area fibre'
Electronics Letters, Vol.33, No.5, pp. 393-394, (1997)
G.P.Lees, D.Taverner, D.J.Richardson, L.Dong and T.P.Newson

'Novel Optical Fibre Distributed Temperature Sensor based on the Landau-Placzek ratio'
CLEO/Baltimore, Paper CThD1 (1997)
G.P.Lees, K.De Souza and T.P.Newson

'A Novel OTDR system using Raman amplification of a 1.64μm probe pulse'
Electronics Letters, Vol. 33, No. 12, pp. 1080-1081, (1997)
G.P.Lees, H.H.Kee, and T.P.Newson

'A High Power Q-switched Erbium fibre laser producing 50μJ pulses'
QE-13 Cardiff, 8-13 Septenber (1997)
H.H.Kee, G.P.Lees and T.P.Newson

'A Novel Method of Increasing the Range of 1.65μm OTDR using a Q-Switched Erbium Fibre Laser'
QE-13 Cardiff, 8-13 September (1997)
H.H.Kee, G.P.Lees, D.Taverner, D.Richardson and T.P.Newson

'Novel Optical Fibre Distributed Temperature Sensor based on the Landau-Placzek ratio'
Optical Fibre Sensors (OFS'97), Williamsburg (1997)
G.P.Lees, P.C.Wait and T.P.Newson

'A method of increasing the range of 1.65μm long range OTDR system based on Raman amplification'
Optical Fibre Sensors (OFS'97), Williamsburg (1997)
H.H.Kee, G.P.Lees and T.P.Newson

1998

'Advances in Optical Fibre Distributed Temperature Sensing using the Landau-Placzek Ratio'
IEEE Photonics Technology Letters, Vol. 10, No. 1, pp. 126-128, (1998)
G.P.Lees, P.C.Wait, M.J.Cole and T.P.Newson

'An extended range OTDR system at 1.65μm based on delayed Raman amplification'
Optics Letters, Vol. 23,No. 5, pp. 349-351, (1998)
H.H.Kee, G.P.Lees and T.P.Newson

'Distributed Optical Fibre Temperature Sensing using the Landau-Placzek Ratio'
International Conference on the Applications of Photonics Technology (ICAPT'98), Paper Number ICAPT98T234, Boston (1998)
G.P.Lees, P.C.Wait and T.P.Newson

'Narrow Linewidth CW and Q-switched Erbium doped Fibre Loop Laser'
Electronics Letters (Submitted)
H.H.Kee, G.P.Lees and T.P.Newson

'Pulse build-up in a Q-switched Erbium doped Fibre Laser'
Electronics Letters (submitted)
S.M.Maughan, G.P.Lees and T.P.Newson